5. Contact formation

In consistence with several investigations (e.g. [73,74,76,77]) the microstructure analysis of silver thick film contacts to crystalline silicon solar cells revealed that silver crystals have grown into the silicon. Although separated from the bulk of the finger by a glass layer it is likely that these crystals are indispensable for the current transport from the emitter into the thick film finger (see also chapter 6). However, most of the investigations on silver thick film contacts to silicon published so far solely focus on the properties of the formed contact. To develop lead free and highly efficient silver pastes it is necessary to investigate the contact formation process, in particular the growth process of the silver crystals, in detail. In this section the experiments and results are presented and summarised in a model of contact formation. The approach is to investigate competing processes during contact formation separately. The role of lead oxide will be considered most carefully. The role of the other paste constituents will be investigated in more detail in chapter 7. After a review of existing hypotheses, the wetting properties, basic reaction and dissolving processes of a typical lead borosilicate glass are investigated. The main focus is on the growth process of the silver crystals. Interactions of the subsystems silver-silicon, silver-glass, glass-silicon, glass-silicon nitride and glass-silver-silicon will be studied. The subsystem silver-silicon nitride will not be investigated because from a thermodynamical point of view this subsystem does not interact.

5.1. Review of existing hypotheses

The interaction of the glass frit with silicon is the key point in electrical contact formation. Although experimental evidence is missing, two main hypotheses exist in literature.

1. Some authors assume that during peak firing silicon [80,81], silver [72,75] or both [77,82] is dissolved in the glass. During cooling down the silicon is assumed to recrystallise epitaxially [80,81]. Silver is supposed to start to randomly grow on the silicon so that inverted pyramids are formed [73,75,77,82]. This hypothesis is mainly based on SIMS studies of the incorporation of elements contained in silver pastes in silicon below a thick film contact [83]. The recrystallised silicon layer beneath the contact is supposed to determine the contact properties at least partly [80,81].
2. Another assumption is that etching occurs via a redox reaction between silicon, well known as a reducing agent [84], and the metal oxides contained in the glass [85]. The resulting metals are supposed to diffuse into the silicon and to damage, in the worst case, the junction [85].

A supersaturation of silicon ions in a silicate glass and a subsequent recrystallisation is not likely because silicon is, in form of SiO_2, a glass component. Dissolution of silicon ions in glass should rather change the glass frit properties like viscosity, transformation point and reactivity [86]. Dissolution of silver is a likely mechanism and is studied in more detail in section 5.3.1 and 5.4.2.

The redox reaction between silicon and the metal oxides in the glass is also a likely mechanism. To the knowledge of the author, so far, however, no experimental evidence for the existence of

such a reaction in a solar cell metallisation process was published. Therefore, this hypothesis will be investigated in detail in section 5.3.3.

5.2. Wetting behaviour

To guarantee a homogeneous and mechanically stable contact the wetting properties of a typical lead borosilicate glass to silicon, silicon nitride and silver are important. If the wetting of silver and/or silicon would be inefficient, the adhesion of the silver thick film contact would be poor [81]. The inefficient wetting of the silicon nitride would lead to an inhomogeneous penetration of this layer and consequently to a reduced contact area, which would affect the electrical properties of the contact. Additionally, a bad silver wetting would not lead to an enhancement of silver particle sintering. The microstructure investigations (chapter 4) revealed a continuous glass layer at the contact interface separating silicon from the silver finger. The existence of this glass layer indicates that the penetration of the SiN_x layer was homogeneous and so the wetting of the SiN_x layer and the silicon is expected to be efficient. The enhancement of sintering (chapter 3) indicates good silver wetting, too. In reference [87] we measured the contact angle of a typical lead borosilicate glass to silicon and silver. It was found that this glass wets both, silver and silicon, similarly well at temperatures above 700°C with an approximate contact angle of 30°. The contact angle was measured at room temperature using the cross section SEM picture. Similar good wetting behaviour of lead borosilicate glass on silver was reported in [88]. Glass on SiN_x coated silicon showed a similar behaviour as on silver [63].

5.3. Basic reactions and dissolving processes

5.3.1. Glass - Silver

As silver is covered by a liquid glass during the contact formation process, the interaction of the silver-glass system was investigated qualitatively. The dominant interaction of a lead borosilicate glass with silver in air atmosphere is silver dissolution in the glass (see e.g. [63,88]). Most effective silver dissolution was obtained using temperatures above the melting point of the silver and long dwell times of about 1 hr. Then up to 4 wt.% silver was dissolved in a lead borosilicate glass extracted from a commercially available paste as EDX measurements revealed. In a more detailed study Forti et al. [89] showed that a lead silicate glass used in thick film pastes for the microelectronics dissolves 3 wt.% silver in 30 min at 850°C, in 15 min at 900°C and in 10 min at 925°C. The composition in wt.% of the glass frit was specified to be $PbO:SiO_2:Al_2O_3 = 68:31:1$. In typical lead glasses used for solar cell processes the SiO_2 content is lower leading to a lower glass transformation point which might lead to a faster dissolving at somewhat lower temperatures. Therefore, tests with lead borosilicate glasses with a higher PbO and a lower SiO_2 content (e.g. $PbO:SiO_2:B_2O_3 = 85:9:5$) were performed. Mixtures of glass and silver with 1 wt.% Ag, 5 wt.% Ag, 10 wt.% Ag were deposited on ceramic substrates (Alsint) consisting of Al_2O_3 and fired in a tube furnace at 800°C with a dwell time of 30 min. It was found that the silver powder was partly dissolved but silver particles still remained undissolved even in the case of 1 wt.% Ag. From these tests it can be concluded that lead silicate glass is able to dissolve silver depending on the glass composition, temperature and dwell time (for details see [63]). Further experiments in the sections below have to clarify whether this process is dominant during the fast firing sequence in solar cell processes.

5.3.2. Glass - Silicon Nitride

In reference [87] we investigated the etching behaviour of a commercially available silver thick film front side paste in d-PECVD SiN_x, deposited on polished, <100> oriented silicon (SiN_x layer thickness: 130 nm). It was found that the etch rate rapidly increases with increasing firing temperature and is very similar to the etch rate of the same paste in silicon. Significant penetration into SiN_x was observed at temperatures higher than 625°C. Reaction products were not observed in these experiments. However, it is likely that etching into SiN_x occurs via a reaction with the metal oxides contained in the glass, mainly with lead oxide. Crystalline lead oxide reacts with Si_3N_4 via subsequent oxidation and reduction processes under N_2 emission [90]. Oxygen is known to act as a catalyst for this reaction [90]. An increased oxygen partial pressure in the atmosphere during peak firing was reported to have a beneficial effect on the fill factor of industrial mc silicon solar [91].

5.3.3. Glass - Silicon

A well known property of silver thick film pastes is the etching into silicon (see e.g. [92,93]). Average results of etching depth measurements of the reference silver thick film paste into polished <100> and <111> oriented silicon substrates without coating resulted in an etching depth of ≈110 nm and ≈80 nm, respectively. The peak temperature in this experiment was 800°C and the ramp up rate 6.7 K/s (for details see [87]). From the microstructure analysis (chapter 4) it is known that silver crystals grow into silicon. The silicon surface below silver thick film finger after removing the finger and the crystals is consequently covered by etch pits with the shape of inverted pyramids. Therefore, etching depth measurements of silver pastes into silicon always measure the combined etching depth of glass and silver.
In this section the etching behaviour of the glass contained in silver thick film pastes is studied separately. At first, the temperature dependency of the glass - silicon interaction is investigated, followed by microstructural analyses.

Etching

Cheek et al. [81] reported an etching depth of 3-4 µm of molten lead borosilicate glass into silicon without silver during a solar cell firing process. However, the firing profile used in this investigation differs from the fast firing profiles used today. In the following experiment 0.4 g glass frit[1] was mixed with a binder system and deposited on etch polished <100> oriented, p-type silicon substrates. The samples were fired in the RTP furnace with a ramp up rate of 20 K/s to 6 different peak temperatures between 650°C and 900°C. Dwell times as well as ramp down rates were also varied. After firing, the glass was completely removed in buffered HF. The etching depth was measured using a DEKTAK surface profiler.
In Figure 5.1 the average etching depth is plotted versus peak temperature. In this firing process, similar to a fast firing sequence in the solar cell industry, the glass frit significantly starts to etch at temperatures above 650°C. At 800°C the Pb glass etches ≈400 nm deep into <100> oriented silicon. Long dwell times as well as slow ramp up rates increase the etching depth strongly. At 650°C and a dwell time of 120 s the etching depth is ≈240 nm .

[1] A lead borosilicate glass was used. Basic composition: 81 wt.% PbO, 11 wt.% SiO_2 , 4 wt.% B_2O_3 and additives like Al_2O_3.

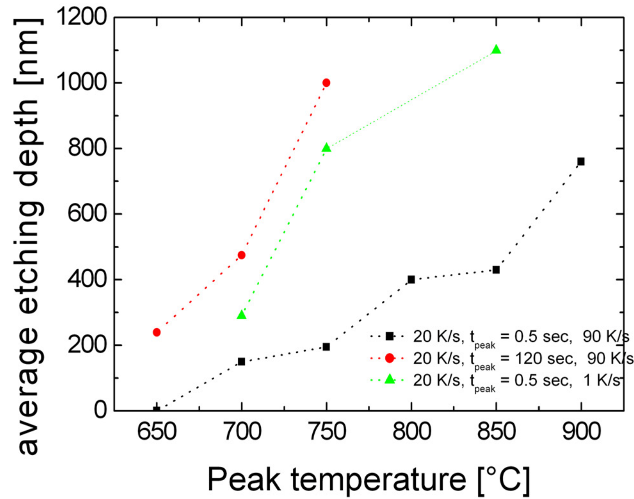

Figure 5.1.: Etching depth of Pb glass in <100> oriented silicon in dependence of the peak temperature

This experiment shows that a lead borosilicate glass alone can deeply etch into the silicon. The glass frit content (and its composition) in a silver thick film paste consequently determines the etching behaviour of such a paste. In the following the etching mechanism of the glass is investigated in more detail.

Reaction

To study the reaction of silicon with lead borosilicate glass, different glass pastes were prepared by mixing glass powder with a binder system (ethyl cellulose + terpineol) or only with a solvent (in general isopropanol) and deposited on polished silicon substrates with different orientations. The samples were fired either in a tube or in the RTP furnace. In both cases the temperature of the samples were monitored.
In Figure 5.2(a) a typical BE-SEM cross section picture of a sample fired in a tube furnace at 780°C for 4 min is shown. At the silicon - glass interface precipitates have been formed. Near the interface the precipitates are small, whereas in the middle of the picture a large sphere is visible. EDX analysis revealed that these precipitates consists of lead, only (Figure 5.2(b)). It is likely that the following redox-reaction occurs:

$$2PbO_{glass} + Si \rightarrow 2Pb + SiO_2 \qquad (5.1)$$

This reaction is exothermal with H = -473.6 kJ/mol under standard conditions [84]. The formation of metallic lead was confirmed by XRD-analysis of the glass powder before firing and after reaction with silicon (Figure 5.2(c)). The glass powder shows the typical spectrum of a high leaded glass. After reaction with silicon Pb peaks occur, indicating the existence of metallic lead. Thus for the first time it was shown that the redox reaction between silicon and lead oxide in the glass (equation 5.1) occurs in a solar cell firing process.

Microstructure

It is interesting to note that hardly any inverted pyramid structures were found in the cross section pictures of the glass - <100> silicon interface. Figure 5.3(a) shows an overview of an

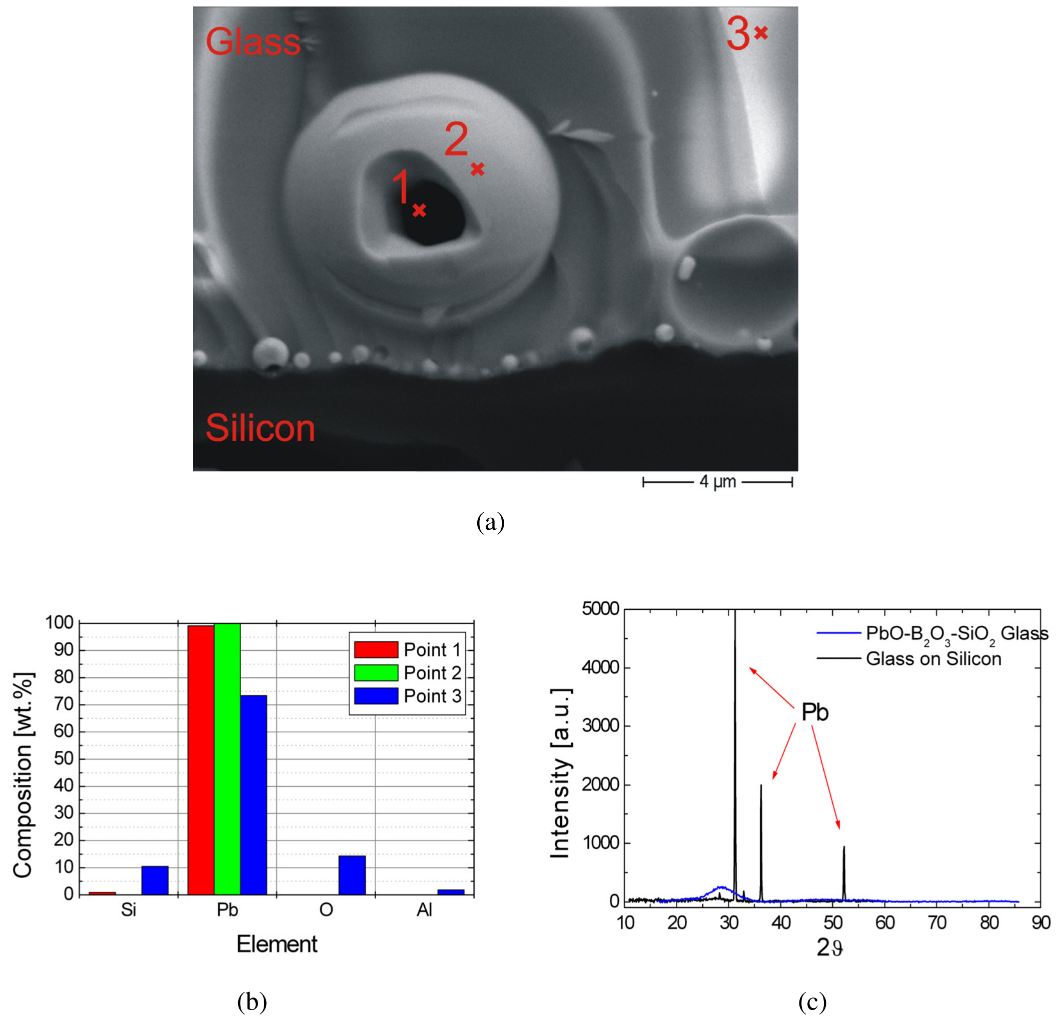

Figure 5.2.: (a) BE-SEM cross section picture glass - silicon interface. The glass was fabricated at our institute (Composition (EDX analysis): PbO:B_2O_3:Al_2O_3:SiO_2=88:(5):4:8) (see chapter 7.1). (b) EDX analysis of the three points marked with a cross. (c) XRD analysis of the lead glass before and after reaction with silicon. The glass spectrum does not show any characteristic peaks, whereas after reaction with silicon lead peaks occur.

cross section. The sample was fired in the RTP furnace at 800°C for 5 min (ramp up: 20 K/s). No inverted pyramid structures are present. The metallic lead does not wet the silicon. The precipitates do not remain at the surface but form spherical crystallites that rise into the glass bulk during the heating process. The hypothesis of Young et al. [85] that the reaction products of the redox reaction diffuse into silicon is unlikely in case of lead oxide because the formed metallic lead precipitates do not wet the silicon.
Analysing the silicon surface after glass removal using SEM and AFM reveals that the surface is corrugated (Figure 5.3). The surface is similar to a wet chemically, isotropically etched surface under agitation with local etch stops. The lead borosilicate glass is therefore assumed to etch at least into <100> oriented silicon isotropically.

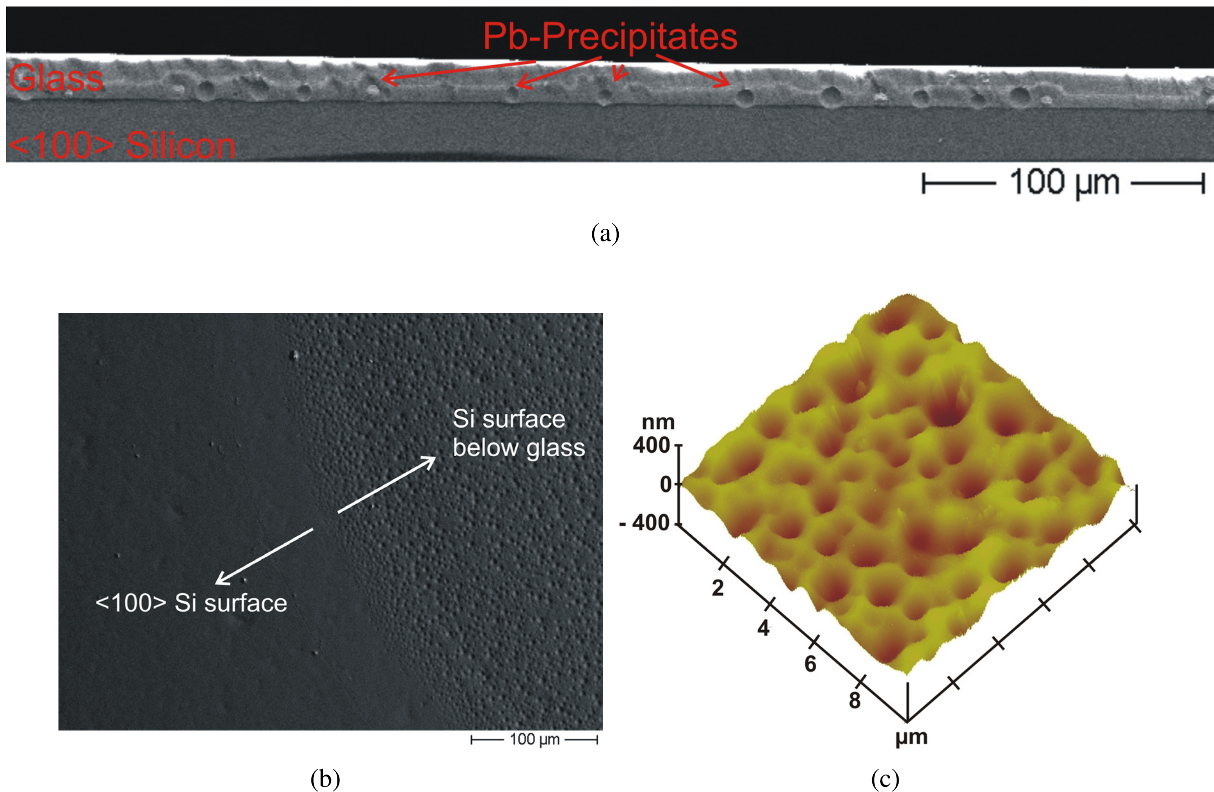

Figure 5.3.: (a) Overview of glass - silicon cross section (Parameters: ramp up: 20K/s, T_{peak} = 800°C, t_{peak} = 300s, ramp down: >75K/s). No hints for anisotropical etching were found. (b) BE-SEM analysis of the silicon surface after etching off the lead borosilicate glass in buffered HF. The sample was fired in the RTP furnace at 750°C for 120 s (Ramp up: 20 K/s, ramp down: as fast as possible). No inverted pyramids are detected. (c) AFM analysis of the silicon surface under the glass. The sample was fired at 730°C for 1 min in a quartz tube furnace in air. The surface is corrugated with deep holes (<400 nm), but pyramidal structures are not detected.

5.4. Growth mechanisms of silver crystals

As silver crystals were found to have been grown onto the silicon without an interfacial layer, it is likely that the silicon - silver crystals contact is responsible for the electrical current transport. The electrical properties of this contact will be investigated in detail in chapter 6. To study the growth mechanism of the silver crystals three systems were analysed: pure silver on silicon, glass containing dissolved silver on silicon and a "near reality" system, a mixture of silver and glass powder on silicon.

5.4.1. Direct silver - silicon reaction

According to the phase diagram of silver and silicon both elements form an eutectic alloy at 836°C with 11 at.% silicon. Recently it was found that there is a finite equilibrium solid solubility of silicon in silver of 0.93 at.% near the eutectic temperature [94]. Furthermore, silicon is able to diffuse in silver at temperatures far below the eutectic temperature [95–97]. Studying the contact formation process, it is unlikely but not excludable that the silver crystals grow into the silicon solely due to a silver - silicon eutectic reaction. To investigate this reaction silver powder was mixed with a binder system and dispensed on etch polished <100> oriented silicon substrates. In Figure 5.4 the SEM analysis of the silver - silicon cross section is shown. Sample

1 (Figure 5.4(a)) was fired in a tube furnace at 900°C for 15 min. Silver crystals are found below the contact, showing the typical inverted pyramid shape and diameters of ≈ 500 nm. In comparison in Figure 5.4(b) the silver - silicon cross section of a sample fired in the RTP furnace (ramp up: 20 K/s, T_{peak} = 800 °C, t_{peak} = 120 s, ramp down: 20 K/s) is shown. No silver crystals were found.

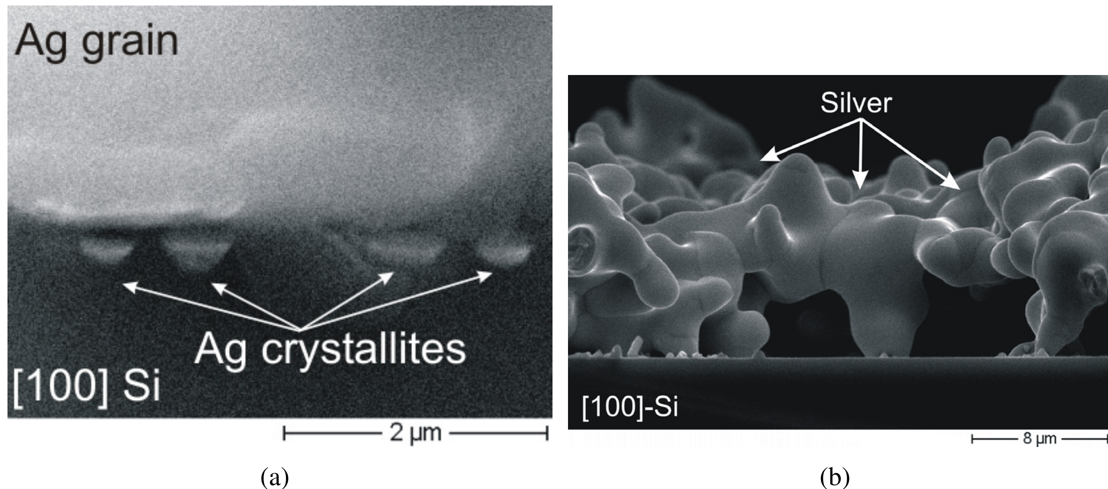

(a) (b)

Figure 5.4.: Interaction of silver and silicon. (a) Firing in a tube furnace at 900°C for 15 min. Silver grows into silicon. (b) Firing in an IR heated RTP furnace with high ramp up rates and a dwell time of 120 s at 800°C.

The results indicate that the silicon - silver reaction starts at T ≥ $T_{eutectic}$ at particular points (e.g. imperfectness in the native oxide layer or defined silver particle contact points to silicon). Silicon dissolves according to the phase diagram similar to the Al-Si eutectic reaction (see chapter 8). Obviously, this dissolving process is anisotropic, [100] planes are dissolved faster, so that inverted pyramids develop. On cooling down, silver recrystallizes and fills up the pyramids. Comparing both results shows that in a standard firing cycle the silver - silicon eutectic reaction is not the dominant process. Much higher temperatures and extremely long dwell times were necessary to grow silver crystals similar in size and shape to those grown in a standard thick film process, indicating that the eutectic reaction is slow at least below the melting point of silver ($T_{melt}(Ag) = 962$°C [84]).

5.4.2. Growth from Ag containing glass

An often proposed contact formation hypothesis is that during firing glass dissolves silver. On cooling down the silver recrystallises from the supersaturated glass to grow onto silicon [72,98,77,75,79,80,87,99]. However, to the knowledge of the author so far no investigations were published that study the silver growth on silicon from silver saturated lead borosilicate separately.

Sample preparation

A commercially available silver thick film paste was heated to 1000°C for 2 hours leading to liquid glass above liquid silver[2]. Due to the high temperatures silver is dissolved in the glass

[2] The density of lead borosilicate glass is between 4 and 7 g/cm^3 [71] and therefore lower than the density of silver (≈10.5 g/cm^3).

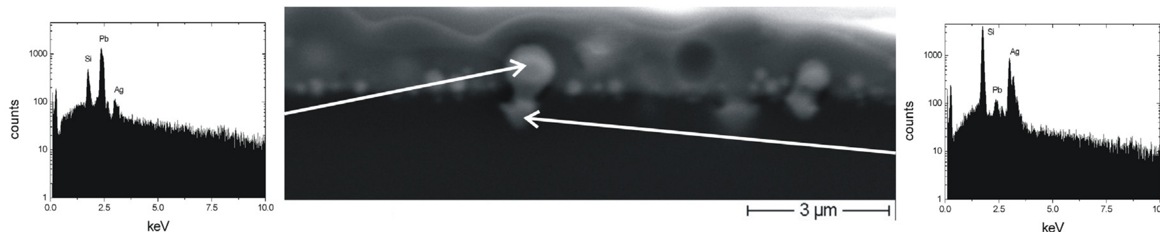

Figure 5.5.: Typical cross section of silver saturated glass on silicon. Silver crystals have been grown into silicon. Pb precipitates, arising from the PbO_{glass}-Si redox reaction, are visible above the crystals.

(see also section 5.3.1). The liquid glass was poured out to keep as much silver dissolved in the glass as possible. ≈4 wt.% silver in the glass was measured with EDX. The glass powder was mixed with a solvent (IPA) and deposited on <100> oriented, etch polished silicon substrates. The firing was performed in the RTP furnace and in a tube furnace at various parameters.

SEM and EDX analysis

The cross section of the silicon - glass interface was investigated with SEM and EDX. In Figure 5.5 the results of a sample fired for 60 s at 810°C in a tube furnace are presented. Inverted pyramids were found to have grown into <100>-oriented silicon. The precipitate above the crystal mainly consists of Pb, whereas the EDX analysis of the pyramid shows that it mainly consists of silver. The growth of silver crystals was confirmed by etching off the glass in HF, leaving behind the silicon surface covered with silver crystals.
As pure lead borosilicate glass does not show a pyramidal etching behaviour, a possible silver growth mechanism would be an anisotropic redox reaction of the silver ions in the glass with silicon, similar to the PbO - Si reaction (equation 5.1). It is remarkably that above the interface Pb precipitates are observed in the bulk of the glass. This is a hint that both redox reactions occur during the firing process.
Simple calculations were made to estimate the amount of silver which has to be dissolved in the glass if silver crystal growth onto silicon occurs via dissolution of silver in the glass and a subsequent reaction between silicon and the silver ions in the glass[3]. 1.4 wt.% silver relative to the frit weight has to be dissolved by the glass during the firing process assuming a 15% coverage of the silicon surface with inverted pyramids. A 50% coverage with larger crystals (diameter: 500 nm) would lead to nearly 8 wt.% silver relative to the frit weight which has to be dissolved in the glass. Comparing this estimation with the results of section 5.3.1 shows that at least 15 min at 850°C are necessary to dissolve 1.5 wt.% Ag in a lead borosilicate glass[4]. These estimations do not seem to fit with the fast firing sequence in a standard industrial solar cell process.

5.4.3. The silver powder - glass system

Reconsidering the results of the contact formation experiments so far, the mechanism of silver crystal growth is not obvious yet. The silver - silicon eutectic reaction is anisotropic, silver

[3]Paste parameters: weight: 1.89×10^{-4} g, area: 120 µm x 1 cm, frit content: 5 wt.%. Silver crystals: shape: inverted pyramids on <100> oriented silicon, diameter: 300 nm, depth: 212 nm, coverage: 15%. Frit: 81 wt.% lead oxide.
[4]A linear relation between dissolution and time was supposed to adapt the results of Forti et al. [89].

pyramids are formed on <100> oriented silicon. However, the temperatures and dwell times, necessary to start the reaction, are too high and too long to explain the silver crystal growth in the fast firing process. Dissolution of silver in glass prior to a possible glass - silicon reaction will occur, thus the observed silver growth from a silver saturated glass into silicon via a redox reaction is a possible mechanism. However, the separated silver dissolution process is also too slow to be dominant during the firing sequence. Consequently, a mechanism must be present that accelerates the transfer of silver through the glass to grow on silicon.

Sample preparation

Following the concept of separating competing processes, the influence of silver on the glass - silicon system was studied. A set of pastes were prepared consisting of a binder system, lead borosilicate glass and a varying amount of silver powder. In Table 5.1 the composition of the pastes is presented. To guarantee identical conditions, all pastes were deposited on etch polished <100> oriented p-type silicon samples side by side and fired in the RTP furnace using different parameters for ramp up, peak temperature, dwell time and ramp down. The interactions were studied by means of SEM, EDX, differential thermal analysis (DTA) and x-ray diffraction analysis (XRD).

Paste	Glass [wt.%]	Silver [wt.%]
0	100	0
1	99	1
2	95	5
3	90	10
4	50	50

Table 5.1.: Paste composition to test influence of silver on glass - silicon interaction

SEM and EDX analysis

As soon as a little amount of silver is added to the glass - silicon system, in addition to the already known precipitates in the glass bulk, inverted pyramids arise. In Figure 5.7(a) a typical SEM cross-section picture of paste 1 is shown. The sample was fired with a heating rate of 20 K/s after combustion of the organics, a peak temperature of 800°C for 120 s and a cooling rate of 1 K/s. EDX analysis showed that the crystals grown into the silicon consist of both, lead and silver. In the precipitates above the interface the amount of lead is much higher but silver is also found. Figures 5.7(a) and 5.7(b) show typical SEM pictures of paste 1 and 2. Analysing the cross sections of paste 2 to 4 reveals that crystals have grown onto the silicon, too, but, most remarkable, the lead rich precipitates in the bulk of the glass have vanished. The same phenomena was observed in the following experiment. A film of lead borosilicate glass (without silver) was prepared on silicon by firing at 760°C for 4 minutes in a tube furnace (average glass layer thickness: 10 µm). After cooling down to room temperature, a 15 µm thick silver foil was placed on the glass layer and the specimen was fired at 750°C for 40 min. Underneath the silver foil no lead precipitates were detected but silver was found to have grown onto the silicon. In the regions without silver foil lead precipitates were formed (Figure 5.7(c)). If a large amount of metallic silver is present in the glass - silicon system, lead precipitates are not detectable with the used SEM.

To circumvent the limited resolution of the EDX analysis, the glass layer was mechanically

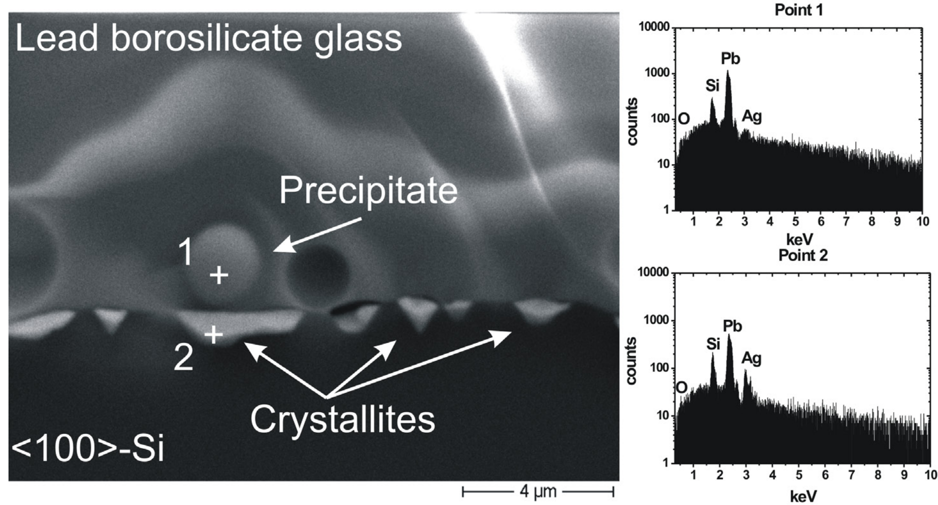

Figure 5.6.: SEM cross section picture of paste 1 on <100> silicon with EDX analysis

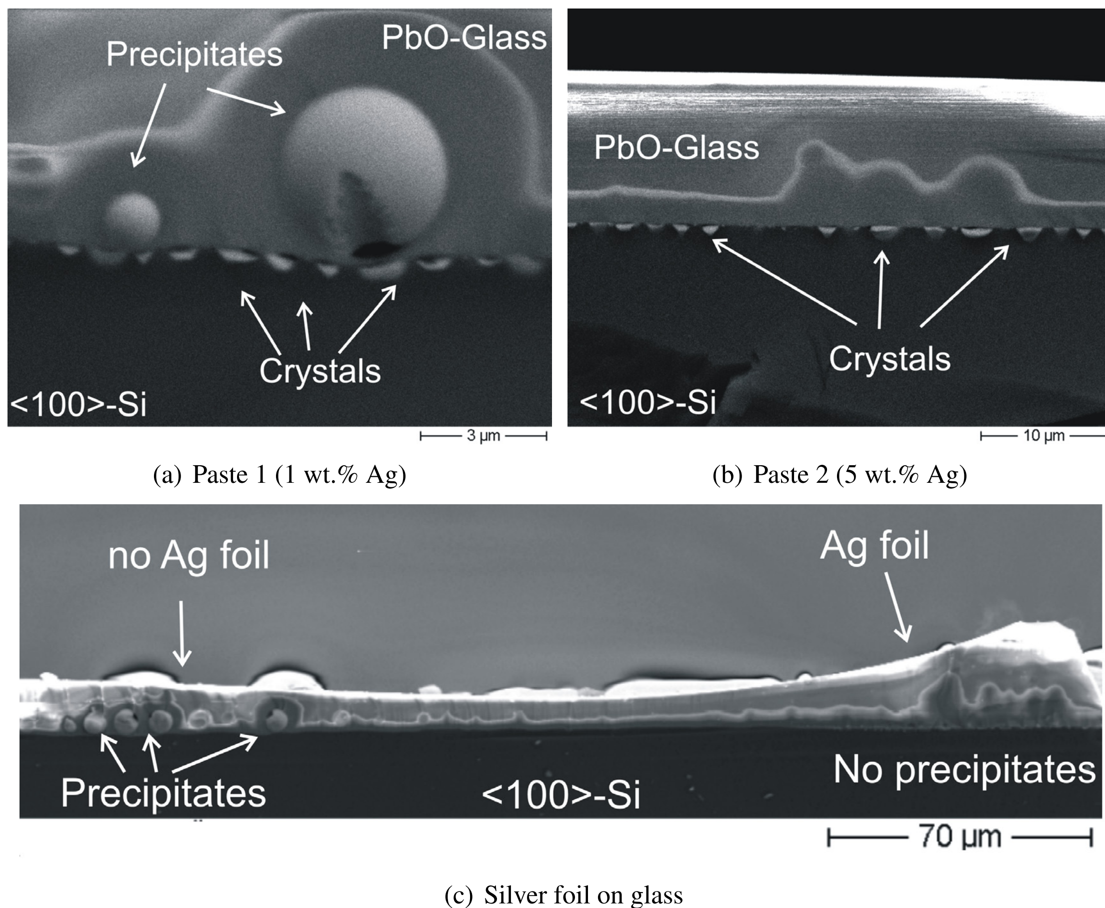

(a) Paste 1 (1 wt.% Ag)

(b) Paste 2 (5 wt.% Ag)

(c) Silver foil on glass

Figure 5.7.: (a) and (b) SEM cross section pictures of silver impurified glass frit paste on silicon (ramp up: 20K/s, 750°C, 120s, ramp down: 20K/s). The lead rich precipitates in the bulk of the glass vanish with increasing silver content in the paste. (c) Cross section of lead borosilicate glass on silicon with (right side) and without (left side) Ag-foil on top. Pb precipitates are clearly visible on the left whereas at the Si-glass interface on the right precipitates are not detectable.

removed to analyse the surface of the silicon below the paste. The crystals (regular white squares) are clearly visible confirming the growth of inverted pyramids (Figure 5.8). The EDX

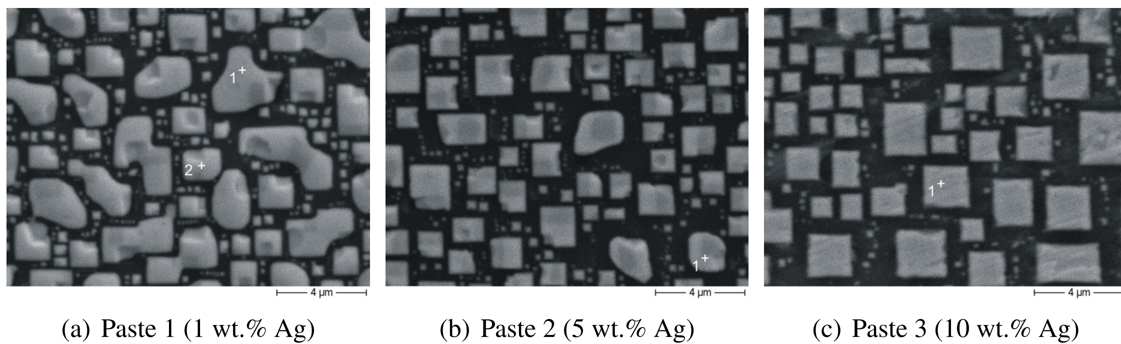

(a) Paste 1 (1 wt.% Ag) (b) Paste 2 (5 wt.% Ag) (c) Paste 3 (10 wt.% Ag)

Figure 5.8.: SEM top view pictures on the <100> silicon surface after mechanical removal of the glass (ramp up: 20K/s, 800°C, 120s, ramp down: 1K/s). In all cases crystals have been grown. The size of the biggest crystals varies between 1.5 and 2 µm. The white crosses mark the location of the EDX analyses presented in Figure 5.9(a).

analysis confirmed the findings above: A little amount of silver added to a glass frit paste leads to the growth of crystals onto silicon consisting of silver and lead. With increasing silver content in the paste the amount of silver in the crystals increases. In Figure 5.9(a) the EDX spectra of typical crystals grown below paste 1, 2 and 3 are shown. As the surface of the investigated structure is not polished, the quantitative analysis is subject to error. The interpretation of the silicon peak in the spectrum is difficult because this peak might occur due to the limited resolution of the EDX analysis. The intensity of the silicon peak decreases with increasing crystal size. Therefore, in Figure 5.9(b) the weight per cent ratio of the detected silver and lead is given, clearly showing the decrease of the lead fraction with increasing Ag amount in the paste. The crystals below paste 3 contain only a very minor amount of lead. As lead and silver do not form a compound, it is likely that both elements occur separated in the crystals. With the SEM and EDX analysis it was not possible to locate the two phases. Nevertheless, these results give a first hint that the silver crystals growth is related to the formation of lead during the firing process.

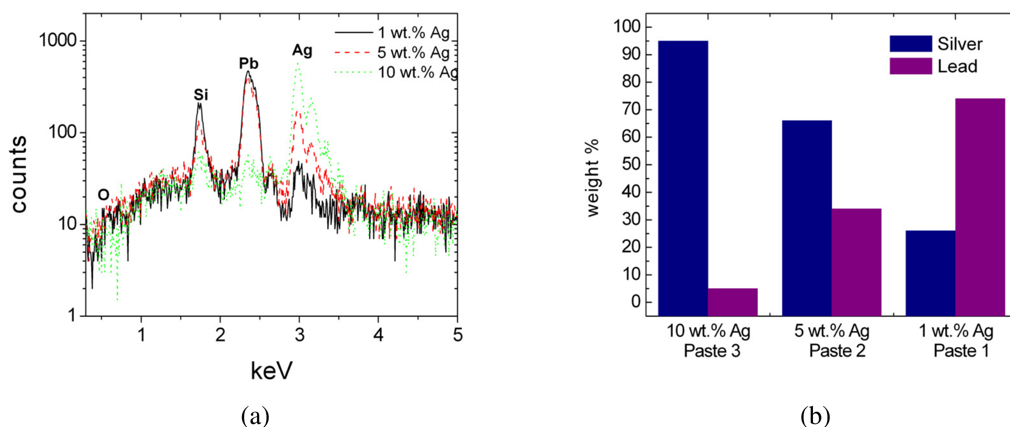

(a) (b)

Figure 5.9.: EDX analysis of crystals below silver impurified glass frit paste

Differential Thermal Analysis

To study the reaction during, firing differential thermal analysis (DTA)[5] was applied to a number of samples. To obtain maximum signal, <100> oriented silicon was crushed into powder and mixed with glass and silver. The used crucibles consisted of an Al_2O_3 ceramics. An empty crucible served as reference. Each sample was heated up at least twice in air to study the reaction. The analysis of the second heating step provides information about the formed reaction products during the first heating step. In Figure 5.10(a) the results of two different samples of the second heating step are presented. The first sample is a mixture of glass frit and 10% silicon powder (dashed line). To the second mixture 5% silver powder was added. In case of mixture 1 the melting of lead precipitates formed during the first firing step is clearly visible (endothermic peak at T = 322°C). When adding a small amount of silver powder (mixture 2) additionally an endothermic peak at T = 298°C is measured. This temperature is only slightly lower than the melting temperature of a lead-silver eutectic ($T_{eutectic}$(Ag-Pb) = 304°C [101]).
The used glass frit consists of 81 wt.% PbO. If the redox-reaction is complete, half of the silicon is consumed and oxidised to SiO_2. Consequently, 68 wt.% of the mixture's weight is then lead. The shifting of the melting point of the lead towards lower temperatures indicates that lead and silver form a liquid alloy during the first heating cycle. On cooling down both phases recrystallise according to the phase diagram (Figure 5.10(b)) ending up in the eutectic composition which melts during the second heating cycle. Again the existence of a lead - silver phase after firing was confirmed suggesting that this phase is formed during contact formation.

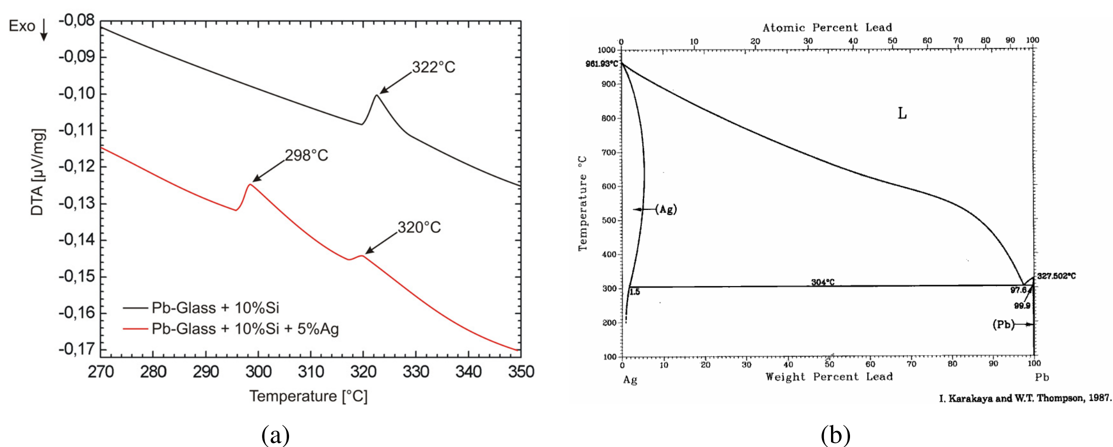

Figure 5.10.: (a) DTA analyses of glass - silicon and glass - silver - silicon systems. (b) Ag-Pb Phase diagram [101] (Reprinted with permission of ASM International™. All rights reserved. www.asminternational.org)

X-ray diffraction analysis

To study the reaction products regarding their crystal structure, x-ray diffraction (XRD) analysis was performed. Paste 0, 1 and 2 were fired on <100> oriented silicon with a heating rate of 20 K/s, a peak temperature of 800°C, a dwell time of 0.5 s and a cooling rate of 20 K/s. The samples were analysed with a Siemens D5000 XRD measurement system. In Figure 5.11 the results are presented. The analyses of paste 0 confirmed again the formation of crystalline lead

[5] A Netzsch (STA 449C) differential thermal analysis system was used. For details about the measurement method see e.g [100].

during firing on silicon occurring in at least three different orientations. Adding a small amount of silver to the glass - silicon system results in the occurrence of only one orientation of lead crystals. Only the <110> orientation is present. Additionally, silver peaks of various crystal orientations occur. The analyses of paste 2 (5 wt.% Ag) showed no lead peaks confirming the SEM and EDX analyses of the paste - silicon cross section.

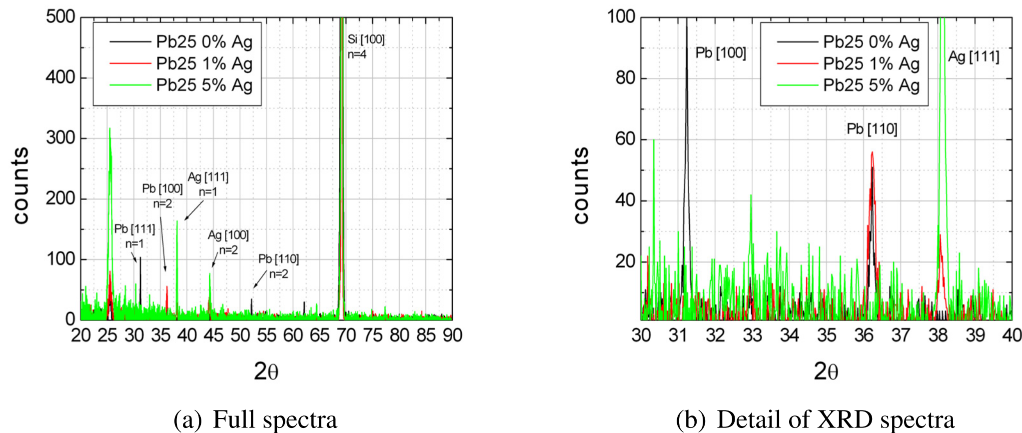

(a) Full spectra

(b) Detail of XRD spectra

Figure 5.11.: XRD analysis of paste 0, 1 and 2 fired on <100> FZ silicon

The results of the different measurements so far suggest four important conclusions:

1. Pyramidal growth of crystals on <100> oriented silicon and hence anisotropical silicon etching occurs when adding silver powder to a glass frit paste. Only minor amounts are necessary to start the reaction confirmed by cross section and top view SEM analysis.
2. The composition of the crystals depends on the amount of silver in the glass paste. >5wt.% Ag is sufficient for Ag:Pb weight per cent ratios of Ag:Pb > 2:1 shown by EDX analysis.
3. Crystalline lead precipitates, resulting from the redox reaction between glass and silicon, are only present when a minor amount of silver is added. At higher mixture ratios of glass and silver lead is not present in a crystalline structure after firing as confirmed by XRD and EDX measurements. This is in consistence with the TEM cross-section analysis of other authors [73,74,76,79]. Ballif et al. [73] reported the existence of lead precipitates in the glass layer of a silver thick film contact to silicon only when overfiring the cell. Khadilkar et al. and Hilali et al. [74,76,79] reported the existence of silver precipitates but did not found lead precipitates in their investigations.
4. The occurrence of both, lead and silver, in the crystals suggests that a lead - silver phase is formed during firing. DTA analysis proved the existence of such a lead - silver eutectic after firing.

Lead, resulting from the redox reaction between glass and silicon, can thus be seen as the key factor for the silver growth on silicon. If this hypothesis is valid, silver growth onto silicon at T < 830°C should be promoted by lead independent of additional components.

Lead promoted silver growth

To test the relevance of lead for the silver crystal growth, two pastes were prepared. Paste 1 consisted of silver and lead (wt.% ratio 2:1), Paste 2 of silver and crystalline lead oxide (wt.% ratio 9:1). After drying, both pastes were fired on etch polished <100> oriented silicon (ramp

up: 20K/s, $T_{peak} = 800°C$, $t_{peak} = 120$ s, ramp down: 20 K/s) in air atmosphere. The adhesion of paste 1 was poor. The paste flaked off after firing. In contrast the adhesion of paste 2 was very good. In Figure 5.12 SEM top view and cross section pictures are presented. Below both pastes crystals are visible. EDX measurements confirmed that they consist of lead and silver. Below paste 1 the lead content in the crystals is higher than for paste 2 as expected from the results above. Here, only a minor amount of lead was detected with EDX.

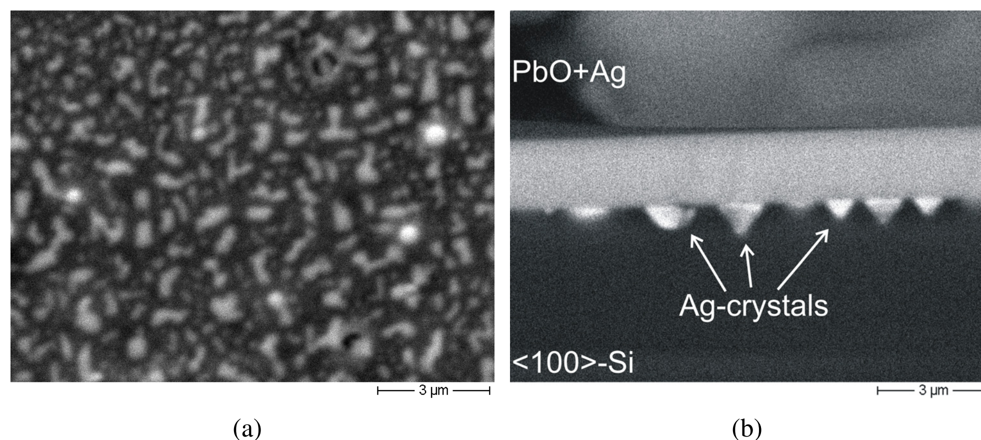

(a) (b)

Figure 5.12.: (a) Top view on silicon surface below paste 1 (Ag+Pb). Crystals have been grown into silicon, consisting of lead and silver. (b) Cross section of paste 2 (Ag:PbO = 9:1). Again, silver crystals are visible.

Discussion

As even lead, contained in paste 1, is covered by a native PbO layer, it is useful to reconsider the interaction of crystalline PbO and silicon. PbO is reduced by silicon resulting in crystalline lead and silicon dioxide which is assumed to form a glass with the excess metal oxide [102]. This reaction starts at T = 600°C, well below a possible direct interaction between silver and silicon. Due to the short reaction time both pastes are therefore expected to provide a liquid lead phase during firing as well as a lead silicate glass without any additional components except silver. For kinetic reasons it is likely that silver interacts with liquid lead. This process is very fast as simple experiments indicate. Mixtures of silver powder and lead become fluid in a reducing atmosphere (Ar-H) at temperatures between 400°C and 800°C. At high temperatures the liquid lead - silver alloy is supposed to interact with silicon resulting in inverted pyramids filled with silver. However, it cannot generally be excluded that the silver growth mechanism is via dissolution of silver in the lead silicate glass and a subsequent redox reaction between the silver ions in the glass and silicon. The most important aspect for further development of environmentally friendly and highly efficient silver thick film pastes for solar cells is, though, that lead, in a glass or as a liquid at high temperatures, is the key component which enables the growth of silver crystals on the silicon at temperatures well below the silver - silicon eutectic.

5.4.4. Influence of the phosphorous surface concentration

As pointed out in chapter 2.2.2, 40-70 Ω/sq emitters with high surface concentrations, exceeding the solubility limit of phosphorus in silicon, are currently necessary to establish an ohmic contact to the n-type region of the solar cell. The high phosphorous surface concentration in

these emitters leads to recombination losses that in turn lead to current and voltage losses.
Recently, several successful attempts were reported to contact emitters with sheet resistances up to 100 Ω/sq with silver thick film pastes [103]. It was also reported that the surface texture influences the contact resistance on emitters with high sheet resistances [104]. In both papers diffusion drive-in steps were not reported. Therefore, a P surface concentration well above 10^{20} cm^{-3} can be assumed. In this chapter the influence of the P surface concentration on the silver thick film contact formation processes is investigated. Hilali et al. [103] assumed the crystal growth to be dependent on the P concentration in the emitter, however, the hypothesis was not systematically examined.
The main focus in the following investigation is on the influence of the phosphorous concentration on the silver growth on silicon.

Sample Preparation

Simple solar cell structures with emitters differing in the phosphorous surface concentration were processed. To exclude shunting or damaging of the space charge region by the metallisation paste we used drive-in steps in order to obtain deep profiles for the emitter P concentration. Four $POCl_3$ pre-deposition steps (820°C low $POCl_3$ flow; 820°C high $POCl_3$ flow; 860°C high $POCl_3$ flow; 950°C high $POCl_3$ flow) were performed on <100> oriented, 12.5x12.5 cm^2 semi-square Cz silicon (thickness: 330 µm, $\rho = 1.5$ Ωcm) after saw damage etching (NaOH, 80°C) and cleaning. After P-glass etching the wafers were divided in a reference and a “drive-in” group. Wafers belonging to the latter group were used to fabricate deep emitters with varying phosphorous surface concentrations by performing a drive-in diffusion at 950°C for 240 min in N_2 atmosphere to avoid pile-up effects. PECVD-SiN_{xx} was deposited and the wafers were cut into 5x5 cm^2 samples. Then front contacts were screen-printed using a commercially available, leaded Ag paste, optimised for 40 - 60 Ω/sq emitters with high P surface concentrations. After printing the Al back contact, the samples were fired in the RTP furnace to ensure an accurate control of the process parameters. The fill factor optimised firing profile was used. To study temperature dependent effects, the peak firing temperature was varied in the range of $T_{peak} = T_{optimal} - 25K$ to $T_{peak} = T_{optimal} + 50K$. Due to the statistical nature of the contact formation processes, three samples per firing parameter and emitter were processed. The pyrometer of the RTP furnace was carefully calibrated using two of the samples with 11 Ω/sq and 83 Ω/sq emitter. The wafers were fired facing the pyrometer.

Emitter characterisation

The fabricated emitters were characterised after P-glass etching by sheet resistance measurements and electrochemical capacitance voltage (ECV) measurement. The results are summarized in Figure 5.13. The variation of R_{sheet} of emitter 4 after drive-in even on one wafer was quite high which might be due to an inhomogenous diffusion due to the low $POCl_3$ flow. The electrical active P concentration was determined by ECV measurements on one wafer of each group. The reference emitters showed a 12 nm to 400 nm deep plateau at N_D = 1 to 3×10^{20} cm^{-3}. The chemical P concentration in the plateau is expected to be a factor 1.2 to 2 higher (see chapter 2.2.2). After drive-in, the resulting profiles of emitter 1 and 2 show similar electrical active surface concentrations but a Gaussian shape, indicating a lower chemical surface concentration because no P-source was present during the drive-in step. Emitter 3 and 4 show Gaussian shapes, too, with P surface concentrations of $N_D \approx 4 \times 10^{19}\text{cm}^{-3}$ and $N_D \approx 3 \times 10^{19}\text{cm}^{-3}$, respectively. For these emitters it can be assumed that the chemical and

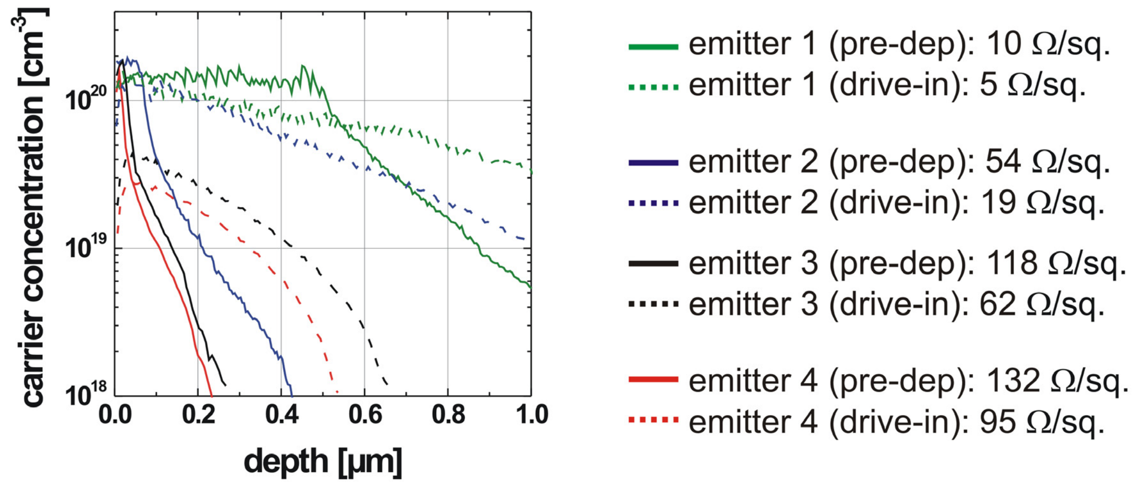

Figure 5.13.: R_{sheet} (mean values of three samples) and electrical active P concentration as a function of depth of the 8 studied emitters

the electrical P concentration depth profiles are identical with the electrically active P profiles.

Cell parameters

The solar cells were characterised by IV-measurements to determine the global cell parameters, I-LIT (Illuminated Lock-In Thermography) to identify shunts, and TLM (transfer length method) measurements to determine the contact resistance. In Figure 5.14 the fill factors (average over three cells) and specific contact resistances (average over 19 fingers of one cell per group) of the "drive-in emitter" cells are presented. Apart from the cells with the highly doped drive-in emitter 1, all samples show very low fill factors due to very high contact resistivities. The contact resistivities of emitter 2-4 are difficult to measure and scatter so that the values given in Figure 2 are only approximate. Dark IV analysis and ILIT measurements revealed that

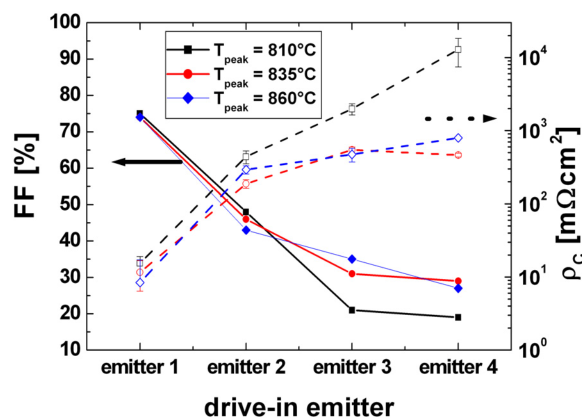

Figure 5.14.: Fill factor and specific contact resistance ρ_C of "drive-in emitter" cells

the fill factor loss is related to the high contact resistance. Although the shunt resistance was

difficult to extract due to the high series resistance, even drive-in emitter 4 - cells showed shunt values in the range of 500 Ωcm^2 < R_{shunt} < 1500 Ωcm^2.

Crystal growth versus doping concentration

The contact formation was investigated by SEM and EDX analysis using the TLM samples. Cross-section investigations of the contact show only limited parts of the finger. To account for the statistical nature of the contact formation process, the focus was set on the analysis of the silicon surface below the silver finger. The silver grid was removed by dipping the samples in diluted HF (2%) for 3 min. This etching procedure guarantees that only the glass layer and the bulk of the silver finger fall off, whereas the silver crystals grown onto the silicon are not affected. 5-10 fingers distributed over an area of 2.5 x 2.5 cm^2 selected from each solar cell were analysed at randomly chosen positions. Firstly, the crystal growth in dependence of the P surface concentration at the optimal peak firing temperature (810°C) was investigated. In Figure 5.15 a selection of representative SEM pictures is presented. As the number and size of the grown crystals is similar on reference emitter 1, 2 and drive-in emitter 1 (size around 500 nm, coverage: ≈9%), only SEM pictures of reference emitter 2 are shown. On all other “drive-in” emitters less and smaller crystals have grown (size: 200-300 nm, coverage: 1.3% - 5%). The differences in Ag crystal growth on those emitters are little. On reference emitter 3 and 4 the crystal growth is comparable to the growth on the corresponding drive-in emitters.

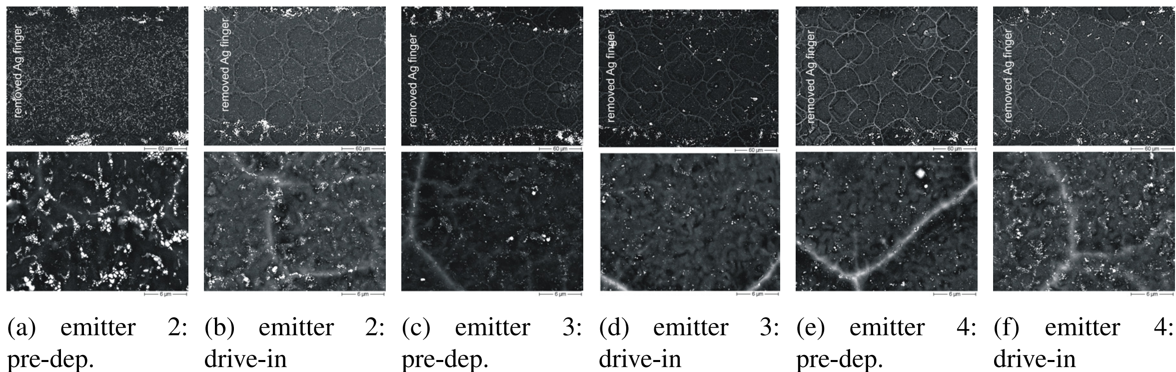

(a) emitter 2: pre-dep. (b) emitter 2: drive-in (c) emitter 3: pre-dep. (d) emitter 3: drive-in (e) emitter 4: pre-dep. (f) emitter 4: drive-in

Figure 5.15.: Dependency of crystal growth on the P surface concentration at the optimal peak firing temperature. The top view on the silicon surface after removal of the silver finger is shown.

It can be concluded that crystal growth mainly depends on the excess phosphorous at the surface. The sheet resistance is not the key parameter. The minor differences between reference emitter 3 and 4 and the corresponding drive-in emitters can be explained by the glass frit etching into the silicon. As the highly doped plateau is only 10 - 15 nm deep for these emitters, it is likely that the effective P surface concentration for silver crystal growth is lower. The activation energy for initiating Ag crystal growth on silicon can be assumed to be lower in the case of highly doped emitters, i.e. crystal growth at a constant peak firing temperature with a given paste system is less effective in case of emitters with lower excess phosphorous at the surface.

Crystal growth versus peak temperature

Increasing the peak firing temperature leads to the growth of more and larger Ag crystals on all emitters. The difference in crystal growth between the optimal fired reference and the drive-in

emitters gets smaller (see Figure 5.16). The average sizes of the crystals grown on drive-in emitter 3 are ≈350nm at 835°C and ≈450nm at 860°C.

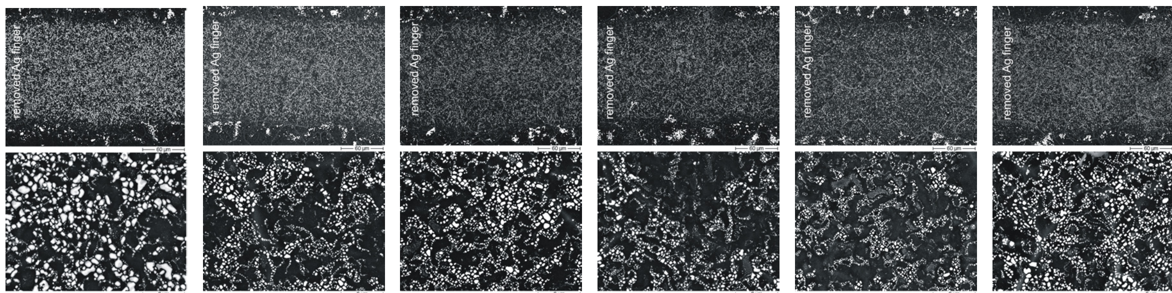

(a) emitter 2: pre-dep, 835°C. (b) emitter 2: drive-in, 835°C (c) emitter 2: drive-in, 860°C (d) emitter 3: pre-dep., 835°C (e) emitter 3: drive-in, 835°C (f) emitter 3: drive-in, 860°C

Figure 5.16.: Dependency of crystal growth on the peak firing temperature and the P surface concentration. The top view on the silicon surface after removal of the silver finger is shown.

In Figure 5.17 the silver coverage is plotted as a function of emitter and temperature. The values given are only approximate but clearly show the tendency that crystal growth is more efficient the higher the temperature is. Although the peak temperature in this experiment exceeds the Ag-Si eutectic of 840°C, it is likely that due to kinetic reasons the eutectic reaction between silver and silicon is not dominant, as the experiments in the previous chapter showed (see chapter 5.4.1).

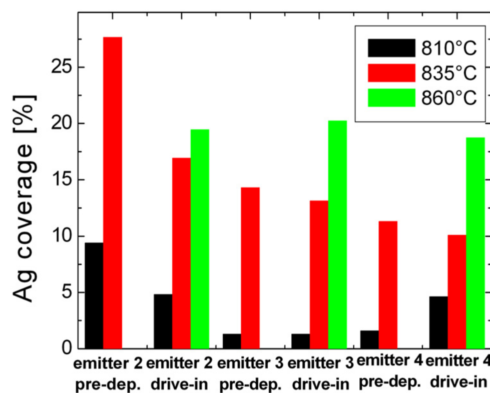

Figure 5.17.: Approximate silver coverage of silicon surface beneath the thick film paste

5.4.5. Influence of the surface texture

Recently it was reported that the surface texture influences the contact resistance on emitters with high sheet resistances [104]. As industrial solar cells are often textured, this hypothesis was investigated on a microscopic level[6]. Two experiments were performed. In the first experiment

[6] Assuming the same finger width, the (geometrical) contact area is enlarged in case of textured surfaces compared to plain surfaces. If the transfer length (see Schroder [59] for details) is $L_T > 1/2W_f$, with the finger width W_f, then the electrical contact area is enlarged, leading to a slightly lower contact resistivity.

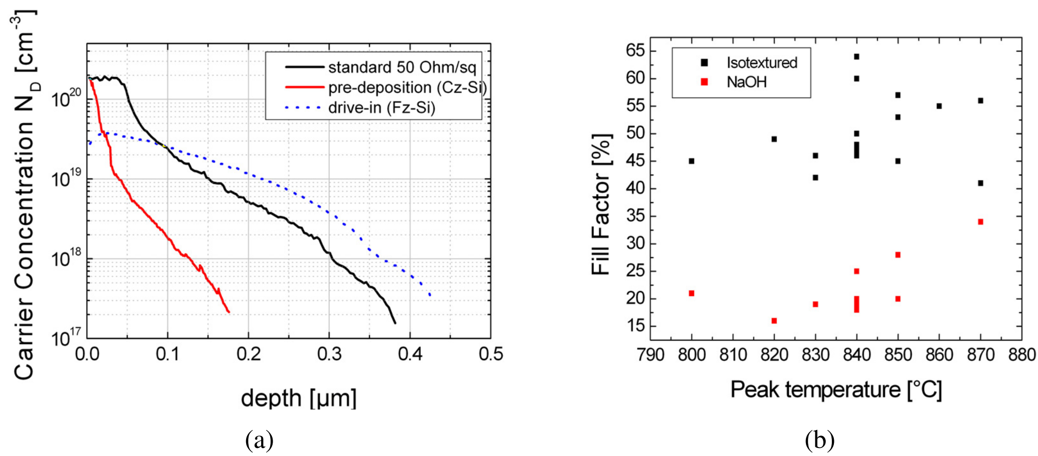

Figure 5.18.: (a) ECV profiles of the pre-deposition diffusion ($R_{sheet} = 110 \pm 11\ \Omega/\mathrm{sq}$) and the drive-in step ($R_{sheet} = 102 \pm 11\ \Omega/\mathrm{sq}$). (b) Fill factor versus temperature.

the influence of an isotextured surface on the solar cell efficiency of mc industrial solar cells with a lowly doped, high efficiency emitter was tested. In the second experiment, the crystal growth on lowly doped, textured surfaces was tested. The influence of the diffusion was eliminated by using phosphorous doped, polished Cz substrates with a bulk doping concentration of $6 \times 10^{19}\ \mathrm{cm}^{-3}$.

Experiment 1: Sample preparation

Neighboured mc silicon substrates (thickness: 325 µm) were successively etched in acidic or alkaline solution to obtain alternating isotextured and quasi not textured surfaces. After a $POCl_3$ pre-deposition step at 820°C the phosphorous glass was etched in diluted HF and a drive-in step at 950°C for 30 min under O_2 flow was performed. The obtained emitter profile was measured with ECV on etch polished, FZ and Cz references and is shown in Figure 5.18(a). After the drive-in step the surface phosphorous concentration dropped to $\approx 4 \times 10^{19}\,\mathrm{cm}^{-3}$. The SiN_x layer was deposited, optimised for the two surfaces. After printing and drying front and back contacts using the standard, commercially available thick film pastes, the cells were fired in a conveyor belt furnace with varying parameters.

Cell results

In Figure 5.18(b) the fill factor in dependence of the cell's peak temperature is shown. Although the absolute level of the fill factor is lower than on 50 Ω/sq emitters ($FF_{50} > 75\%$) it can be stated that for all investigated temperatures the fill factor was highest on the isotextured cells (FF(iso, max) = 64%, FF(NaOH, max) = 34%). A slight tendency for better fill factors towards higher temperatures might also be deduced. The fill factor is not limited by low shunt values. Even on the cells with NaOH etched surfaces shunt values above $1 \times 10^4\,\Omega\mathrm{cm}^2$ were fitted from the dark I-V curves. Therefore, the textured surface seems to be beneficial for contacting lowly doped emitters with a standard silver thick film paste.

Experiment 2: Sample preparation

To test the influence of the surface texture on the crystal growth, polished, <100> oriented n-type wafers with a bulk doping of $N_D = 6 \times 10^{19}\,\mathrm{cm}^{-3}$, measured with ECV, were used to exclude differences in the diffusion profile due to texturing. Half of the wafers were alkaline-etched to obtain a pyramidal surface with <111> oriented surface planes. After printing the front grid using the same Ag paste as in the previous experiments, the samples were fired in the RTP furnace at fill factor optimised parameters varying the peak temperature. SEM and EDX analysis were performed after removal of the fingers in diluted HF (2%) for 6 min.

Crystal growth versus surface texturing

In Figure 5.19 representative SEM pictures are presented. The crystals start to grow on the side surfaces of the pyramids at lower temperatures compared to the <100> oriented surface. This experiment indicates that the Ag crystal growth depends besides temperature and P concentration on the orientation of the silicon[7]. The activation energy for Ag crystals to grow on <111> oriented surfaces is supposed to be lower in comparison to the energy required to start growing on <100> Si surfaces.

5.5. Model of contact formation

Based on the results of this chapter, the following microscopic model for the contact formation of silver thick film pastes to a phosphorous doped silicon emitter during a solar cell firing process is proposed.

T < 550°C
After drying, the organics contained in the silver thick film paste are combusted. During the burn-out process initial sintering of the silver particles might occur. The viscosity of the glass frit decreases.

550°C < T < 700°C
At temperature above 550°C the lead borosilicate glass frit, typically contained in the paste, is fluid enough to wet the silver particles and the silicon nitride layer. Rapid silver particle sintering presumably due to a rearrangement process assisted by the liquid glass frit starts at ≈ 580°C. Silver is dissolved in the glass. However, at temperatures below the melting point of Ag (940°C) this process was found to be slow compared to the fast heating and cooling ramps in the firing process. At T>625°C significant penetration of the glass frit into the silicon nitride layer was observed presumably due to a reaction of the silicon nitride with the metal oxides (mainly lead oxide) contained in the glass (Figure 5.20(b)).

700°C < T < 800°C
As soon as the silicon nitride layer is penetrated, a redox reaction of PbO_{glass} with silicon occurs resulting in the reaction products SiO_2 and Pb (Figure 5.20(c)). SiO_2 is assumed to be dissolved in the silicate glass whereas lead is liquid at these temperatures and does not wet the silicon. In this temperature range silver crystals are assumed to start growing. It is likely that

[7] As mentioned before, the dwell time at T_{peak} also influences the crystal growth. Similar prepared samples were fired at the same temperatures for 30 s. More and bigger crystals were found to have been grown (see Figure 6.6).

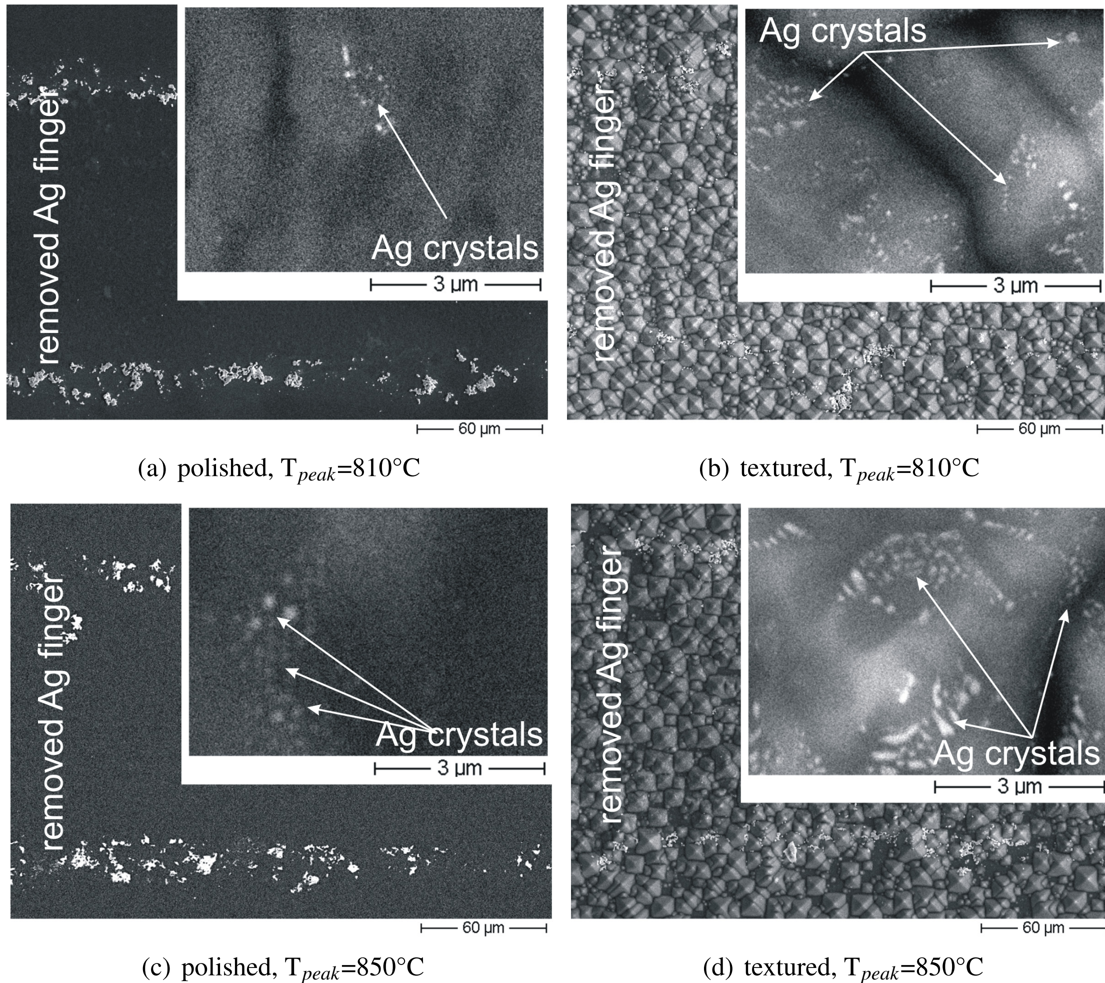

(a) polished, T_{peak}=810°C (b) textured, T_{peak}=810°C

(c) polished, T_{peak}=850°C (d) textured, T_{peak}=850°C

Figure 5.19.: Ag crystal growth on polished <100> Si surfaces and on alkaline textured Si surfaces with $N_{D,surface} = 6 \times 10^{19}\,\mathrm{cm}^{-3}$ at different peak firing temperatures.

two processes occur:

1. Silver growth from silver saturated glass
The silver, dissolved in the glass, is reduced by silicon. The dissolution of silver in glass is a slow process but might be accelerated by the simultaneous occurring redox reaction of the silver ions with silicon.

2. Silver growth via liquid lead phase
Many hints indicate that metallic lead, the reaction product of the glass - silicon interaction, plays the dominant role for the fast transfer of silver to grow into silicon.
As soon as liquid lead comes into contact with the silver grains of the finger, the silver melts to form a liquid silver - lead phase (Figure 5.20(d)). According to the phase diagram this alloy consists of $\approx$72 wt.% Ag at 800°C. The liquid silver is supposed to be highly reactive. It might be dissolved by the surrounding glass and subsequently reduced by the silicon leading to the growth of the inverted crystals on <100> oriented silicon. The dissolving process of silver and glass would be enhanced by the formation of the silver - lead phase.
Another possible mechanism would be the dissolution of [100] silicon planes in the liquid silver similar to the direct reaction between silver and silicon at elevated temperatures. Inverted

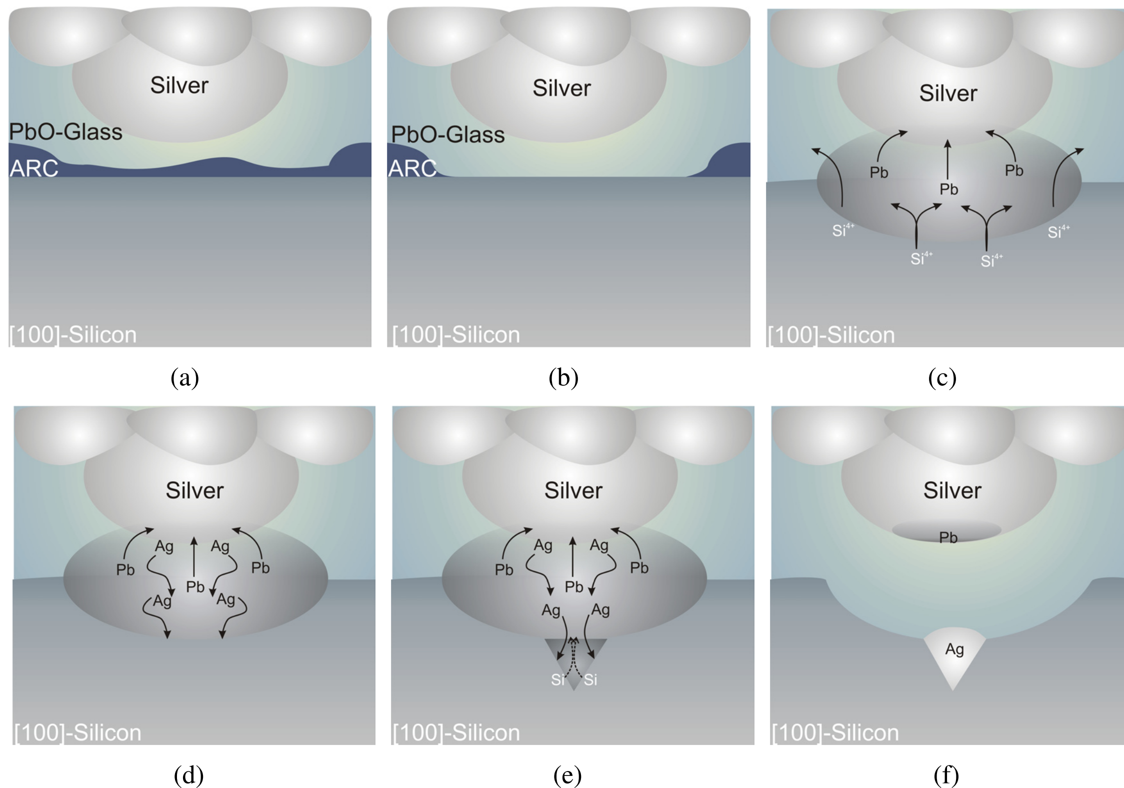

Figure 5.20.: Simplified model of contact formation. (a) Schematic cross section of Ag thick film paste on <100> Si after combustion of organics. (b) Glass etches through SiN_x layer. (c) Redox reaction between Si and glass. Pb is formed. (d) Liquid Pb starts to melt Ag. (e) Ag - Pb melt reacts with Si. Inverted pyramids are formed. (f) On cooling down Ag recrystallises on (111)-Si planes.

pyramids are formed on <100> oriented silicon substrates (Figure 5.20(e)). The task of lead would then be to lower the temperature of the silver - silicon interaction. On cooling down, silver recrystallises on the [111] planes of the inverted pyramid (Figure 5.20(f)). The lead - silver interaction would occur at the silver grains in contact with the glass layer. Therefore it is likely that lead is dissolved in metallic silver present in the system. At 800°C up to 5 wt.% lead can be dissolved according to the phase diagram. The amount of lead which is needed to dissolve enough silver to lead to a 15% coverage of the silicon surface with inverted pyramids in a standard firing process, is quite low[8]. Only 0.8 wt.% Pb relative to the amount of Pb in the glass or 0.03 wt.% Pb relative to the total amount of silver is necessary. The consumed silicon due to the redox reaction between glass and silicon would lead to an etching depth of 1 nm. Even a 50% coverage with larger crystals (diameter: 500 nm) would consume only 0.2 wt.% Pb relative to the total silver weight and cause an etching into silicon of 8 nm. This minor amount of lead is likely to be dissolved by the silver of the finger.
On cooling down, lead precipitates according to the phase diagram. The excessive lead is supposed to be oxidised again and dissolved by the surrounding glass or, most likely, is located at the bottom of the silver grains of the finger above the glass layer (Figure 5.20(f)). Lead or lead oxide precipitates were indeed found at the bottom side of silver fingers (chapter 4.2.2). Lead was also found in or on the silver crystals grown into silicon, when adding only a small

[8]Paste parameters: weight: 1.89×10^{-4} g, area: 120 µm x 1 cm, frit content: 5 wt.%. Silver crystals: shape: inverted pyramids on <100> oriented silicon, diameter: 300 nm, depth: 212 nm, coverage: 15%. Frit: 81 wt.% lead oxide.

amount of silver to a glass frit paste (section 5.4.3). However, adding a larger amount of silver lead precipitates were not found neither in or on top of the silver crystals grown into silicon nor in the separating glass layer (see section 4.2 and [73,76]). Lead containing precipitates were solely found on the bottom side of the silver fingers. The amount of silver seems to influence the precipitation of lead.

Both dissolving - precipitation processes are supposed to occur simultaneously. It is likely that the silver transfer via liquid lead is faster than the transfer via glass. Regardless, which detailed process leads to the growth of silver crystals on [111] silicon planes, it is important to point out that lead is the key component which promotes the silver growth in the fast firing process.

The activation energy for dissolving the [100] silicon planes respectively inverted pyramid formation depends on the excess chemical phosphorous concentration and on the surface texture. It is likely that lattice faults serve as seeds for the above proposed reactions. These lattice faults are induced by the high phosphorous concentration at the surface, exceeding the solubility limit, or by the surface texturing. Additionally, silver growth on [111] silicon planes is energetically favoured compared to the growth on [100] planes due to the better lattice match. In these experiments the paste composition was kept constant to study the influence of the substrate properties. Recent studies showed that the crystal growth is additionally influenced by the silver particle size [74] and the softening point of the glass [75,76].
Overfiring of contacts leads to a more pronounced crystal growth. The proposed reactions occur faster. However, the average glass layer thickness, separating the crystals from the bulk of the finger, increases. The sintering of the silver crystals might result in larger distances between crystals and fingers. Additionally, silver diffusion into silicon is accelerated. This might increase the recombination in the space charge region leading to high J_{02} current and consequently fill factor losses.

Based on the studies above one reason for unsuccessful contacting of moderately doped emitters with standard silver thick film pastes is the insufficient growth of silver crystals at standard firing parameters. Higher temperatures lead to the growth of more and bigger crystals, however, typical overfiring effects occur that lead to high contact resistances and/or to high J_{02} currents. The model explains the growth of silver crystals into silicon and points out the importance of the glass frit for contact formation. According to the results, lead contained as lead oxide in the glass frit plays the most important role in electrical contact formation. Regarding the development of optimised Ag-pastes, the important question to be answered is, whether these silver crystals play the major role in establishing a current path from the silicon into the finger. The electrical properties of the silver thick film contact to silicon will be investigated in the next chapter.

6. Current transport in silver thick film contacts

The investigations in chapter 4.1 on the microstructure of the silver thick film contact showed that silver crystals are in direct contact with the silicon. However, they are separated from the bulk of the silver finger by a glass layer with varying thickness. The glass layer is the transport medium for silver to grow onto silicon. In none of the microstructure investigations, published so far, hints for direct interconnections between silver crystals and the silver finger were found. A typical lead borosilicate glass is typically insulating[1]. Regarding the current transport from the emitter of the solar cell into the silver fingers, two questions arise:

1. What are the electrical properties of the silver - silicon contact?
2. What is the role of the glass layer covering the crystals?

In the following section a short review about existing hypotheses regarding the current transport in a silver thick film contact to silicon is given. After theoretical considerations the electrical properties of the silver crystal - silicon contact are investigated. The influence and properties of the glass layer will be examined subsequently. The electrical properties of silver thick film contact to p-type silicon and its impact on the efficiency of the solar cell will be analysed. Finally, a model of current transport summarises the results.

6.1. Review of existing hypotheses

In literature two main hypotheses regarding current transport in a silver thick film contact to the n-type emitter of silicon solar cells exist.

1. The glass layer at the interface is assumed to be insulating and is therefore responsible for high contact resistances. The current is consequently supposed to be transported via (local) direct interconnections between silver fingers and silicon [81,85,108,109] or quasi-direct interconnections at locations with a glass layer thickness smaller than 1 nm [73,77,78]. Young et al. [85] suppose that optimal fired contacts show direct silver - silicon interconnections that are not distributed locally, but can be found over a large area.
2. Some authors [72,98] assume an increased tunnelling probability in the glass layer due to dissolved silver. The current is supposed to be transported via a multi-step tunnelling process from the emitter to the silver through the glass layer. The increase in conductivity of a lead borosilicate glass due to a tunnelling process from metal precipitate to precipitate has been reported [110–112].

These hypotheses have to match with macroscopic phenomena. As reported in chapter 4, the microstructure investigations showed that the silver crystals locally grow on the emitter. The hypothesis of a large area direct silver - silicon interconnection [85] could not be confirmed. The assumption of sparsely distributed direct silver - silicon interconnections would explain the necessity of a highly doped emitter to achieve low contact resistances [73]. If the current is

[1] Details about electrical conduction in glasses can be found for example in [105,106,71,107].

transported only via few interconnections, the contact resistivity at these contact points must be very low. This would be guaranteed by high emitter doping. Another reason for high emitter doping is given by Fath [93]. The emitter doping concentration typically shows a highly doped plateau of several tens of nm. Behind that plateau the doping concentration sharply decreases with depth. Consequently, excess etching of the paste into the emitter is supposed to lead to a lower doping concentration at the local contact points. Therefore, a highly doped deep plateau is assumed to be necessary to provide low contact resistivities. Nakajima et al. [98] showed that annealing of the fired contact in a hydrogen atmosphere at around 400°C improves the contact resistance. The authors suppose that this macroscopic effect can be explained by the reduction of silver dissolved in the glass layer existing at the silver - silicon contact interface in a hydrogen atmosphere. This would increase the conductivity of the glass layer and in turn decrease the contact resistance. Another macroscopic observation is a specific temperature at which the contact resistivity exhibits a minimum (see chapter 2). Prudenziati et al. [72] use the multi-step tunnelling hypothesis to explain this effect. At low firing temperatures the glass layer is thin, but only a small content of silver is dissolved. The tunnelling probability is too low to provide a low contact resistivity. At high temperatures the increased amount of silver in the glass cannot compensate the higher thickness of the glass layer. The best compromise between glass layer thickness and silver "doping" of the glass is given at optimal firing conditions; the contact resistivity shows its minimum. This short review shows that it is possible to explain several macroscopic properties using different hypotheses which are oppositional in describing the current transport. In the next sections investigations will be presented to bring more light into the discussion.

6.2. Simulation

Before discussing experimental investigations on the current transport, the metal-semiconductor contact basics are briefly reviewed. Simple models are used to simulate the influence of the contact geometry as well as the influence of the emitter doping gradient on the contact resistance.

6.2.1. Metal-Semiconductor contacts

For almost all semiconductor devices understanding and tailoring of the metal - semiconductor contact are most important issues. Therefore, metal - semiconductor contacts have been subject to many investigations. Schottky [113,114] developed a first detailed model. Today, metal - semiconductor contacts are still called "Schottky contacts". A good review of this model and its extensions is given for example by Schroder and Meier [115] and by Rhoderick and Williams [116]. In this work, only the aspects relevant for thick film contacts to silicon are briefly resumed.

For the subsequent calculations the following definition of the contact resistivity ρ_C is used [117].

$$\rho_C = \left(\frac{\partial J}{\partial V}\right)^{-1}_{V\to 0} \tag{6.1}$$

with the current density J and the applied voltage V.
Following the Schottky model (Figure 6.1), the barrier height ϕ_B is given by

$$\phi_B = \phi_M - \chi \tag{6.2}$$

with ϕ_M, metal work function, and χ, the semiconductor electron affinity. ϕ_B is independent of the position of the Fermi level in the bandgap of the semiconductor. A more detailed description

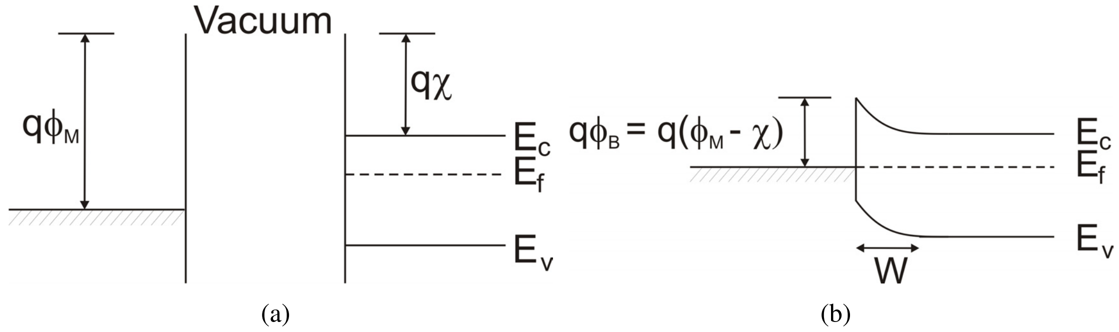

Figure 6.1.: A rectifying metal - semiconductor contact in the Schottky model. (a) Metal and semiconductor separated (b) Metal and semiconductor in intimate contact with W: Depletion layer width

includes barrier lowering due to the electric field in the semiconductor at the contact interface. The image-force lowering $\Delta\phi$ is proportional to the square root of the electric field E, which depends on the doping concentration (equation 6.3) [32,115].

$$\Delta\phi = \left(\frac{q^3 N_D \left(V_{bi} - kT/q\right)}{8\pi^2 K_s^3 \varepsilon_0^3}\right)^{1/4} \tag{6.3}$$

with V_{bi} being build-in voltage and K_s being dielectric constant of silicon. The effective barrier height $\phi_{B,eff}$ is

$$\phi_{B,eff} = \phi_B - \Delta\phi \tag{6.4}$$

To obtain ohmic contacts, the metal work function should be equal or smaller than the semiconductor electron affinity, i. e. ϕ_B would be zero or negative. The majority carries in contact near regions are accumulated or unchanged, respectively, compared to their density in the neutral substrate. Those contacts are frequently named “accumulation” or “neutral contacts” [59]. If ϕ_M is greater, ϕ_B is positive and a rectifying contact is formed. The majority carries in the contact near regions are depleted. However, the predicted linear dependency of the barrier height on the metal work function was not confirmed experimentally (see e.g. [118]). Frequently, the Fermi level at the metal - semiconductor interface is supposed to be pinned by surface states leading to rectifying contacts independent of the metal work function, especially for n-type silicon substrates [115,116,118]. Ohmic contacts have to be fabricated with other means. In the following the current transport in a metal - semiconductor contact is therefore briefly discussed.

Thermionic emission

The current in contacts to lowly doped material ($N_D < 1\times10^{17}\,\mathrm{cm}^{-3}$) is transported via thermionic emission. Only those electrons with an energy greater than the barrier contribute to the current transport. The current - voltage relation is

$$J = A^* T^2 e^{-q\phi_B/kT} \times \left(e^{qV/kT} - 1\right) \tag{6.5}$$

with $A^* = A \times m_R^*/m$, A: Richardson constant, m_R^*: effective mass in effective Richardson constant, V: applied voltage (positive in forward bias). The effective mass used to calculate

the effective Richardson constant depends on the type of dopant in silicon and the crystal orientation. The underlying theory is well described in [32]. For the following calculations $A^* = 112\ \mathrm{Am^{-2}K^{-2}}$ for n-type and $A^* = 32\ \mathrm{Am^{-2}K^{-2}}$ for p-type, given by Andrews and Lepselter [119], are used. Contacts to lowly doped material with the thermionic emission transport mechanism are rectifying. The contact resistivity for thermionic emission is then calculated to

$$\rho_C(TE) = \frac{k}{qA^*T}\exp\frac{\mathrm{q}\left(\phi_\mathrm{B} - \Delta\phi\right)}{\mathrm{kT}} \tag{6.6}$$

Thermionic field emission (TFE)

With increasing doping concentration the depletion layer width of the metal - semiconductor contact decreases. Electrons thermally excited to an energy less than the barrier height are in that case able to tunnel through the thin barrier. The contact resistivity in this doping region can be calculated using the WKB (Wentzel-Kramers-Brillouin) approximation [117]. The functional dependency of ρ_C on the semiconductor doping level N_d is given by equation 6.7 [117].

$$\rho_C(TFE) = \frac{k}{qA^*T} \times C_1 \times \exp\left(\frac{2\sqrt{\mathrm{K_s}\varepsilon_0\mathrm{m^*_{tunnel}}}}{\mathrm{q}\hbar}\frac{\left(\phi_\mathrm{B} - \Delta\phi\right)}{\sqrt{\mathrm{N_D}}\coth\left(\frac{\mathrm{E_{00}}}{\mathrm{kT}}\right)}\right) \tag{6.7}$$

and C_1 is given by

$$C_1 = \frac{kT\cosh\left(\frac{\mathrm{E_{00}}}{\mathrm{kT}}\right)\sqrt{\coth\left(\frac{\mathrm{E_{00}}}{\mathrm{kT}}\right)}}{\sqrt{\pi\left(\phi_B + E_F\right)E_{00}}} \times \exp\left(\frac{\mathrm{E_f}}{\mathrm{E_{00}}\coth\left(\frac{\mathrm{E_{00}}}{\mathrm{kT}}\right)} - \frac{\mathrm{E_f}}{\mathrm{kT}}\right) \tag{6.8}$$

E_{00} is a characteristic energy given by

$$E_{00} = \frac{q\hbar}{2}\sqrt{\frac{N_D}{m^*_{tunnel}K_s\varepsilon_0}} \tag{6.9}$$

Equation 6.7 is valid, if

$$\frac{\cosh^2\left(\mathrm{E_{00}/kT}\right)}{\sinh^3\left(\mathrm{E_{00}/kT}\right)} < 2\left(\phi_B + E_f\right)/(3E_{00}) \tag{6.10}$$

m^*_{tunnel} is the tunnelling effective mass. In general, the tunnelling effective mass is not equal to the effective mass used to calculate the effective Richardson constant. In literature different values are used. Following Ng [120] and Schroder [59], for the following calculations $m^*_{tunnel}/m_e = 0.3$ was used for metal contacts on n-type silicon[2].

Field emission

Very high doping surface concentrations, $N_D \geq 1 \times 10^{20}\,\mathrm{cm^{-3}}$, lead to $kT/E_{00} << 1$ at room temperature. Tunnelling is possible near the bottom of the conduction band because the depletion layer width is now thin enough. Following Yu [117], the dependency of the contact resistivity on the doping concentration including image force lowering writes

[2] The used value for m^*_{tunnel} is close to the density of states effective mass for <111> oriented n-type silicon ($m^*_{DOS}/m_e = 0.33$).

$$\rho_C(FE) = \frac{k}{qA^*T} \times C_2 \times \exp\left(\frac{2\sqrt{\mathrm{K_s}\varepsilon_0\mathrm{m}^*_{\mathrm{tunnel}}}}{\mathrm{q}\hbar}\frac{(\phi_\mathrm{B}-\Delta\phi)}{\sqrt{\mathrm{N_D}}}\right) \tag{6.11}$$

with

$$C_2 = \left[\frac{\pi}{\sin\left(\frac{\pi\mathrm{kTln}\left(\frac{4\phi_\mathrm{B}}{\mathrm{E_F}}\right)}{2\mathrm{E}_{00}}\right)} - \frac{2E_{00}}{kT\ln\left(\frac{4\phi_\mathrm{B}}{\mathrm{E_F}}\right)}\exp\left(\frac{-\mathrm{E_f}\ln\left(\frac{4\phi_\mathrm{B}}{\mathrm{E_F}}\right)}{2\mathrm{E}_{00}}\right)\right]^{-1} \tag{6.12}$$

This equation is valid if

$$1 - \frac{kT}{2E_{00}}\ln\left(\frac{4\phi_\mathrm{B}}{\mathrm{E_F}}\right) > \mathrm{kT}\sqrt{\left(\frac{1}{2\mathrm{E}_{00}\mathrm{E_f}}\right)} \tag{6.13}$$

The ratio kT/E_{00} indicates the relative importance of the thermionic process compared to the tunnelling process. For $KT/E_{00} \gg 1$ thermionic emission, for $KT/E_{00} \ll 1$ field emission is dominant. Thermionic-field emission connects the two regimes ($KT/E_{00} \cong 1$).
In Figure 6.2 the contact resistivity for an silver - silicon contact is plotted versus the doping concentration for the three contact resistivity regimes including image force lowering. For $N_D > 1 \times 10^{17}\,\mathrm{cm}^{-3}$ thermionic-field emission is dominant, for $N_D > 8 \times 10^{19}\,\mathrm{cm}^{-3}$ the current transport mechanism is field emission. The calculated values slightly differ from the calculations presented in [115]. The difference mainly occurs due to the different effective mass used for the calculations. In [115] $m^*_{tunnel}/m = 1$ was used. In this work the more actual ratio $m^*_{tunnel}/m = 0.3$ given by Ng and Liu [120] is used.

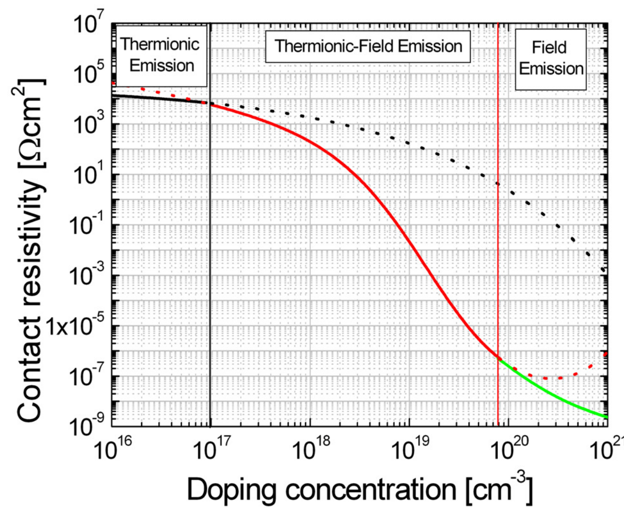

Figure 6.2.: Contact resistivity versus doping concentration for the three transport mechanism. Parameters: n-type <111> oriented silicon, $\phi_B = 0.78$ eV [32], $m^*_{tunnel}/m_e = 0.3$ [59], $A^* = 112\ \mathrm{Am^{-2}K^{-2}}$ [119], $T = 300$ K, image force lowering

6.2.2. Geometrical effects on contact resistivity

In an <100> oriented silicon substrate silver crystals typically grow as inverted pyramids. The crystal is therefore in contact with the [111] planes of the n-type silicon emitter. To account for the geometry, simple calculations[3] on the contact resistivity of one single inverted pyramid were performed. Two aspects are important:

1. The doping concentration of a typical industrial emitter is decreasing with increasing depth (see chapter 2.2.2). As the crystals penetrate up to 100-400 nm deep into the emitter, the impact of the decreasing doping profile on the contact resistivity has to be considered.
2. High electric fields at the tip of the pyramids can lead to barrier lowering [121,122]. The impact of this effect on the contact resistivity is also estimated (section 6.7).

In a first step three typical doping profiles used in solar cell devices[4] were applied to calculate the contact resistivity varying with depth for planar contacts. It is assumed that the doping concentration is constant in planes perpendicular to the doping gradient[5]. In Figure 6.3 the calculated contact resistivities of the three emitters are plotted using equation 6.7 and 6.11. In a standard 50 Ω/sq emitter field emission dominates in the highly doped plateau. In case of a shallow 110 Ω/sq emitter without drive-in step the highly doped region is small leading to a thermionic-field emission dominated current transport. In case of a drive-in emitter with 100 Ω/sq with a moderate phosphorous surface concentration the current is solely transported due to thermionic-field emission.

For the following considerations silver crystals grown on the [111] planes of a perfect inverted pyramid in a <100> oriented silicon substrate without defects are assumed. The silver pyramid with side length a can then be divided into arbitrary small area elements ΔA (Figure 6.4). For each element the average contact resistivity is calculated with the depth dependent doping concentration as the parameter. The total contact resistance of the crystal is then assumed to be the parallel connection of the individual contact resistivities divided by the area element. To compare calculated and measured experimental contact resistivity values, it is useful to define a specific resistivity of a single crystal by relating the total contact resistance to the base area of the crystal.

$$\rho_{t,\text{singlecrystal}} = R_{C,\text{singlecrystal}} \times a^2 = a^2 \times \left(\frac{1}{\sum \rho_{C,\Delta A}/\Delta A} \right)^{-1} \tag{6.14}$$

Then, the theoretically expected macroscopic contact resistivity of an ideal silver contact (all silver crystals are in direct contact with silver contact) can be calculated by dividing the single crystal resistivity $\rho_{t,\text{singlecrystal}}$ by the coverage fraction of crystals below a silver finger. For typical side lengths of silver pyramids on a 50 Ω/sq emitter (for the doping profile see Figure 6.3(a)) the results are summarised in Table 6.1.

The differences for varying crystal sizes are very small. The reason is that the contact resistivity in the highly doped region is extremely low. Because of the pyramidal shape, the area fraction in the surface near emitter regions is the highest. With a total depth of around 200 nm, 50% of the 300 nm crystal area is located in the first 60 nm, thus in the highly doped plateau region. The bigger the crystal, the smaller the fraction of the area located in the surface near region,

[3] Throughout the calculations Boltzmann-statistics were applied. Band bending effects were not considered.

[4] The electrical active carrier concentration was measured with ECV. In case of the 100 Ω/sq drive-in emitter, the depletion at the surface might result from phosphorous out-diffusion during the drive-in step.

[5] The depletion layer width is estimated to be between 10 nm ($N_d = 5 \times 10^{20}$ cm^{-3}) and 100 nm ($N_d = 6 \times 10^{18}$ cm^{-3}). In this calculation the effects of the doping gradient within the depletion layer for planar contacts are not considered.

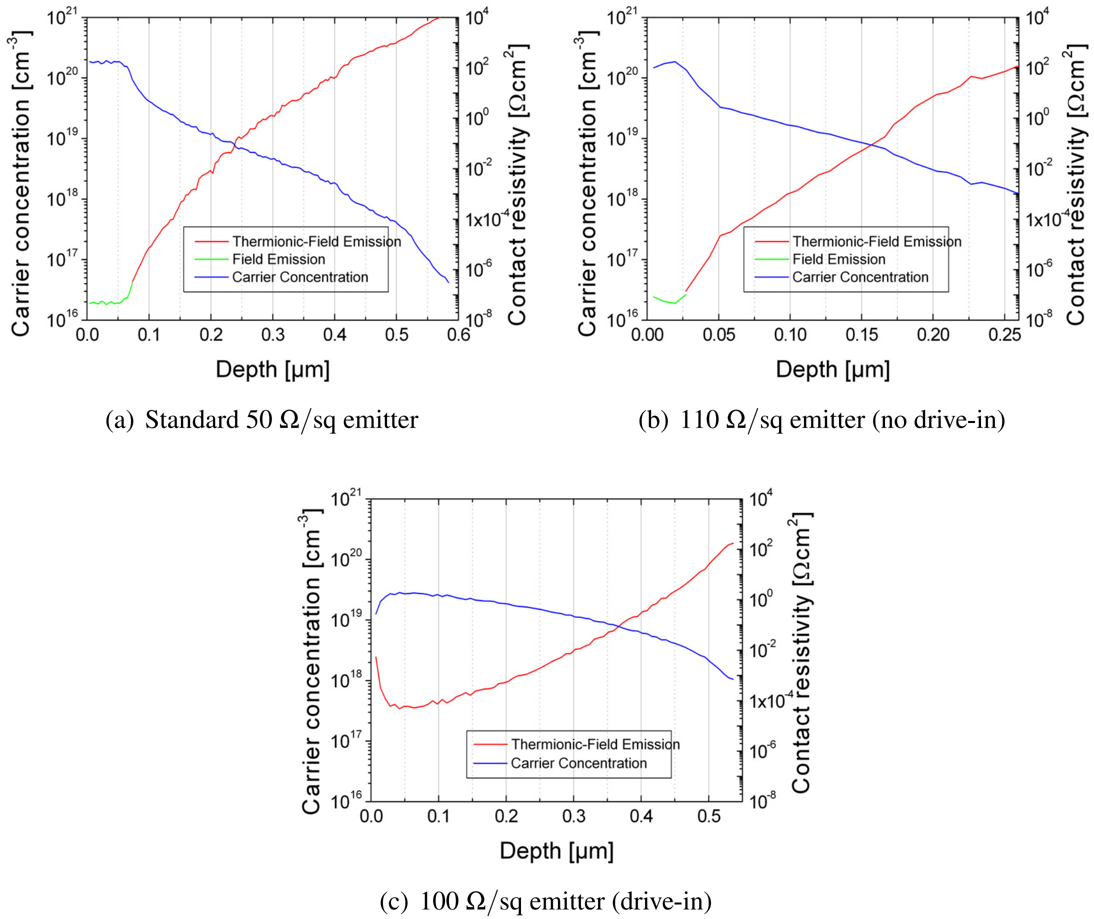

(a) Standard 50 Ω/sq emitter (b) 110 Ω/sq emitter (no drive-in)

(c) 100 Ω/sq emitter (drive-in)

Figure 6.3.: Calculated contact resistivity in dependence of the doping profile for three differently diffused emitters. The profiles were measured with ECV.

consequently the contact resistivity increases slowly. In comparison with plane contacts of silver crystals to <111> oriented silicon substrates, the contact resistivity, which is related to the base area and calculated using equation 6.14, is somewhat larger due to the larger contact area in the case of silver contacts to <100> oriented silicon ($\rho_{C,(\mathrm{Ag\ to\ <111>-Si})} = 4.64 \times 10^{-5}\mathrm{m\Omega cm}^2$, $N_d = 1.85 \times 10^{20}\,\mathrm{cm}^{-3}$). In these calculations it was not considered that the glass frit etches into the silicon prior to silver - silicon contact formation. The influence of the glass frit can be estimated by starting the calculation at an assumed etching depth. In Figure 6.5 the contact resistivity of a silver pyramid (side length 300 nm) to the 50 Ω/sq emitter in dependence of the

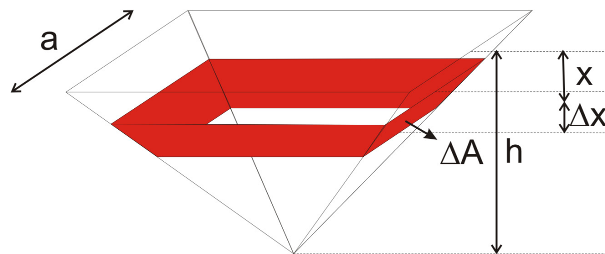

Figure 6.4.: Schematic drawing of an inverted pyramid, grown into silicon. To calculate the doping profile dependent contact resistivity, the pyramid is divided in arbitrary small area elements ΔA.

Side length a [nm]	Depth h [nm]	ρ_C(single crystal) [mΩ cm^2]	ρ_C(10% coverage) [mΩ cm^2]	ρ_C(50% coverage) [mΩ cm^2]
100	71	2.68×10^{-5}	2.68×10^{-4}	5.35×10^{-5}
300	212	2.68×10^{-5}	2.68×10^{-4}	5.35×10^{-5}
500	354	2.79×10^{-5}	2.79×10^{-4}	5.58×10^{-5}

Table 6.1.: Calculated contact resistivities for pyramidal shaped silver contacts to phosphorous doped silicon.

etching depth is shown. Significant increase of the contact resistivity occurs when the highly doped plateau is etched away as expected from the calculations above.

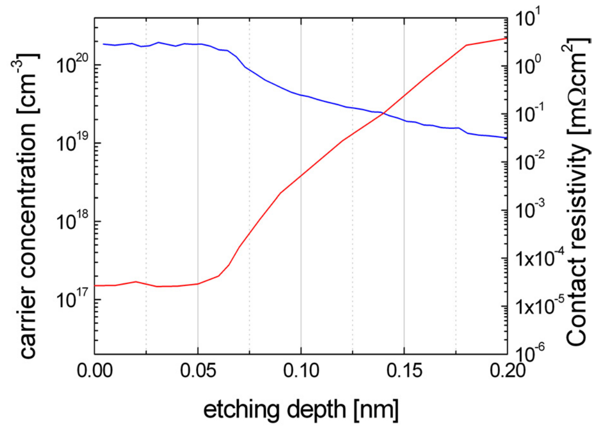

Figure 6.5.: Contact resistivity of a single inverted pyramid (side length: 300 nm) on an industrial 50 Ω/sq emitter in dependence of the etching depth.

In a silver thick film paste with 5 wt.% glass frit content (density: 5 g/cm^3, PbO content: 81 wt.%) the maximal etching depth would be 170 nm, assuming that the total PbO content in the glass reacts with silicon (equation 5.1). The glass layer thickness at the interface would be 1570 nm. However, the measured maximal glass layer thickness in an optimal fired contact is around 500 nm (see chapter 4.1). With this glass layer, a maximal etching depth of 60 nm is likely.
The calculations above (Figure 6.5) show that the glass frit etching in an optimal fired silver thick film contact to a standard 50 Ω/sq emitter does not influence the contact resistivity remarkably. Consequently, the doping concentration in the surface near region (<60 nm) is determining the contact resistivity of ideal silver-silicon contacts to n-type emitters regardless of the contact geometry.

The calculated contact resistivity is, however, four orders of magnitude lower than the measured contact resistivities on industrial solar cell with 50 Ω/sq emitter. Three reasons can be assumed:

1. The contact resistivity of the silver crystals to silicon, grown below a thick film paste, is not adequately described with the used model. However, varying effective tunnelling masses and effective Richardson constant masses lead only to changes in one order of magnitude in the calculated ρ_C. To explain the measured resistivities, barrier heights greater than 2 eV are

necessary, which cannot be explained by interface states or other band bending phenomena.
2. Assuming a 20% coverage of silver crystals with a side length of 300 nm, only 0.013% of the silver crystals need to be directly interconnected with the finger silver to explain the experimental values [73]. The resistance from crystal into finger was neglected as well as glass frit etching and current crowding effects. The number of direct interconnections would be the limiting factor for the contact resistivity.
3. Assuming that the glass layer covers the silver crystals completely, the resistance induced by the tunnelling process through the glass layer would determine the contact resistivity. In case of optimal fired contacts, the average specific resistivity of the glass layer would be in the range of 1 mΩcm^2 to 10 mΩcm^2. The average glass layer resistivity respectively the tunnelling process through the glass would limit the macroscopic ρ_C.

In the next sections experiments are performed to study the nature of the current transport in a silver thick film contact.

6.3. Electrical properties of silver - silicon contact

The study of the current transport mechanism in a silver thick film contact requires detailed knowledge about the electrical properties of the silver crystals - emitter contact. The first question to answer is, whether the silver crystals grown onto the silicon play the major role for the current transport. Ballif et al. [73] measured the contact resistivity by scanning the cross-section of a silver thick film contact on silicon with a conductive AFM. The potential drop between silicon and single silver crystals was measured. With this approach contact resistivities in the range of 2×10^{-7} Ωcm^2 on a 35 $\Omega/$sq emitter were determined.
In this study a different approach was chosen. To account for the statistical nature of the crystal growth process, the contact resistivity of silver crystals grown below a 1 cm long and $\approx$130 µm wide finger was determined.

6.3.1. Sample preparation

Following the calculations above, the expected contact resistance even on moderately doped emitters with a surface phosphorous concentration of $N_{D,\ surface} = 5 \times 10^{19}\,\text{cm}^{-3}$ is in the order of 10^{-4} Ω for a silver finger (width: 130 µm, length: 1 cm) directly connected to 300 nm crystals with a coverage fraction of 20 %. To measure this contact resistance with the transfer length method (TLM), it is necessary to reduce the contribution of the emitter to the measured total resistance to the same order of magnitude. This can be done by reducing the sheet resistance, the finger spacing and/or by increasing the stripe width (i. e. the finger length used in the measurement). Emitter sheet resistances lower than 5 $\Omega/$sq are not easily obtained with $POCl_3$ diffusion due to very long diffusion times especially by demanding a moderate surface phosphorous concentration. The finger spacing for thick film pastes is limited to $\approx$0.5 mm. Increasing the stripe width can lead to lateral resistance losses in the finger, which would lead to uncertainties in the contact resistivity determination. Even for extreme parameters ($R_{sheet} = 5$ $\Omega/$sq., finger spacing $d = 0.5$ mm, stripe width $W = 50$ mm) the minimal contribution to the total resistance would be 50 mΩ. The calculated contribution of the contact resistance would be ≈ 0.1 mΩ, assuming a moderately doped emitter with $N_{D,\ surface} = 5 \times 10^{19}\,\text{cm}^{-3}$ and a crystal coverage of 10%. Small deviations in the sheet resistance between the fingers, in the contact formation, etc. make it difficult to obtain a measurement accuracy, high enough to guarantee reliable values[6].

[6]For limitations of the TLM measurement method for screen-printed contacts see also e.g. [8].

To overcome these limitations, homogeneously phosphorous doped, polished, <100> oriented n-type silicon samples with a thickness of 380 μm were used. Both, ECV and specific resistance measurements accomplished by subsequent simulation with PC1D [55] resulted in a bulk concentration of $N_D = 6 \times 10^{19}$ cm^{-3}. The sheet resistance measured with a four-point probe setup was determined to be $R_{sheet} = (0.034 \pm 0.009)\Omega/\text{sq.}$. This low sheet resistance guarantees an accurate measurement of the expected contact resistance.
The test samples were prepared in a similar way as described in chapter 5.4.5. After printing the front grid (finger width after firing: 130 μm, finger spacing: 2.64 mm), using the same Ag paste as in the previous experiments, the samples were fired in the RTP furnace. Starting from fill factor optimised parameters, two peak temperatures were chosen, $T_1 = 770°\text{C}$ and $T_2 = 850°\text{C}$. The dwell time was in both cases 30 s. After firing, two 1 cm wide stripes were cut out of the samples and the contact resistance was measured with the TLM setup. To account for inhomogenous contact formation that might occur in case of thick film contacts, up to 30 fingers on each stripe (i.e. 60 fingers per sample) were included in the measurement. The silver fingers were then removed in diluted HF (2%) for 2-5 min. Only the silver crystals grown into the silicon remained, which was confirmed by SEM and EDX measurements. After determining the number and size of the crystals, using the method described in chapter 4.2.1, liquid conductive silver was deposited on the silver crystals. A drying step was performed for 1 min at 50°C and the contact resistance was measured using the TLM measurement setup. The electrical contact width was assumed to be the same as the original finger width after firing, although the deposited conductive silver fingers were larger. Therefore, the selectivity of this contacting method was tested by applying liquid conductive Ag on the bare surface of the substrates.

6.3.2. Results and discussion

Crystal growth

In Figure 6.6 two representative SEM pictures of the silicon surface are shown after removal of the silver fingers. In case of sample 1, fired at 770°C, only a few and very small silver crystals were found to have been grown into the silicon. The edges of the fingers are, however, covered by a large number of crystals (see chapter 4.2). The surface of sample 2, fired at 850°C, is covered by large crystals. As the conductive silver finger also contacts the edge crystals, the silver crystal coverage fraction, determined at six independent positions for each sample, has to be analysed carefully. The coverage fraction for sample 2 is $(23.5 \pm 2.2)\%$, independent of in - or excluding the edge crystals. In case of sample 1, the role of the edge crystals is more important. The crystal coverage fraction in the middle of the finger is only $(0.9 \pm 0.3)\%$. Including the silver crystals at the finger edges, the coverage fraction was determined to be $(2.7 \pm 0.9)\%$. Assuming that only the edge crystals would contribute to the current transport, the coverage fraction of the edge crystals alone was determined to be $(6.7 \pm 0.9)\%$.

Contact resistance

After firing, the contact resistances of the samples were much higher than the emitter contribution to the total resistance. Independent of the finger distance an average resistance of (123 ± 24) Ω was measured on sample 1. As the maximal emitter contribution (measured from finger 1 to finger 5) is only 0.036 Ω. Therefore the measured resistance can be approximated to be twice the contact resistance R_C[7]. On sample 2 a total resistance of (48 ± 17) Ω was mea-

[7]The contact resistance is calculated by dividing the contact resistivity by an effective contact area [59].

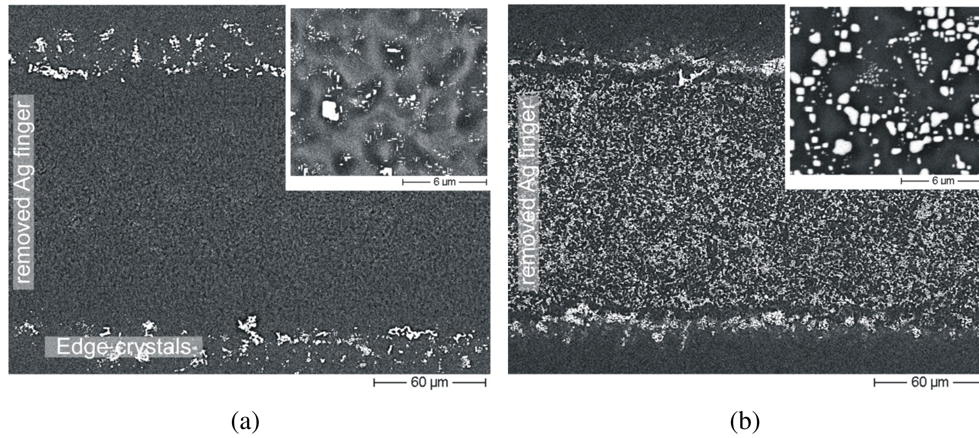

(a) (b)

Figure 6.6.: Top view on silicon surface after removal of silver paste. (a) Sample 1, $T_{peak} = 770°$C. Only very small and few crystals have been grown in the middle of the finger. The edges are surrounded by larger crystals. (b) Sample 2, $T_{peak} = 850°$C. Many large crystals have been grown.

sured. After depositing liquid conductive silver on the silver crystals, the resistances dropped drastically. In both cases the contact resistance was in the order of magnitude of the sheet resistance so that the TLM model was applied to extract the contact resistivity. On sample 1 $\rho_C = (0.094 \pm 0.002)$ mΩcm^{-2} and on sample 2 $\rho_C = (0.047 \pm 0.018)$ mΩcm^{-2} was measured. As the conductive silver contacts the bare silicon areas between the crystals, the selectivity of this method was tested by directly applying the silver on the substrate at locations without any crystals. The total resistance was measured to be (51 ± 23) Ω independent of the finger distance. This is three orders of magnitude higher than the total resistance measured when contacting areas with the silver crystals present. The selectivity of this method was confirmed.
The measured contact resistivities on sample 1 and 2 differ by a factor of 2 to 3. Comparing the silver crystal coverage fractions determined in middle of the samples, sample 1 shows a 26 times smaller coverage than sample 2. Assuming the current to be solely transported via the edge crystals in case of sample 1, the coverage fractions differ by a factor of 3 to 4, which is closer to the difference in the electrical measurement.

Comparison with contact resistivity model

The experimental results are compared with the calculations presented in section 6.2.2. It is assumed that no significant resistance is induced by contacting with conductive silver. As the substrate is homogeneously doped, the specific contact resistivity is independent of the crystal size. Dividing the calculated resistivity for a single crystal by the crystal coverage fraction gives the expected theoretical value. With $m^*_{tunnel}/m_e = 0.3$, $A^* = 112$ Am^{-2}K^{-2} and $\phi_B = 0.78$ eV the calculated contact resistivity does not fit to all measured values. Assuming the current to be solely transported via the crystals in the middle of the finger of sample 1 (Ag coverage: 0.9%), the calculated ρ_C matches the measured one. However, the calculated contact resistivity for sample 2 underestimates the measured one by a factor of 10 (Table 6.2). Assuming the current to be solely transported via the edge crystals of sample 1 (Ag coverage: 6.7%), the parameters in the contact resistivity model have to be adapted to match the measured contact resistivities. The thermionic-emission mechanism is most sensitive for changes in the tunnelling effective mass, m^*_{tunnel} (equation 6.7). Increasing it only slightly to $m^*_{tunnel}/m_e = 0.5$ results in $\rho_C(6.7\%) = 0.089$ mΩcm^2 and $\rho_C(23.5\%) = 0.025$ mΩcm^2, which is closer to the experimental values (Table 6.2). Due to the uncertainties in the measurement and unconsidered or

uncertain parameters (interface states, tunnelling effective mass, layer on the surface of silver crystals) that might influence the silver - silicon contact, final conclusions regarding the theoretical contact resistivity model cannot be drawn from this experiment. Further experiments have to clarify if the parameters determining the current transport mechanism change with increasing firing temperature or if the edge crystals regarding this experimental setup are the main contributors to the current transport. In the latter case, the contact resistivity would be determined by additional factors, either by an additional resistance induced by the contacting method or by slightly changed parameters in the contact resistivity model, e.g. the tunnelling effective mass.

Sample	$\rho_{c,\ measured}$	$\rho_{c,\ calc}$ ($m^*_{tunnel}/m=0.3$)			$\rho_{c,\ calc}$ ($m^*_{tunnel}/m=0.5$)		
		0.9%	6.7%	23.5%	0.9%	6.7%	23.5%
1	0.094 ± 0.002	***0.086***	0.012		0.636	***0.085***	
2	0.047 ± 0.018			0.003			***0.024***

Table 6.2.: Comparison of calculated and measured contact resistivities (in mΩcm^2). Best matches are given in italic.

Summary

This experiment leads to four important conclusions:

1. The silver crystals, grown into the silicon, are indispensable for the current transport from the emitter into the silver finger.
2. The reason for the high macroscopic contact resistivity is the separating glass layer between silver crystals and silver finger. It prevents the formation of a large number of (quasi-) direct interconnections and the resistivity of this layer is orders of magnitude higher than the crystal - emitter contact.
3. It is in principal possible to contact moderately doped phosphorous emitters with silver thick film pastes, assuming a suitable emitter design and good conductivity between silver crystals and silver finger.
4. The silver coverage is of influence on the contact resistivity. The silver crystals at the finger edges, occurring due to paste bleed out and shrinkage of the finger during firing, seem to be in electrical contact with the silicon. In silver thick film contacts the contribution to the total contact resistance is supposed to be minor. However, in the experiment performed the effect of the edge crystals led to small the differences in the contact resistivity due to the silver crystal growth.

6.4. Kinetics of electrical contact formation

To gain insight in the temperature and time dependence of the electrical contact formation, a new contact resistance measurement setup was developed. The resistance between two thick film fingers on phosphorous doped silicon is simultaneously measured with the temperature, using the same setup as for the in-situ line resistance measurement (see chapter 3.2.1).

6.4.1. Sample preparation

A commercial Ag thick film paste was printed on polished n-type silicon 5x5 cm^2 substrates ($N_D = 6 \times 10^{19}$cm^{-3}, thickness: 380 µm) in a finger pattern. The finger length was defined as 1 cm by a sawing step. Two fingers (distance: 2.5 mm, width: 120 µm) were contacted using

a silver wire (diameter: 25 µm) to allow a four point measurement of the resistance between the fingers. In Figure 6.7 the experimental setup is shown. During firing in the RTP furnace both the sample temperature and the resistance between the two fingers were simultaneously measured every 200 ms (see also chapter 3.3(a)). A constant current with alternating polarity in the range of 1 to 100 mA was applied. The firing profile was varied in peak temperature, peak dwell time and ramp down rate. To confirm the in-situ measurement, R_C was also determined using the TLM measurement setup after firing.

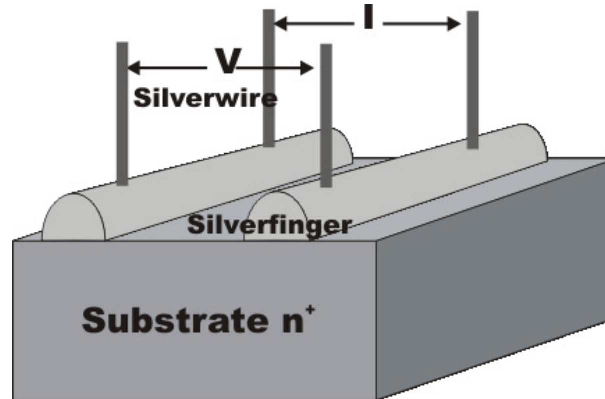

Figure 6.7.: Sample design for the in-situ R_C measurement

Various firing sequences were applied. In Table 6.3 the parameters are summarised. In all cases the same ramp up rate was chosen. Peak temperature, dwell time and cooling rate were varied.

Sample	ramp up [K/s]	T_{peak} [°C]	t_{peak} [s]	ramp down 1 [K/s]	ramp down 2 [K/s]
200	75	810	0	3.3 (sinus-shape)	—
307	75	800	10	25	3.3 (plain)
500	75	800	1	33	3.3 (plain)
600	75	800	40	lamps off	—
700	75	850	40	lamps off	—

Table 6.3.: Firing parameters of in-situ R_C measurement

6.4.2. Results

In Figure 6.8 the total resistance R_{total} between two fingers on n-type samples during the firing process for four samples is presented. The in-situ R_C measurement in case of sample 500 failed because the silver wires disconnected during the firing process. In all other cases the electrical contact formation started during the ramp up period. A sharp decrease in R_{total} was measured at $T \approx 700°C$[8]. At T_{peak}, the resistance reached a constant but noisy level. In case of fast cooling (sample 600 and 700) R_{total} decreased only slightly during the cooling step. However, on both samples that were cooled down very slowly, a sharp decrease in R_{total} was measured during the cooling step. This decrease starts in both cases at about $T \approx 650°C$. Although the ionic glass conductivity increases with increasing temperature, the contribution to the total contact resistance is supposed to be not dominating [71].

[8]It has to be remarked that the resistance measurement is scattered and the temperature increase is fast. Per resistance measurement the increase in T is 15K. Therefore, an accurate determination of the characteristic temperature is difficult.

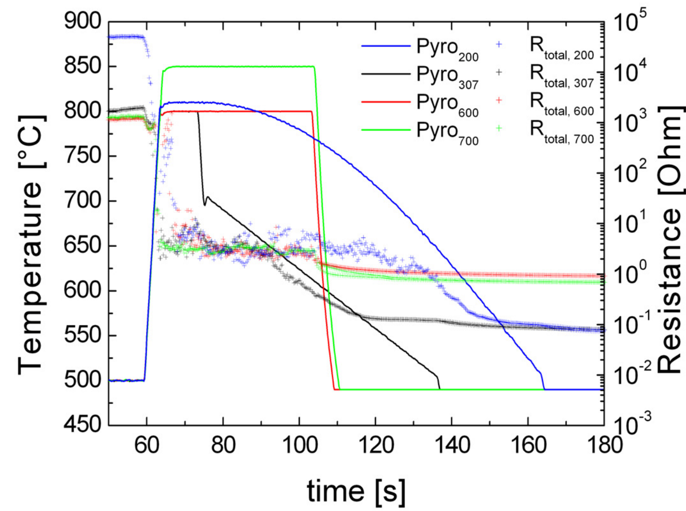

Figure 6.8.: In-situ R_C measurement on n-type samples. The dotted curves represent the R_{total} measurement, the straight line the temperature measurement. The used pyrometer was calibrated in the temperature range between 490°C and 900°C.

The slow decrease of the total resistance when cooling down from 490°C to room temperature can be explained with the temperature dependence of the sheet resistance R_{sheet}. Simulations using PC1D [55] showed that $R_{sheet}(T)$ is dominated by the temperature dependence of the majority carrier mobility in case of a substrate doping of $N_D = 6 \times 10^{19}\text{cm}^{-3}$. The impact on R_{sheet} is, however, minor.

Contact resistivity measurements after firing confirmed the measurement with the in-situ method. The TLM measurement was applied on up to 15 fingers per sample (up to five measurements of the contact resistivity on sets of five fingers). The total resistance between two fingers of sample 307 was between 0.01 and 0.02 Ω. Taking into account a sheet resistance of the n-type substrate of 0.034 Ω/sq , a contact resistivity $\rho_C = 0.015 \pm 0.002$ mΩcm^2 is calculated using the transfer length method. In contrast, on sample 600 the total resistance varied between 0.1 and 1 Ω independent of the finger distance, which is 10 to 100 times the maximal emitter contribution. The contact resistivity was therefore not determinable accurately. In case of sample 700 the resistance was even more scattered from finger to finger. Resistances in the range of 0.3 to 70 Ω were measured. The resistances measured between two fingers on sample 200 varied between 0.006 and 0.05 Ω. Consequently, the contact resistivity could be calculated, but shows a large error ($\rho_C = 0.02..0.24$mΩcm^2). Although the in-situ resistance measurement failed for sample 500, the contact resistivity was measured after firing. Again, the resistance between some fingers is higher (0.04 to 4 Ω) indicating a non-homogeneous contact formation process. The contact resistivity determined for low resistance fingers was $\rho_C = 0.24 \pm 0.05$mΩcm^2.

6.4.3. Summary and discussion

The in-situ contact resistance measurements showed that the electrical contact formation to a bare (without an ARC coating) silicon emitter starts around $T \approx 700$°C. It has to be considered that the conductivity of a lead borosilicate glass increases with increasing temperature [106]. However, the sharp decrease in R_{total} is more likely to be related to the initial growth of silver crystals (chapter 5.4). The results indicate that slow cooling improves the contact resistance

of a silver thick film paste to a moderately phosphorous doped silicon sample. The reached contact resistivities are in the same order of magnitude as in the case of directly contacting the grown silver crystals with conductive silver (section 6.3). Very slow cooling ramps in a silver thick film firing process seem to lead to an enlarged number of direct silver crystal - silver finger interconnections. It is interesting to note that the number and size of crystals, grown onto the [111] planes of the silicon, are not the only critical parameters to guarantee a low contact resistivity. Below fingers of sample 700 even larger crystals were found than below fingers of sample 307.
The transfer of this result to n^+-p diodes is difficult, because silver diffusion deep into silicon and excessive etching of the glass frit have to be considered. From the results above it is likely that fast cooling can be applied in the high temperature regime. The slow cooling has to set in not until the sample reaches a temperature of $T = 700°C$ (see sample 307 and 500). It has to be tested wether the slow cooling can be applied at even lower temperatures to minimise impurity diffusion and excessive etching. The TLM results of sample 500 indicate that the slow cooling process can be applied to a dwell time of 1 s or lower. However, further tests have to clarify whether the homogeneity of the formed contact is guaranteed.
Based on these results, Grupp et al. [123] studied the influence of a temperature plateau, a temper step, in the cooling cycle of an industrial thick film solar cell process at $T > T_{Al-Si,\ eutectic}$ for different plateau dwell times. They found that the efficiency of over-fired solar cells can be increased by such a temper step due to a reduced series resistance and hence an increased fill factor. The potential of a slow cooling ramp or temper step on the contact resistance of moderately doped emitters has not been investigated yet.
In general, the in-situ R_C measurement proved to be useful to study the kinetics of electrical contact formation. Applying the in-situ Rc measurement method to n^+-p diodes is in principle possible but analysis is extended. At high temperatures the number of carriers in the lowly doped p-base rapidly increases due to thermal generation. Consequently, the n^+-p diode - in this measurement setup the p-base is isolated from the emitter at room temperature - is in forward bias. Therefore, the temperature dependence of the specific resistivity in the base will dominate the measurement. Consequently, the analysis of the in-situ R_C measurement involves simulations of the J-V characteristic of the n^+-p junction at high temperatures.

6.5. Impact of the forming gas anneal on the contact resistance

In previous sections it was shown that the limiting factor for the contact resistance of silver thick film pastes to phosphorous doped silicon is the conductivity of the silver crystal - silver finger interconnection. It was found that direct contacts to silver crystals covering maximal 7% of the contact area would be sufficient to obtain contact resistivities in the order of magnitude of 0.1 $m\Omega cm^2$ on moderately doped emitters (section 6.3). In this section the mechanism behind the beneficial effect of a forming gas anneal on solar cells with thick film metallisation is investigated. Understanding this mechanism in detail is assumed to be one of the keys to achieve a complete picture of the current transport mechanism in silver thick film contacts.
The process window related to the peak firing temperatures in a typical industrial "firing through silicon nitride" process for achieving fill factors above 75% is about 50 K or larger for a $R_{sheet} = 50\ \Omega/sq.$ emitter, using a commercially available silver paste (see section 2.6). This process window narrows with increasing sheet resistance. Lower peak firing temperatures lead to a sharp decrease in fill factor due to a high series resistance because the glass frit contained

in the silver paste has not penetrated the SiN_x layer fully. Higher peak temperatures (or long dwell times) exceeding the process window lead to a decrease in fill factor, too. As shown in section 4 and in accordance with several authors (see e.g. [79]), it seems to be most likely that the thickness of the glass layer, separating the silver crystals and the silver finger, increases with increasing firing temperatures. Additionally, sintering of the silver particles in the finger is enhanced with increasing firing temperature (chapter 3). Both effects lead to a greater distance between the silver crystals that are in direct contact with the emitter and the silver particles in the bulk of the contact finger. The current transport via direct interconnections is therefore unlikely for those contacts. Another possible current path is via tunnelling through the glass layer. The tunnelling probability decreases with increasing tunnelling distance. This could be the reason for higher contact resistances and thus lower fill factors in case of overfired samples. Very high firing temperatures result in additional effects that also lead to a reduction of the fill factor: Impurities (e.g. silver from the tip of the crystals) diffuse towards the junction, increasing the recombination in the space charge region. Schottky-like shunting can occur and the ohmic shunt resistance can be decreased. Applying a forming gas anneal (FGA) typically for 15 min at 400°C in an argon-hydrogen atmosphere leads to an increase in fill factor of overfired cells (see e.g. [98,124,125]). Applying this anneal, the process window can be enlarged towards higher peak firing temperatures. Optimal fired cells with high fill factors after the solar cell process can only be slightly improved by FGA.
To get more insight in the mechanism occurring during the forming gas anneal, the dependency of the beneficial effect on the annealing temperature and time is investigated, accomplished by microstructure analysis and long term stability tests. The section is completed with investigations on the current transport in annealed silver thick film contacts.

6.5.1. The forming gas anneal

Sample preparation

To study the influence of the forming gas anneal (FGA) Cz ($A = 12.5\,\text{cm} \times 12.5\,\text{cm}$, $d = 270$ µm, $\rho = 1\ \Omega\text{cm}$) and FZ etch polished silicon industrial solar cells ($A = 5\,\text{cm} \times 5\,\text{cm}$, $d = 250$ µm, $\rho = 0.5\ \Omega\text{cm}$) were fabricated using the process sequence described in chapter 1.1 with a NaOH saw damage etch in case of the Cz cells and no additional texturisation of the surface. The $POCl_3$ diffusion resulted in a sheet resistance of $R_{sheet} = (51.2 \pm 0.6)\ \Omega/\text{sq}$. Standard commercially available aluminium and silver thick film pastes were screen-printed and dried. Subsequently, the cells were fired in a conveyor belt furnace with three heating zones. The temperature of the third zone was varied. The forming gas anneal was performed in a tube furnace. The tube was evacuated and vented with N_2. Then it was loaded with the samples. After evacuating, the tube was vented again with the desired gas (N_2, O_2, Ar-H(10%)) and a constant gas flow was applied during the process. The annealing time was defined as the time difference between reaching a pressure of 1 bar in the tube with the specific atmosphere and evacuating before unloading. The impact of the forming gas anneal on the diode parameters was determined by J_{sc}-V_{oc}, dark J-V, illuminated J-V analysis and spectral response measurements. The impact on the contact resistance was determined by TLM measurement on stripes that were cut out of representative cells. To account for light induced degradation of the Cz solar cells, these cells were annealed at 200°C for 20 min prior to the J-V measurements before and after FGA.

6.5.2. Influence of forming gas anneal on the diode parameters

In Figure 6.9 the parameters of under- ($T_{peak} = 745°C$), optimal ($T_{peak} = 795°C$) and extremely overfired ($T_{peak} = 885°C$) solar cells after a standard forming gas anneal (atmosphere: Ar-H(10%), temperature (inside tube): 400°C, time: 15 min) are plotted. Two cells per group were analysed. As expected, after the forming gas anneal the fill factor of the overfired solar cells is more than doubled and the difference between the two cells vanish. The fill factors of the under- and optimal fired cells remain constant within the accuracy of measurement. The overfired cells show an increase in J_{sc} probably due to the reduced series resistance. The increase in J_{sc} of the underfired cells is less. The optimal fired cells do not show significant changes. Most of the cells show a little loss in V_{oc} (0.1-0.3% relative) after the forming gas anneal. In total the efficiency is drastically increased in case of the extremely overfired cells. The efficiency of the optimal fired cells is constant within the accuracy of measurement and the efficiency of the underfired cells is increased due to the increase in J_{sc}. Analysing the J-V characteristics

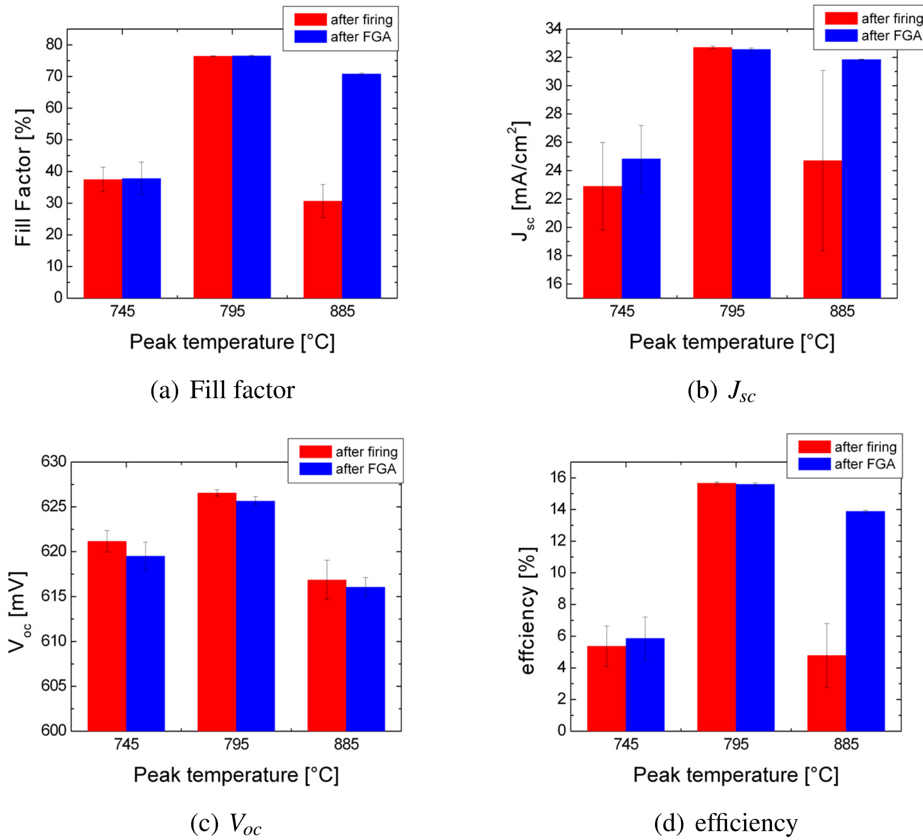

(a) Fill factor

(b) J_{sc}

(c) V_{oc}

(d) efficiency

Figure 6.9.: The solar cell parameters before and after FGA (400°C, 15 min) of under-, optimal and overfired cells

with the simulation program IV-CC [58], revealed that the fill factor increase is attributed to the decrease in series resistance (Table 6.4). In some cases J_{02} was fitted to be increased after the anneal. As all investigated cells show a inhomogenous series resistance distribution prior to the forming gas anneal, extracting J_{02} might be inaccurate. The drop in series resistance is caused by a significantly reduced contact resistance (Figure 6.10). Additionally, the scattering of ρ_C from finger to finger is reduced. The shunt resistance remains constant. Only little differences in J_{01} before and after the anneal are extracted. The difference in J_{01} for the optimal fired cells is negligible. The difference for the overfired cells can be related to the uncertainty in

Temp.-Nr	Fill factor [%]	R_{sh} [Ωcm^2]	R_s [Ωcm^2]	J_{01}[pA/cm^2]	J_{02}[nA/cm^2]
795-1	76.4	3780	0.8	0.88	6.94
795-1 fga	76.6	3710	0.6	0.88	6.26
885-1	26.0	2850	50	1.539	6.06
885-1 fga	70.6	2890	1	1.315	8.52

Table 6.4.: Diode parameters for two cells extracted from the dark J-V and J_{sc}- V_{oc} measurements before and after anneal.

the extraction of J_{01} before the forming gas anneal due to the very high series resistance. The

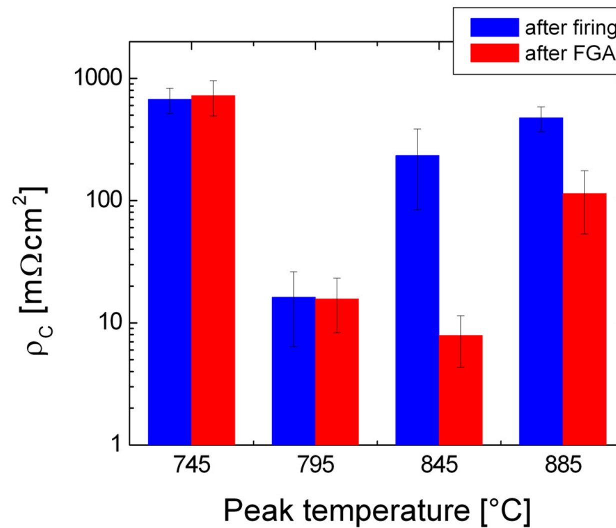

Figure 6.10.: Contact resistivtiy before and after forming gas anneal of differently fired solar cells

influence of the forming gas anneal on the aluminium back surface field was tested by extracting the effective diffusion length from spectral response measurements on FZ industrial solar cells before and after anneal fired at the optimal peak temperature. In Figure 6.11 the IQE of the two cells before and after anneal is plotted. No differences in the long wavelength region are found. L_{eff} was found to be between 490 µm and 520 µm for all cells.

The microstructure was investigated with SEM and EDX. To study the differences in the cross section before and after anneal, cells were cleaved perpendicular to the finger grid. Only one of the two stripes was annealed.
It was found that no changes in the silver crystal growth are visible with the used SEM. No hints for more or bigger crystals were found. Additionally, the glass layer thickness was not found to be decreased. However, the resolution of the SEM does not allow for exact measurements below 50 nm so that microstructural changes in the glass layer (e.g. increased number of metal particles due to a reduction process) could not be observed. Transmission electron microscopy should give more insights in these changes.

6.5.3. Influence of atmosphere

In Figure 6.12(a) ρ_C for two overfired lead free pastes on a typical industrial emitter (see chapter 7) after annealing at 400°C for 25 min in air and subsequently for 15 min at the same

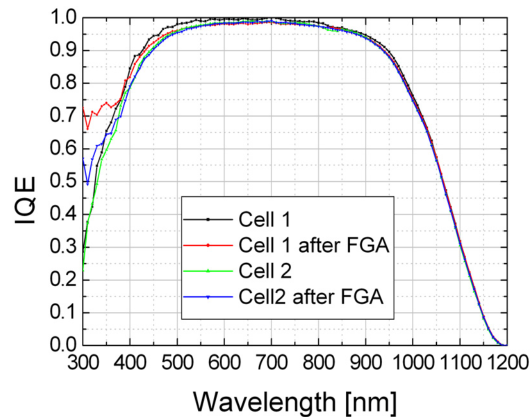

Figure 6.11.: Internal quantum efficiency of two optimal fired FZ industrial solar cells before and after forming gas anneal. The extracted L_{eff} was ≈ 500 µm for all cells.

temperature in Ar-H is shown. Annealing in air atmosphere has a negative effect on the contact resistance and thus on the fill factor of the cell. Subsequent forming gas anneal leads to a sharp decrease in the contact resistivity. The influence of N_2 was tested on overfired solar cells of the previously described experiment. In accordance with Rohatgi et al. [124], it was found that annealing in N_2 for 15 min at 400°C has a negative impact on the fill factor and on the contact resistance (Figure 6.12(b)).

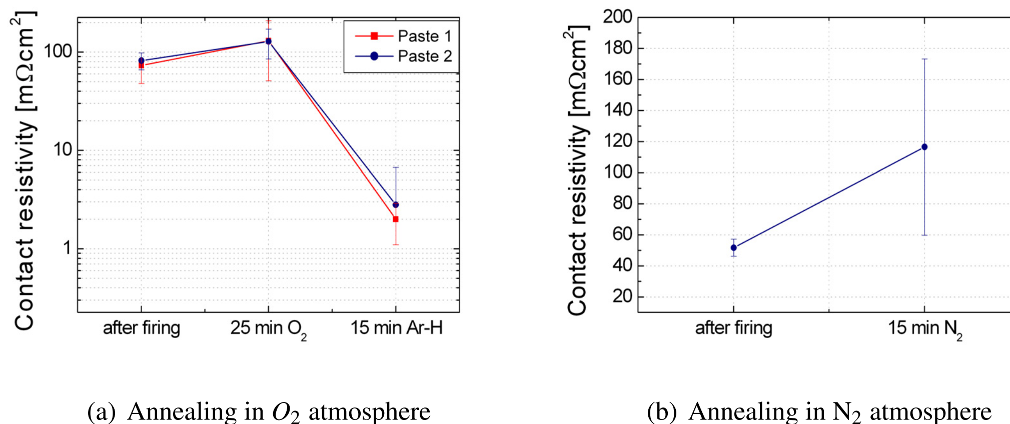

(a) Annealing in O_2 atmosphere (b) Annealing in N_2 atmosphere

Figure 6.12.: Annealing at 400°C in different atmospheres. Only the hydrogen atmosphere leads to a significant decrease of the contact resistivity. Note the different scaling (Log and Lin) for the two graphs.

6.5.4. Irreversibility of effect

It is interesting to note that the beneficial effect of the forming gas anneal seems to be irreversible. A standard forming gas anneal (400°C, 15 min) was applied to industrial solar cells (Cz, alkaline textured) processed using different silver thick film pastes and various firing parameters (a reference paste and two lead free silver pastes, chapter 7). After firing, cells with paste 1 (Pb free) and 2 (Pb free) showed very poor fill factors. A forming gas anneal increased

the fill factors of both cells reaching values comparable to the fill factors of the two reference cells. After an oxygen anneal for 15 min at 400°C the fill factors of all cells remain stable, indicating that the reaction occurring during FGA in an reducing atmosphere cannot be reversed (Figure 6.13).

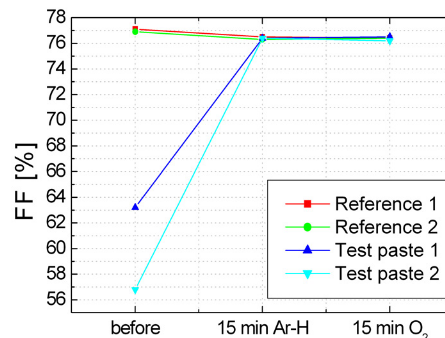

Figure 6.13.: After applying the forming gas anneal in Ar-H atmosphere, the overfired cells with pastes 1 and 2 show increased fill factors. A subsequent O_2 anneal has no effect.

6.5.5. Long term stability

The irreversibility of the positive effect of the forming gas anneal on the fill factor gives a first hint that this effect is long term stable. Regarding a transfer into solar cell industry, the long term stability is one of the critical requirements for new process sequences. Therefore, the stability was tested on one cell for up to now 17 months compared to a reference cell. In Figure 6.14 the evolution of the fill factor and the efficiency of two industrial solar cells is plotted. Both cells were identically processed except for the used silver paste[9] and firing conditions. The forming gas anneal increased the fill factor of the overfired solar cell remarkably. After 17 months both solar cells are stable within the accuracy of measurement. The cells were stored in a box at room temperature in darkness.

6.5.6. Influence of annealing temperature and time

To get more insight in the processes occurring during the forming gas anneal, temperature and dwell time of the anneal was varied. The temperature in the tube furnace was increased from 200°C to 400°C. Two overfired solar cells and two contact resistance stripes of overfired solar cells were used per annealing parameter. In Figure 6.15 a characteristic development of the fill factor after subsequent annealing steps is plotted. After firing at an elevated peak temperature ($T_{peak} = 845°C$), the fill factor of this solar cell was reduced due to an increased contact resistance ($FF_{inital} = 72.5\%$). After two annealing steps at 200°C for in total 30 min and another annealing step at 350°C for 15 min, the fill factor did not change significantly. The annealing step at 375°C for 15 min led to a sharp increase in fill factor. Subsequent annealing at the same temperature for another 15 min did not lead to changes within the accuracy of measurement. In Figure 6.16 the development of the fill factor of a solar cell, fired at 845°C, and the contact resistance, measured with the TLM method on a stripe cut out off a neighbouring cell fired also

[9] A reference paste and a lead free test paste was used.

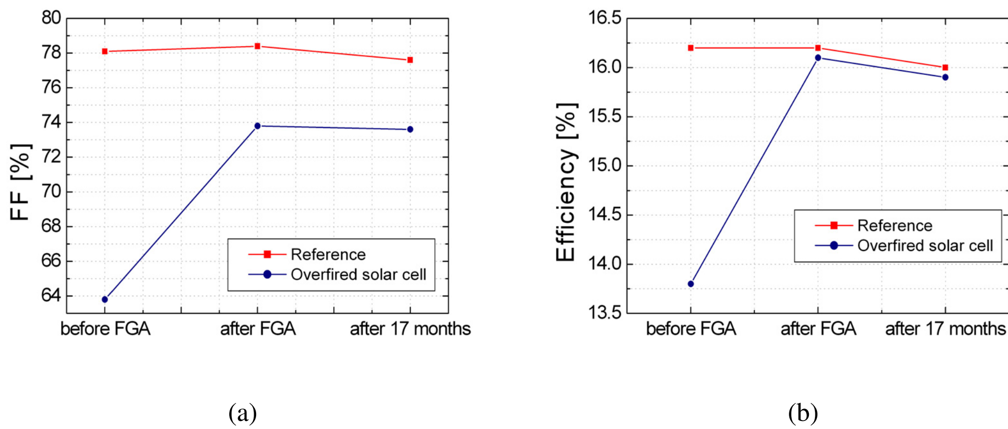

(a) (b)

Figure 6.14.: Long term stability of forming gas anneal effect

at 845°C, is plotted versus subsequent annealing steps. Again, it is shown that the increase in fill factor starts at $T = 375$°C. A subsequent annealing step at 400°C did not lead to further improvements. Analysis of the diode parameters revealed that the fill factor is limited by J_{02} ($J_{02} \approx$ 66 nA/cm^2), extracted from the illuminated J-V characteristics[10]. The contact resistivity was determined at the top, in the middle and at the bottom of the stripe. Due to inhomogenous contact formation, the contact resistivity was lowest in the bottom and highest in the middle regions of the stripe cut out off the solar cell. Annealing at 290°C and 350°C led to a decrease in the contact resistivity especially in the middle region of the stripe. At 375°C a sharp decrease of ρ_C in the middle and a slight decrease in the bottom region was measured. At 400°C ρ_C decreased drastically in all regions in all regions. Applying forming gas annealing steps at 450°C

[10]The analysis of the dark characteristics resulted in $J_{02} = 20$ nA/cm^2. This is a hint that an inhomogeneous series resistance distribution might be one origin of the high J_{02} value extracted from the illuminated characteristics (see chapter 2).

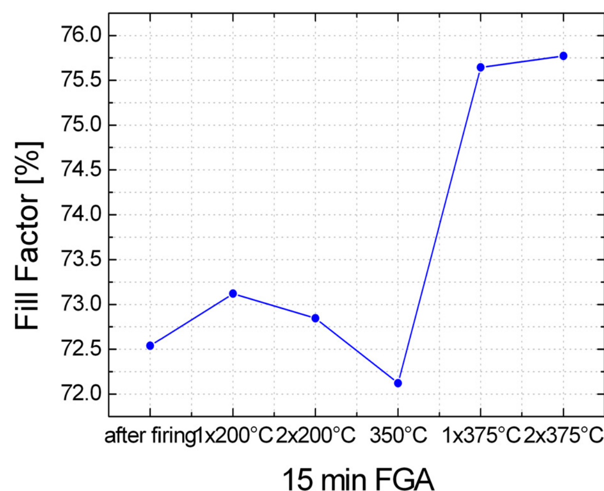

Figure 6.15.: Subsequent forming gas anneal steps at different temperatures. The beneficial effect on the fill factor arises at T = 375°C.

or higher did not lead to improvements in the fill factor.
Varying the dwell time during the forming gas anneal at 400°C showed that the process is time

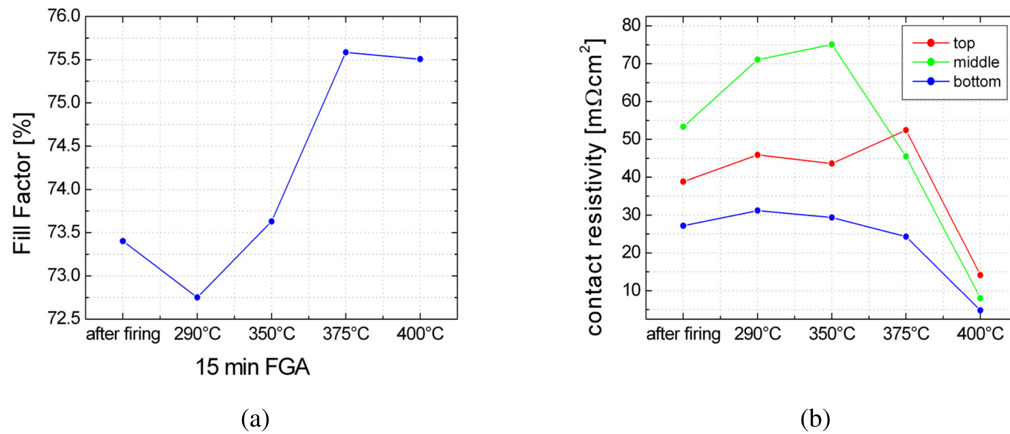

Figure 6.16.: Fill factor and contact resistivity development in subsequent forming gas anneal steps. The fill factor is limited by a high second diode saturation current.

dependent. After 5 min the beneficial effect starts. After 15 min the maximal improvement in the fill factor is reached. Annealing for longer times does not lead to further decrease in contact resistance. Ebong et al. [125] showed that the beneficial effect on the fill factor can be reached in 3 min when using a rapid thermal processing (RTP) furnace. Possible reasons for the reduced annealing time are the high ramp up and ramp down rates.

Summarising these results, it is likely that a chemical reaction occurs during the forming gas anneal. A temperature of $T \approx 375$°C or higher is necessary to start the reaction. Additionally it was found that the reaction is not fast, compared to the contact formation processes in a rapid thermal firing sequence. It has to be pointed out that the forming gas anneal was applied to pastes with different glass frits characterised by different glass transformation temperatures. In all cases the forming gas anneal works best at $T = 400$°C. A reduction of the metal oxides in the glass to metallic precipitates is the most likely reaction occurring during the annealing step. These observations support the hypotheses formulated earlier [87,98,72]. Taking into account the results of the microstructure investigations (chapter 4.2.2), it is also plausible that the lead or lead oxide precipitates, found at the bottom of the silver finger facing towards the glass layer, are, in case of being lead oxide precipitates, reduced to metallic lead as well. Then, the existence of current channels from the silver crystal via the lead precipitate directly into the silver finger would be likely.
The formation of metallic precipitates in lead borosilicate glass during the forming gas anneal was observed earlier. It was also observed that the distributed metal particles after the forming gas anneal lead to an increase in the surface conductivity of glass, especially if the glasses contain, beside lead oxide, bismuth oxide [110–112]. According to these publications, Bismuth is supposed to act as a resonant centre for the resonant tunnelling conduction mechanism. This effect was successfully applied to fabricate channel electron multipliers [126].
In case of a limitation of ρ_C by an increased glass layer thickness due to overfiring, it is therefore likely that the current is transported from the silver crystal in direct interconnection with the silicon to the silver finger via a multi step tunnelling mechanism from precipitate to precipitate. The tunnelling probability through thick glass layers is assumed to be increased by a forming

gas anneal.

6.5.7. Estimation of the average glass layer conductivity after FGA

The investigations performed so far lead to the assumption that the conductivity of the glass layer, the most probable limiting factor in silver thick film contacts, is increased during the forming gas anneal. To estimate this effect, the contact resistivity of a commercially available silver thick film paste to a moderately doped n-type sample is measured before and after a standard forming gas anneal step[11]. The TLM stripe used for this experiment was cut out off the same sample used for the estimation of the contact resistivity of the silver crystals grown into silicon (see section 6.3). The peak temperature of this sample, fired in the RTP furnace was $T_{peak} = 850°C$ and the dwell time 10 s. The silver crystal coverage fraction on the neighbouring stripe was determined to be 23.5%. The sample was annealed in Ar-H(10%) atmosphere at 400°C inner tube temperature for 15 min. The TLM measurements before the annealing step resulted in $R_{total} = 44.34 \pm 5.46\ \Omega$[12] regardless of the finger distance. The maximal sample contribution measured from finger 1 to finger 5 is 0.036 Ω so that the total resistance can be assumed to be $2 \times R_C$. After applying the forming gas anneal step, the total resistance dropped to $R_{total} = 0.75 \pm 0.09\ \Omega$, which is 1.7% of the previously measured value. Again, the sample contribution to R_{total} is negligible. The contact resistance can then be estimated to be $R_{C,FGA} \approx 0.38\ \Omega$. This is factor 100 higher than $R_C = 0.0036 \pm 0.0015$ measured when directly applying conductive silver on the silver crystals grown into silicon (section 6.3). The contact resistance of optimal fired silver thick film pastes to 50 Ω/sq emitters is in the range of $R_C \approx 0.5\ \Omega$ assuming a transfer length of 89 µm and a specific contact resistivity of 4 mΩcm^2. It can be concluded that the forming gas anneal leads to an average decrease of the glass layer resistance to values comparable with the contact resistances measured on optimal fired contacts.

6.6. Contacts to moderately doped emitters

One way to increase the efficiency of a screen-printed industrial solar cell is to lower the emitter doping in particular the surface phosphorous concentration (chapter 2.2.2). In chapter 5.4.4 it was shown that it is possible to grow silver crystals on moderately doped emitters. However, higher peak firing temperatures are necessary when using commercially available silver thick film pastes. In chapter 6.3 it was shown that the contact resistivity to emitters with a surface doping of $N_D = 6 \times 10^{19}\ \text{cm}^{-3}$, obtained when contacting the silver crystals directly, is at least two orders of magnitude lower than the macroscopic contact resistivity of silver thick film contact to highly doped 50 Ω/sq emitters. The requirements for contacting are therefore fulfilled. Assuming a suitable emitter design, which prevents shunting and impurity diffusion effects, the limiting factor to reach suitable contact resistivities on moderately doped emitters is not the contact resistivity of the crystals to the emitter as many authors assumed (see e.g. [73,77,93]). The limiting factor is rather the silver crystal growth and related effects.
Currently, as stated above, it is necessary to use high firing temperatures to grow enough silver crystals that enable the contact to the moderately doped emitter. The current transport from the emitter into the silver finger is then, however, limited by the resistance induced by the thick glass layer between the silver crystals and the silver grains in the finger, typically for "overfired" contacts. If this hypothesis is valid, a forming gas anneal should increase the conductivity of

[11] $N_D = 6 \times 10^{19}\ \text{cm}^{-3}$. Finger width: 130 µm, length: 1 cm.
[12] Average over 80 measurements on 10 different fingers.

the glass layer and thus lead to a decreased contact resistivity. This hypothesis is tested in the following.

6.6.1. Sample preparation

The same solar cells fabricated to test the influence of the surface phosphorous concentration on the crystal growth were used (section 5.4.4). In a first experiment the electrical properties of the emitter - crystal contact were measured to test the potential of the forming gas anneal. The samples were prepared in the same way as described in chapter 6.3. The silver fingers of the TLM test structures were removed in diluted HF. The remaining Ag crystals grown onto the emitter were selectively contacted by conductive silver. A drying step at 50°C for 1 min was performed and the contact resistance was measured using the TLM measurement setup. The contact width was assumed to be same as the original finger width after firing.
After etching off the Ag crystals in NH_3:H_2O_2 (1:1) followed by an HF-dip, the selectivity of this contacting method was tested by applying conductive Ag on the bare "drive-in" emitter 1. SEM analysis revealed that all crystals were removed. The forming gas anneal (400°C, 15 min) was then applied to solar cells with drive-in emitters 2, 3 and 4 with phosphorous surface concentrations of $N_{D,\ surface}(2) \approx 1 \times 10^{20}\,\text{cm}^{-3}$, $N_{D,\ surface}(3) \approx 4 \times 10^{19}\,\text{cm}^{-3}$ and $N_{D,\ surface}(4) \approx 3 \times 10^{19}\,\text{cm}^{-3}$ (see Figure 5.13).

6.6.2. Results and discussion

The results of direct contacts to the silver crystals are summarised in Figure 6.17. The contact resistivity decreases drastically when contacting the Ag crystals directly. The contacts to drive-in emitter 2 and 3 are homogeneous (log scale). As the sheet resistance of drive-in emitter 4 varies, the contact resistivity scatters considerably. Contacting the bare drive-in emitter 1 with conductive Ag resulted in $\rho_C \approx 600$ mΩcm^2, proving the selectivity of this method. To eval-

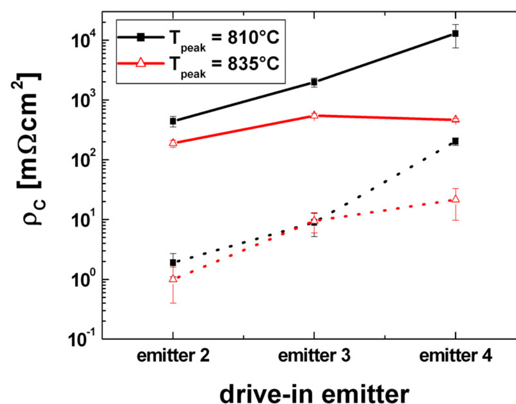

Figure 6.17.: Contact resistivity of "drive-in emitter" cells (mean values) after firing (straight lines) and after direct contacting the Ag crystals (dotted lines).

uate the experimental results, the doping profiles and the crystal coverage fractions were used to estimate the expected contact resistivity. For all samples an average crystal size of 350 nm was assumed. It has to be considered that the doping profile of emitter 3 and 4 increases in the first 30 nm to the peak concentration. This effect is presumably the result of phosphorous

out-diffusion during the drive-in step. However, another origin might be a rough surface of the analysed substrate that might lead to errors in the ECV profiling in the surface near regions. In Table 6.5 the calculated contact resistivities are given. For emitter 3 and 4 the calculations were performed assuming no glass frit etch and 30 nm etching of the glass frit.
The experimentally determined ρ_C in case of emitter 2 (high electrical surface concentration)

Emitter	Coverage [%]	ρ_C(no etch) [mΩcm^2]	ρ_C(30 nm etch) [mΩcm^2]	experimental [mΩcm^2]
2, 810°C	4.9	1.9×10^{-3}	-	1.9 ± 0.8
2, 835°C	16.9	5.4×10^{-4}	-	1 ± 0.6
3, 810°C	1.3	17.9	0.43	9 ± 3.8
3, 835°C	13.1	1.8	0.04	9.5 ± 3.5
4, 810°C	4.6	67.6	0.90	202 ± 29
4, 835°C	10.1	31.0	0.41	21.5 ± 11.7

Table 6.5.: Calculated ρ_C for different emitter profiles and crystal coverage fractions. The average crystal size was assumed to be 350 nm.

is much higher than the calculated one. The reasons are experimental limitations as described in the following. For comparison reasons the contact resistivity was measured on stripes cut out off the solar cells. The finger distance was 2.6 mm leading to a minimal contribution of the emitter to the measured total resistance of $R_{emitter,min} = 4.94\ \Omega$. The expected contact resistance for silver on emitter profile 2 is between 0.03 mΩ and 0.1 mΩ. The measurement accuracy of the TLM method should hence be below 0.001%. As the sheet resistance varies as well as the contact resistance, the measurement accuracy is limited. The extracted ρ_C is therefore only a rough estimation for an upper bound of the real ρ_C in case of emitter 2. For emitter profile 3 and 4 the comparison of experimental and calculated values suggests that the effective surface phosphorous concentration is indeed lower than the maximal concentration.
From this experiment it is expected that the forming gas anneal can lead to improvements in the fill factor.

The results of the forming gas anneal are plotted in Figure 6.18. The squares indicate the fill factors measured directly after firing, the rhombuses the fill factor after the forming gas anneal. The samples with drive-in emitter profile 2 show fill factors between 73% ($T_{peak} =$ 810°C) and 77% ($T_{peak} =$ 860°C) in contrast to 42% and 37% after firing. This result clearly indicates the dependency of the contact resistivity on the crystal coverage fraction. The solar cells with drive-in emitter 3 and 4 fired at $T_{peak} =$ 810°C do not show an increased fill factor. However, J_{sc} was found to be increased after the forming gas anneal. This is a hint that the series resistance is lowered. At $T_{peak} =$ 835°C the fill factor of cells with these emitter profiles doubles after the FGA. At $T_{peak} =$ 860°C the fill factor of cells with emitter profile 4 is not further increased. Analysis with IV-CC showed a still high series resistance of $R_s \approx 4.5\ \Omega$cm^2. The main loss factor is, however, the high second diode saturation current ($J_{02} =$ 180 nA/cm^2). The origin is presumably silver (or other metals of the paste) diffusion to the junction. The best cell results were reached on the cell with emitter profile 3 with a higher junction depth and a slightly increased surface doping. This cell has a fill factor of 73.8%, an open circuit voltage of 616.5 mV and a short circuit current density of 32.74 mA/cm^2 resulting in an efficiency of 14.9%. The limiting factor is again the high second diode saturation current (J_{02} = 84 nA/cm^2). The series resistance contribution was extracted to be 0.68 Ωcm^2. With a reduced J_{02} ($J_{02} \approx$

20 nA/cm^2) a fill factor of 77% can be estimated.

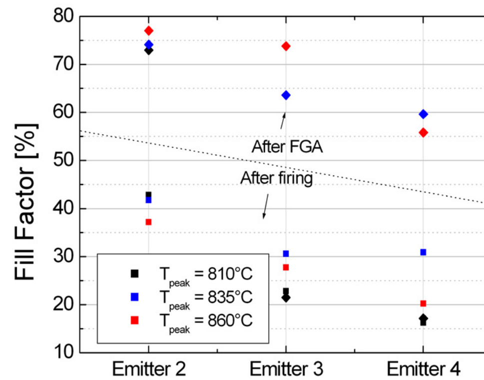

Figure 6.18.: Fill factor after firing and after forming gas anneal for different emitters and peak firing temperatures.

The experiment proved that it is possible to fabricate solar cells with moderately phosphorous surface concentrations using silver thick film metallisation. A solar cell was fabricated with a maximal surface phosphorous concentration of $N_{d,surface} \approx 4 \times 10^{19}$ with an efficiency of 14.9% and a fill factor of 73.8%. The fill factor and the efficiency are limited by J_{02} due to silver diffusion to the junction at high peak firing temperatures. In the next section the impact of the emitter profile on the formation of shunts is investigated.

6.7. Silver thick film contacts to p-type silicon

Contacts of the silver paste to p-type silicon are not only the origin for ohmic leakage currents. Point-like contacts of the silver paste to the base can also lead to leakage currents with a diodic characteristic [63,64]. These shunts lead to deviations from two diode model with ideality factor $n_2 = 2$ and to a characteristic hump in the maximum power point region, reducing FF and V_{oc} [37]. The point like contacts can occur due to mechanical emitter damage by handling or printing or due to penetration of the silver paste through the emitter. Especially on <100> oriented silicon substrates it is likely that the tips of the pyramidal silver crystals penetrate the emitter.
To characterise the silver thick film contact to boron doped silicon substrates, the diode characteristics of metal - silicon diodes were measured. Points with varying diameter were printed on the front side of two substrates with 0.5 Ωcm and 10 Ωcm, respectively. On the rear side a full area aluminium contact was applied. After drying and firing at fill factor optimised parameters in the IR heated conveyor belt furnace, the dark I-V characteristic was determined. In Figure 6.19 two representative I-V characteristics of point contacts with a radius of 90 µm are plotted. The series resistances are in both cases dominated by the spreading resistance. For the given geometry and substrate doping the spreading resistance is calculated to be approximately $R_{spread} = 13\ \Omega$ on the 0.5 Ωcm sample and $R_{spread} = 257\ \Omega$ on the 10 Ωcm sample (see e.g. [59] for details). Following the calculations in chapter 6.2.1, thermionic emission is predicted to be the dominant current transport mechanism. A rectifying behaviour would be expected. The simulated I-V characteristic is included in the graph (dotted lines). The fitted and the calculated spreading resistance coincide. Obviously, the shunt resistance of the metal-silicon diode

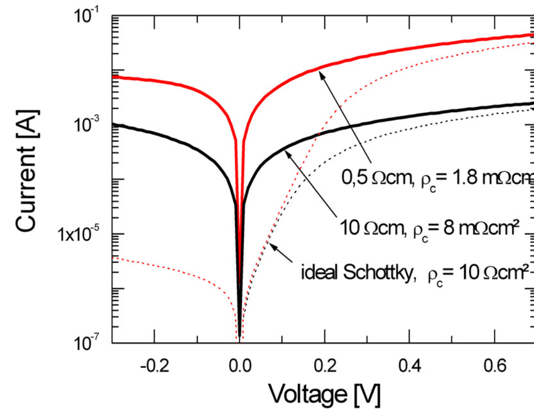

Figure 6.19.: I-V characteristics of silver thick film paste to p-Si substrates. Diode parameters: $I_0 = 6.46 \times 10^{-7}$A (calculated following equation 6.5 with $\phi_B = 9{,}54$ eV, $A^* = 32$ A K^{-2}cm^{-2}), $R_s = R_{spread} = 13\ \Omega$ respectively 257 Ω, $R_{shunt} = 1 \times 10^5\ \Omega$.

is remarkably reduced (see also [64]). The contact resistivities calculated using equation 6.1 resulted in 1.8 mΩcm^2 and 8 mΩcm^2, respectively, compared to 10 Ωcm^2 for the simulated characteristics. In [64] the hypothesis was formulated that the shunt in the Ag-p-Si contacts originates from barrier lowering at the tip of the pyramid due to high electrical fields. To test this hypothesis, the I-V characteristics of silver thick film contacts to <111> oriented silicon was measured. In chapter 4 it was shown that the predominant geometry of the silver crystals grown onto these substrates is lens-shaped. However, similar shunt resistances were extracted on both orientations. Additionally, simple numerical calculations were performed. The tip of the pyramid is regarded to be rounded with a radius r. Then the electrical field and the induced barrier lowering can be calculated following the approach of Chi et al. [122]. Assuming a tip radius of 10 nm, the barrier lowering is estimated to be $\Delta\phi_B \approx 0.07$ resulting in a 10 times smaller ρ_C. However, the discrepancy between model and experiment is still two to three orders of magnitude. As only simple calculations were performed, it cannot be excluded that a high electrical field at sharp edges lead to ohmic shunts in the Ag-p-Si contact (see e.g. [121] for details). Nevertheless, the origin for the reduced shunt resistance is not obvious.

6.8. Summary

Summarising the investigations on the electrical properties of silver thick film contacts to phosphorous doped silicon emitters, the following conclusions can be drawn:

- Calculations show that the geometry of the silver crystals in direct contact to the silicon has only a minor effect on the contact resistivity. The greatest area of inverted pyramids is in contact with the surface near region of the emitter. It is likely that the etching depth of a typical lead borosilicate glass is less than 60 nm. Considering the glass frit etching, calculations lead to no significant changes in ρ_C for typical industrial emitter profiles.
- The silver crystals grown into the silicon are indispensable for the current transport from the emitter into the silver finger.
- The contact resistivity of silver to moderately doped emitters ($N_D = 6 \times 10^{19}\,\mathrm{cm}^{-3}$) was measured to be in the range of $\rho_C(\mathrm{singlecrystal}) = (7..60) \times 10^{-7}\ \Omega\mathrm{cm}^2$. Even a crystal cover-

age of 0.1% would be sufficient to reach sufficient low contact resistivities ($\rho_{C,macroscopic} \approx$ 6 mΩcm^2) assuming direct connections between silver fingers and crystals.
- The number of crystals grown into the silicon gets more important the lower the phosphorous concentration at the surface is because the specific resistivity of each crystal increases. Therefore, two limiting factors determine the macroscopic contact resistivity of silver thick film contacts. 1. The number of silver crystals grown into the silicon and 2. the current transport from the silver crystal to the silver finger.
- The in-situ R_C measurements showed that the process parameters have a great impact on the contact resistivity, presumably on the formation of (quasi-) direct silver crystal - finger interconnections. Overfired, fast cooled samples resulted in high contact resistivities, whereas slow cooling led to contact resistivities comparable to direct contacts to the silver crystals.
- A forming gas anneal leads to an improvement in ρ_C of silver thick film fingers, if the origin for high contact resistivities is related to an increased average distance between silver crystal and finger due to sintering effects and a thicker glass layer. The average resistance between crystals and finger drops to $\approx 1-2\%$ of the initial value.
- The forming gas anneal has a significant influence on ρ_C and thus on the series resistance related losses, only. Other parameters are not remarkably influenced [13].
- The reaction occurring during the forming gas anneal is slow compared with the fast contact formation processes. The minimal temperature for efficient annealing was found to be 375°C. After 15 min annealing in a tube furnace no further improvements were measured.
- The improvements by FGA are irreversible and long term stable.
- No changes in the crystal coverage fraction or size of the crystals were found.

According to these results, the current transport in a silver thick film contact depends on the firing sequence. The following model for the current transport in a silver thick film contact is proposed.

1. **Underfired contacts ($T < T_{opt}$)** (Figure 6.20(a))
   Underfiring leads to incomplete penetration of the SiN_x layer and to an inefficient silver crystal growth. As the growth of silver crystals on the silicon is the requirement for electrical conduction, the obtained contact resistivity is high. Subsequent FGA does not have an impact on the crystal growth, so no further improvements are measured.
2. **Optimal fired contacts ($T = T_{opt}$)** (Figure 6.20(b))
   Optimal fired contacts show macroscopic contact resistivities higher than expected from calculations taken into account the emitter profile and the crystal coverage fraction. Only about 0.01% of the crystals covering 20% of the silicon surface need to be directly connected with the silver finger to explain the macroscopic resistance (see calculations in chapter 6.2.2). Current crowding effects make it likely that the current is transported via ultra thin glass layers occurring distributed over the contact.
3. **Overfired contacts ($T > T_{opt}$)** (Figure 6.20(c))
   The contact resistivity increases with increasing firing temperature, although the number and the size of crystals grown into silicon increases as well. As shown in chapter 4, it seems to be most likely that the thickness of the glass layer, separating the silver crystals and the silver finger, increases with increasing firing temperatures. Additionally, sintering of the silver particles in the finger is enhanced with increasing firing temperature (chapter 3). Both effects lead to a greater distance between the silver crystals that are in direct contact with the emitter and the silver particles in the bulk of the contact finger. The tunnelling probability

[13] As the contact resistance is improved, it cannot be ruled out that leakage currents induced by the metallisation diodic or ohmic in nature are also increased.

decreases, however, with increasing tunnelling distance, which is supposed to be the reason for higher contact resistances. This hypothesis is supported by the beneficial effect of the forming gas anneal (Figure 6.20(d)). During this anneal metal oxides contained in the glass layer, PbO, Ag_2O and others, are supposed to be reduced and hence evenly distributed. It is likely that the current is transported via a multi-step tunnelling mechanism from precipitate to precipitate.

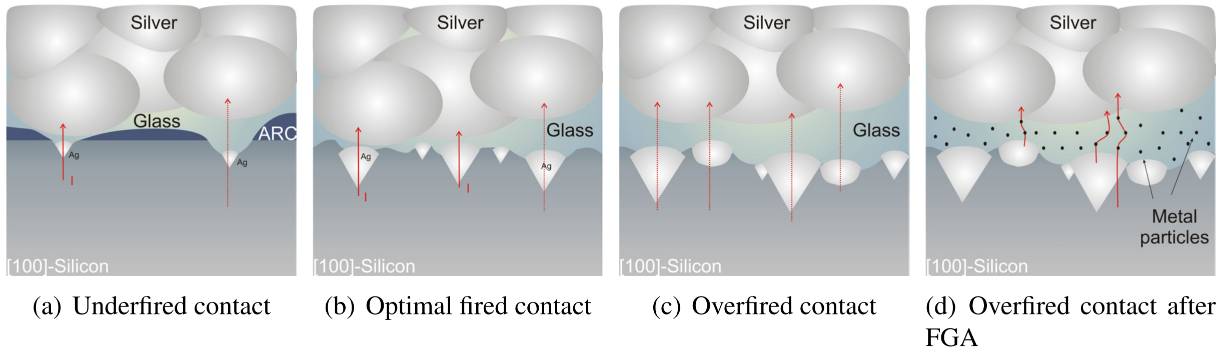

(a) Underfired contact (b) Optimal fired contact (c) Overfired contact (d) Overfired contact after FGA

Figure 6.20.: Simple current transport model. (a) Underfired contact: Incomplete penetration of the SiN_x layer. Only a few current path via quasi-direct interconnections can be established. (b) Optimal fired contact: The current is assumed to be transported via locally distributed quasi-direct contacts (c) Overfired contact: The glass layer is too thick leading to a high resistance between crystal and finger. (d) FGA is supposed to lead to reduced metal particles distributed in the glass layer. A multi-step tunnelling mechanism is supposed to reduce the resistance of the separating layer.

The combination of current transport model with the contact formation model resulted in the fabrication of a solar cell with a lowly doped phosphorous emitter. The achieved series resistance was $R_s = 0.68\ \Omega\text{cm}^2$, however, the fill factor and V_{oc} were limited by a high second diode saturation current. It was shown that in principle it is possible to contact lowly doped emitters with silver thick film pastes.

These results can serve as a basis to develop silver thick film pastes for contacting moderately doped emitters[14]. The critical point is to reduce the average resistance between silver crystals

[14] Self doping pastes were reported to be successfully applied to contact high sheet resistance emitters [127–130]. The proposed contact formation mechanism was the following [127,128]. The paste, containing phosphorous, is fired at $T_{peak} > 840°\text{C}$. It was proposed that during the high temperature step a silicon - silver alloy forms. On cooling down, it would recrystallise and phosphorous was supposed to be incorporated leading to a high doping concentration below the contact. However, the experiments in the thesis lead to a slightly modified mechanism behind the contact formation of self-doping silver pastes on high sheet resistance emitters. The cross-section of the paste-silicon interface was found to be similar to the cross-section of a standard paste to silicon. A glass layer separates silver crystals, grown into the emitter, from the silver bulk [79]. This indicates that also in case of self doping pastes the silver crystal growth is promoted by a transfer process of silver through the liquid lead phase. As shown in chapter 5.4 even on 100 Ω/sq emitters with a narrow highly doped plateau, the temperature for efficient silver crystal growth is higher than in the case of a standard 50 Ω/sq emitter. As the self doping pastes are usually fired at high temperatures, the silver crystal growth is expected to be sufficient. A phosphorous diffusion from the paste into the surface-near emitter region might not be excluded so that the crystal growth mechanism is further accelerated. Additionally, the junction depth might be increased so that silver diffusion does not affect J_{02} to a great extend. Rohatgi et al [129] and Hilali et al. [130] report the use of a forming gas anneal to achieve low contact resistances and high efficiencies. The FGA is therefore supposed to account for the thicker glass layer due to the high peak firing temperature. The contact formation and current transport mechanism of self-doping pastes are therefore assumed to be basically similar to standard pastes but contact formation starts at higher temperatures.

and silver finger ensuring at the same time the effective growth of silver crystals. Three ways are proposed:

1. Optimisation of paste system
   The glass frit should be modified to allow for crystal growth on lowly doped emitters at lower temperatures avoiding excessive silver diffusion. Additionally, the layer between crystals and finger should be as thin as possible.
   The silver particles should be modified to support silver growth and to prevent early sintering.
2. Separating contact formation and silver sintering
   A new approach would be to separate contact formation from increasing the line conductivity during the firing process completely. A paste should be optimised for crystal growth at low temperatures. In a subsequent processing step the line conductivity should be build up, e.g. by plating.
3. Another possibility to reduce the average resistance between silver crystals and silver finger while providing enough crystals on moderately doped emitters would be the implementation of a forming gas anneal in cell production. First experiments showed that stack annealing is possible, which is necessary to reach the high throughputs in solar cell industry. The long term stability of the forming gas anneal on cell level was also shown but has to be verified on module level. The emitter design and the firing process would have to be carefully adapted to account for the silver diffusion at higher peak temperatures.

Part III.

Development of lead and cadmium free thick film pastes

From July 2006 on, the "Directive on the restriction of the use of certain hazardous substances" (RoHS) regulates that electrical and electronic equipment put on the EU-market must not contain lead and cadmium and other hazardous substances [2]. This directive was further specified in this way that a maximum concentration value of 0.1 wt.% lead and 0.01 wt.% cadmium shall be tolerated in homogeneous materials. Lead is contained in modules of crystalline silicon solar cells e.g. in the solder used to interconnect cells in a module with tabs, in the glass used for encapsulation and in the glass frit used in aluminium and silver paste to fabricate contacts. Cadmium was also used in glass frits for metallisation pastes, but a data sheet survey of pastes (status: March 2006), supplied by the main producers Ferro and Dupont, revealed that state-of-the-art pastes are already cadmium free. Therefore, the hazardous substance in metallisation pastes is lead. Presently, photovoltaic modules are excluded from this directive, but the situation may change in the future [3]. If the RoHS directive would apply to the solar cell itself and not to the complete module, lead originates solely from the glass frits contained in the thick film pastes. The contribution of a standard aluminium thick film paste is about 0.17 mg/cm^2 [131] assuming a full area aluminium rear side contact. As the tendency in photovoltaic industry is to use thinner wafers, the concentration of lead related to the silicon weight increases. The lead concentration in a 300 µm thick solar cell originating from the Al thick film paste is about 0.24 wt.% and increases to about 0.7 wt.% for a 100 µm thin cell[15], exceeding the limit of the RoHS directive by far. The contribution of standard silver thick film pastes to the total lead amount is less, about 0.016 mg/cm^2 [131]. The lead concentration originating from the silver paste for a 300 µm thick silicon wafer is about 0.02 wt.%. For a 100 µm thick wafer the lead concentration increases to about 0.07 wt.% assuming the same amount of paste per square centimetre. Even if a lead free aluminium paste would be used (see chapter 8), the lead content in standard silver thick film pastes would approach the limit of the RoHS directive when fabricating thin wafers. Furthermore, there is motivation amongst the solar cell producer to fabricate environmentally friendly, completely lead free solar cells.
One task in this thesis is therefore to develop lead free thick film pastes for the metallisation of industrial solar cells. In the next chapter investigations on lead free silver pastes are presented. Lead free aluminium pastes will be investigated in chapter 8.

[15]The same amount of deposited aluminium was assumed.

7. Development of lead and cadmium free silver paste

A literature survey, performed starting to work on the study contained in this thesis, revealed that only a few investigations were published dealing with silver thick film paste compositions without PbO. Ross [132,133] investigated metal pastes without glass frit. The glass frit was substituted by lead or tin, both metals with a low melting point. To etch through oxide layers SiF was used. However, only results for lead containing pastes were given. Mertens et al. [80] and Eyckmans [134] reported about the fabrication of "home-made" silver pastes. Different glass frit systems were studied: pure PbO, PbO+B_2O_3 +SiO_2 glass, ZnO+B_2O_3 +SiO_2 glass, B_2O_3 +SiO_2 glass, pure Bi_2O_3 and Bi_2O_3 +B_2O_3 +SiO_2 glass. In their study Bi_2O_3 based frits performed better than PbO based frits. However, a combination of these frits led to the processing of a solar cell with a maximal fill factor of $FF = 71.4\%$. It has to be taken into account that the dwell time in the firing process at a peak temperature of about 810°C was 4 min [81] (limited by available equipment), different from the temperature profiles used in fast peak firing sequences today. A survey among paste suppliers showed that at the beginning of this study no commercially available lead free silver pastes for contacting the emitter of industrial solar cells were offered.
In this chapter the development of a lead free silver paste is presented. The approach is to apply the results of the investigations on contact formation and current transport mechanism of successful lead containing silver pastes. After a short introduction into glass theory, fabrication, properties and characterisation, the investigations on several lead free metal oxides and glass systems are presented leading to the development of lead free silver thick film pastes.

7.1. Glass basics

Substituting a constituent of a glass requires a basic knowledge of the glass structure. In this section the theory of glasses is therefore briefly summarised. In this work commercially available as well as "home-made" glasses were used. The advantage of using self-fabricated glasses is to control the composition exactly. The fabrication process is and glass characterisation methods are described.

7.1.1. Glass theory

The glass theory is introduced following the random network hypothesis of Zachariasen [135] restricting to SiO_2-glasses. The basic assumption is that in a SiO_2 glass the smallest units, [SiO_4]-tetrahedrons, are randomly interconnected to form a network. The main difference between a glass and a crystal is that on solidifying a glass shows a continuous change in a physical property (e.g. specific volume) over a range of temperature. A crystal, in contrast, exhibits a well-defined melting point at a singular temperature at which there occurs a discontinuous

change in that property. In general, oxides that are able to form a glass are called “glass formers”. Beside SiO_2 typical glass formers are B_2O_3 and Al_2O_3. Melting of a glass-former with other metal oxides like Na_2O, PbO, ZnO and many others leads to the incorporation of metal cations into the network. In SiO_2 glasses the Si-O-Si bridges are partly disrupted and the metal cations are placed in the free spaces. The oxide anions are bonded by the silicon (Figure 7.1) [86].

$$\mathrm{Si{-}O{-}Si} \rightarrow \mathrm{Si{-}O^{-}\ 2M^{+}\ {}^{-}O{-}Si} \text{ respec. } \mathrm{Si{-}O^{-}\ M^{2+}\ {}^{-}O{-}Si} \tag{7.1}$$

The metal cations and the oxygen anions are evenly distributed following the network hypothesis. The metal cations are called “glass modifiers”. With these modifiers the properties of a glass can be tailored. A typical example is the softening point of a glass. As the structure of the glass becomes weaker by introducing a modifier, the softening point is lowered. The impacts of certain metal oxides especially in combination with others are often empirically investigated due to the complex interactions [86].

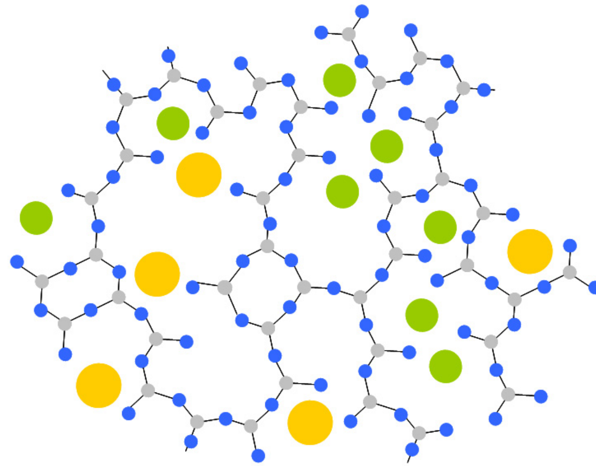

Figure 7.1.: Silicate glass with glass modifiers. Grey dots symbolise silicon, blue dots oxygen. Yellow dots symbolise e.g. Pb^{2+} ions, green dots e.g. Na^{+} ions.

7.1.2. Glass fabrication

In leaded commercially available silver thick film pastes various glass compositions are used. In a previous study [63] glasses of typical silver pastes were extracted[1] and analysed with EDX. Two systems were found: PbO-ZnO-(B_2O_3)-SiO_2 and PbO-(B_2O_3)-SiO_2 (Table 7.1). The determination of the boron content was not possible because elements lighter than carbon cannot be extracted with the used EDX system. However, the data sheets of the pastes show that boron is included in the paste. In both pastes additional oxides in minor concentrations were found such as Al_2O_3, P_2O_5 or TiO_2. It is interesting to note that both pastes lead to acceptable fill factors of industrial solar cells, although they remarkably differ in the glass frit composition. In this work mainly glasses with a high lead oxide content were used as test and reference glasses. To get more insight in the fabrication of glass frits and to develop individual compositions, glass was prepared by using oxide powders. After mixing the appropriate amount of the metal oxides, SiO_2 and B_2O_3 the powder was heated up in a tube furnace to about 1100°C. This temperature was held for several hours constantly stirring with a rod consisting of an Al_2O_3

[1] Glass and silver were separated in a high temperature step above the melting point of silver.

Glass	PbO	ZnO	SiO_2	B_2O_3
A	12	85	3	?
B	90	0	10	?

Table 7.1.: Typical glass compositions in leaded commercially available silver thick film pastes in weight per cent. Only the ratios of the main constituents are given.

ceramic (Alsint). It has to be taken into account that B_2O_3 is very hygroscopic and forms boric acid in air atmosphere [84]. During heating up, the water evaporates leading to bubbles if too fast ramp up rates are applied. The used crucibles consisted of Alsint. A little amount of Al_2O_3 was therefore constantly dissolved by and incorporated in the glass.
With this method several glasses were fabricated summarised in Table 7.2.

Glass	PbO	B_2O_3	SiO_2
I	29	31	40
II	89	2	9
III	85	5	9

Table 7.2.: Compositions of fabricated glass in weight per cent.

7.1.3. Characterisation of glasses

In the following the glass characterisation methods used in this work are briefly summarised. These methods are similar to the methods used in the glass industry.

Composition of glasses

The composition of glasses was studied with EDX. However, a quantitative analysis is subject to error because the surface of the glasses was in general not polished. The boron content was not determinable because with the used EDX system elements lighter than carbon are not detectable. In case of glass powders, the powder was prepared on a substrate (e.g. quartz-glass, silicon, ALsint ceramic) and heated up to obtain a homogeneous film. In this case additional errors can occur due to the interactions of the glass with the substrate.
The EDX analysis of the fabricated glass III is summarised in Table 7.3. As expected, Al_2O_3 originating from the crucible was dissolved in the glass during glass fabrication. The PbO and SiO_2 content is similar to the weighted oxide powder content.

Glass	PbO	B_2O_3	SiO_2	Al_2O_3
III (preparation)	85	5	9	-
III (EDX)	88	?	8	4

Table 7.3.: EDX analysis of fabricated glass in weight per cent. Al_2O_3 was incorporated in the glass.

XRD analyses

The fabricated glasses were studied with the x-ray diffraction system (XRD). The glasses were crushed into powder and irradiated with a monochromatic x-ray beam under different angels. With the Bragg equation $n\lambda = 2s\sin\theta$ the atomic layers and thus the structure of the sample can be determined. A glass is not expected to show sharp peaks in the spectrum because of the lack of an ordered structure. In Figure 7.2 the spectrum of two glasses and crystalline PbO powder is shown. Glass II does not show any maxima. Glass III shows a flat, widely spread maxima in the region of typical PbO peaks occurring due to the very high PbO content (85 wt.%).

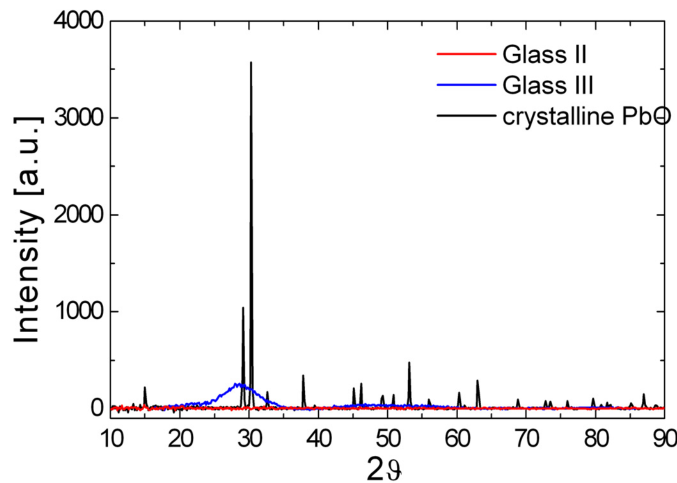

Figure 7.2.: XRD analyses of two fabricated glasses compared with the spectrum of crystalline lead oxide.

Thermal analysis

The viscosity of a glass decreases continuously with increasing temperature. In contrast to the step in the specific heat $c_p = \partial H / \partial T$ (H: Enthalpy) at $T = T_{melt}$ occurring in crystals (first order phase transition), the $c_p - T$ characteristic of glasses is continuous. The increase in c_p is the glass transformation region (see e.g. [86]). A glass can be characterised using its transformation temperature T_g often defined as the inflection point of the $c_p - T$ characteristic after a defined thermal history of the glass [86].
Throughout this work the transformation temperature was determined using Differential Thermal Analysis (DTA). An empty Alsint crucible served as reference. In Figure 7.3 a typical measurement of glass III is shown (ramp up: 10 K/min, cooling: 5 K/min). The transformation region during heating up ranges from 385°C to 424°C. The transformation temperature extracted from the cooling curve was 380°C.
As most of the glasses used in this work were present in form of powders, in general two heating cycles were necessary to determine the transformation temperature. During the first heating, the powder sinters and shrinks causing a noisy signal. After cooling down the glass is homogeneous and T_g can be extracted during a second heating cycle.

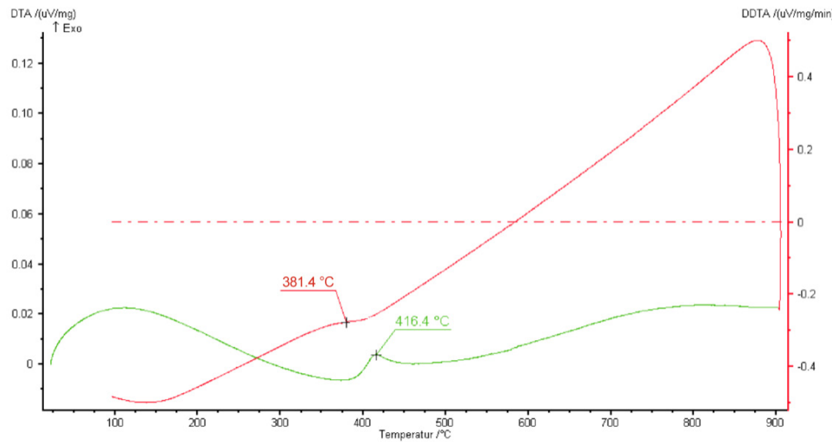

Figure 7.3.: DTA measurement of glass III. Green line: Heating up. Red line: Cooling down

7.1.4. Temperature dependent measurement of the viscosity

The viscosity - temperature ($\eta - T$) characteristic of a glass can provide additional information about a glass. The viscosity is often used to define characteristic temperatures [86]:

- Softening point: $\eta = 4^7$ Poise
- Flow point: $\eta = 10^5$ Poise
- Working point: $\eta = 10^4 7$ Poise

The gradient of the $\eta - T$ characteristic denotes whether a glass is long (low gradient) or short. In case of glass containing thick film pastes this characteristic is important. If a glass has a low viscosity at temperatures below the combustion of the organics, bubbles can occur leading to a mechanically unstable contact. If a glass has a high viscosity at moderate temperatures (in the range of 700°C-800°C), high peak firing temperatures and/or long firing dwell times are necessary to start the interaction between glass, silicon and silver.

In this work the viscosity-temperature characteristic was measured with a rotating cylinder setup. Glass was heated in a tube furnace, a stirring rod was rotating with a constant frequency and the torque was measured. With this setup viscosities in the range of 1×10^3 Poise $< \eta < 1 \times 10^5$ Poise could be measured (for details see [63] and [87]). In Figure 7.4 the $\eta - T$ characteristic of two high leaded glasses is shown (glass III and extracted glass B) is shown. The gradient of both glasses is comparable, however, glass III is fluid (i.e. has a viscosity below 10^3 Poise) at $T > 550$°C, whereas glass B is fluid at $T > 625$°C.

7.2. Application of the contact formation model

The silver crystals below the thick film paste, directly contacting the emitter, were found to be indispensable for the current transport from the emitter into the silver finger (chapter 6). The investigations on the contact formation of lead containing silver pastes, presented in chapter 5, led to the hypothesis that two key properties determine the growth of silver crystals on phosphorous doped emitters.

1. The glass should contain metal oxides that are reduced by silicon in the relevant temperature regime.
2. The resulting metal should be liquid during the peak firing process and serve as a transport medium for silver to grow onto the silicon.

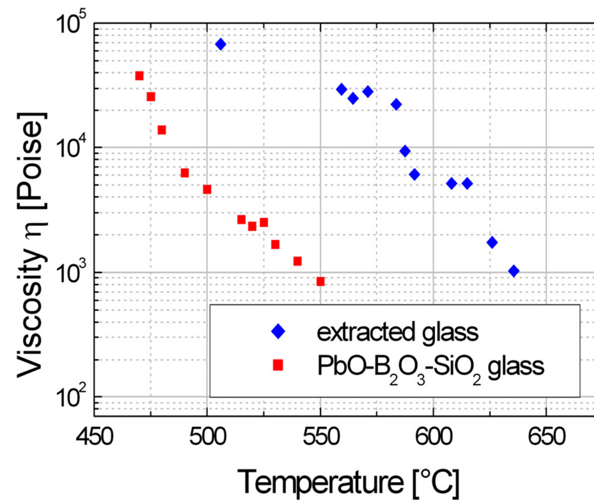

Figure 7.4.: Viscosity - temperature characteristic of glass III and extracted glass B

It was shown that it is sufficient to use lead oxide without being embedded in a glass to promote the silver growth. A redox reaction of silicon and PbO leads to liquid lead serving as the transport medium for silver. To find substitutes for PbO in a borosilicate glass, the ability of several metals, liquid in the relevant temperature range, were tested to serve as a transport medium for silver.
Initially, a phase diagram survey was performed to find the most promising metals. As these metals are supposed to substitute lead oxide in the glass matrix, experimentally silver transport properties of oxides of these metals were investigated.

7.2.1. Survey of binary silver-metal phase diagrams

A survey of binary silver-metal phase diagrams was performed to select promising candidates. The two key requirements led to the selection of three possible substitutes, the oxides of zinc, tin and bismuth. In Figure 7.5 the binary phase diagrams of these elements with silver are shown. In contrast to lead, tin and zinc form compounds with silver, thus it is likely that on cooling down a liquid tin-/ zinc-silver alloy separates in compounds. These compounds own different properties concerning the electrical contact to silicon and the conductivity, which might have a negative impact on the electrical performance of the thick film contact due the lower specific conductivity of silver alloys.
The phase diagram of silver and bismuth is very similar to the lead-silver interaction. According to Ugai et al. [102] Bi_2O_3 is reduced by silicon in the relevant temperature regime (500°C < T < 850°C). If the contact formation in silver thick film pastes is related to a transfer process of silver accelerated by a liquid metal phase, then Bi_2O_3 seems to be the most promising candidate to substitute PbO.

7.2.2. Experimental verification

To test the contact formation model, pastes were prepared containing 10 wt.% crystalline metal oxide and 90 wt.% silver (binder system: ethyl cellulose and terpineol). After drying on a hot plate these pastes were fired on a <100> FZ silicon substrate in the RTP furnace. The firing

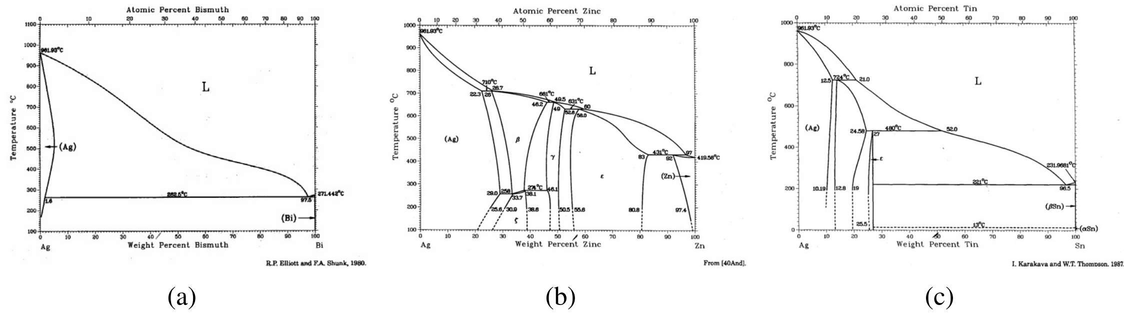

Figure 7.5.: (a) Ag-Bi phase diagram [101]. (b) Ag-Zn phase diagram [101]. (c) Ag-Sn phase diagram [101]. The Ag-Pb phase diagram is shown in Figure 5.10(b). (Diagrams reprinted with permission of ASM International™. All rights reserved. www.asminternational.org)

parameters were adapted to test the interaction at a typical firing temperature of 800°C[2]. A long dwell time of 120 s was chosen to visualise differences in the crystal growth.
In Figure 7.6 SEM photographs of the silicon surface after mechanical removal of the metal oxide - silver pastes are presented.

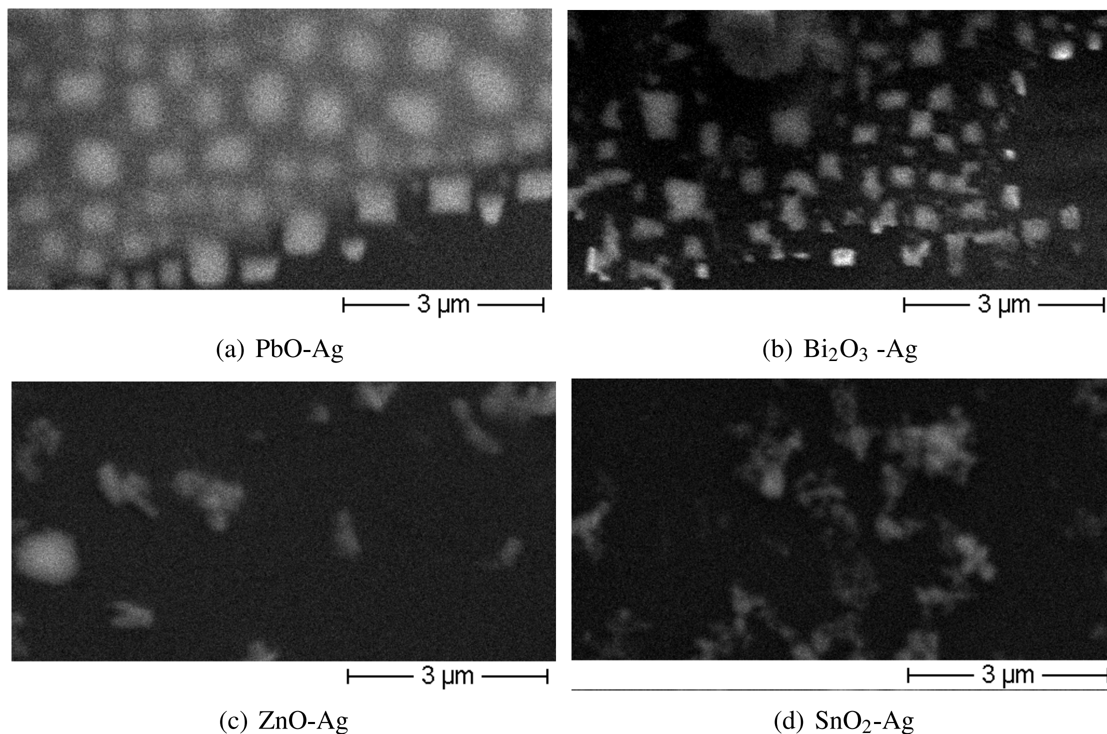

(a) PbO-Ag (b) Bi_2O_3 -Ag

(c) ZnO-Ag (d) SnO_2-Ag

Figure 7.6.: SEM top view on silicon surface below metal oxide - silver pastes. Silver growth is most effective below the PbO and Bi_2O_3 paste.

SEM and EDX analysis proved that the transfer process of silver to grow onto the silicon surface is more effective at $T = 800°C$ when using Bi_2O_3 compared to SnO_2 and ZnO, respectively. Below the latter two pastes hardly any silver crystals were found to have been grown into silicon. Bi_2O_3 is therefore supposed to be the most promising substitute for PbO in a glass frit. This supports the contact formation model formulated in chapter 5.5.

[2] The firing temperature was chosen to be slightly below the silver - silicon eutectic to exclude the occurrence of this reaction.

Bi_2O_3 and ZnO served as a basis for fabricating several silicate glasses varying in metal oxide species and content[3]. In the next section the essential properties of these frits are tested and evaluated.

7.3. Investigations on lead free glass frits

Glass properties are very sensitive to changes in the glass composition. Commercially available optimised glasses consist therefore of a number of metal oxides. Empirical methods are often used to find optimal compositions. In this work a different approach is used. Based on the investigations in chapter 5 and 6 basic requirements of the glass frit are reconsidered. These requirements define test methods to decide, whether a glass frit has the potential to lead to well performing silver thick film pastes. For these experiments glass frits with a limited number of metal oxides were chosen. The most promising glass frits were then investigated to understand the role of additional components. Finally, Metalor used the optimal glass frit composition to prepare silver thick film pastes, tested on a large number of solar cells at ECN and afterwards in the production line of the solar cell producer RWE SCHOTT Solar.

7.3.1. Requirements

Before investigating lead free glass frits, it is useful to reconsider the basic requirements of a frit system in silver thick film pastes. A glass frit should ...

1. ... enhance sintering of silver particles. The glass should wet silver.
2. ... etch through the dielectric layer. It is important that SiN_x is wetted by the glass.
3. ... serve as the long term stable adhesive to silicon to guarantee the mechanical and electrical stability of the contact.
4. ... not etch too deep to avoid junction damaging.
5. ... act as the transfer medium for silver to grow on silicon.

These processes should preferable occur in the same temperature range as the simultaneous formation of the aluminium back surface field and rear side contact in a co-firing sequence. The process window for the contact firing step should be large.

In this work the following test methods were used: The glass transformation temperature was determined, if not available from data sheet. Furthermore, the etching ability into a silicon nitride layer, the wetting and reaction of the glass with silicon and the silver transfer process to silicon were investigated.

7.3.2. Characterisation of lead free glass frits

To get a first idea of the properties of lead free glass frits, glass frits were tested supplied by glass producers. These frits were prepared as a thick film paste by Metalor to be deposited on substrates. The components and the softening temperatures T_{soft} specified by the suppliers are given in Table 7.4. The softening temperatures are comparable to T_{soft} of a leaded reference glass frit ($T_{soft} = 450°C$).

[3]Fabricating a glass with a high SnO_2 content was difficult, because very high temperatures were necessary to melt the oxide powders

Paste	Composition (main components)	T_{soft} [°C]
AG ref	$PbO+SiO_2+B_2O_3$	450
AG1	$ZnO+P_2O5$+Alkali metals	>360
AG2	$Bi_2O_3+B_2O_3+SiO_2$	526
AG3	$ZnO+B_2O_3+SiO_2$	500
AG4	$Bi_2O_3+SiO_2+B_2O_3$	450

Table 7.4.: Glass frits used in the following experiments

Etching through silicon nitride layer

The ability of etching through the silicon nitride is one of the key properties required for a successful lead free glass frit. In a simple experiment the etching properties were qualitatively studied. Two pastes were fabricated containing only glass frit AG3 or AG4, respectively. These pastes were printed on a 170 nm thick PECVD SiN_x layer deposited on polished FZ silicon. After drying and combustion of the organics on a hot plate, the samples were fired in the RTP-furnace with equal ramp up and cooling rates (10 K/s) and a peak temperature of $T_{peak} = 820°C$. The dwell time was zero. The slow ramp rates were chosen to visualise the effect. Both pastes etched into silicon nitride visible due to the transparency of the glasses and the colour change with decreasing SiN_x layer thickness. This confirms that glasses based on these metal oxides are able to penetrate through the SiN_x layer. Further experiments were performed to study, if the etching rate is high enough to etch through the SiN_x layer in a fast firing process (see below).

Interaction with silicon

The interaction of the different glass frits with silicon was investigated using different reaction temperatures. It was found that the adhesion of the ZnO based glass on silicon was poor. In Figure 7.7(a) the cross-section of the ZnO based glass (AG3) on polished, <111> oriented FZ silicon fired at 800°C for 2 min in a tube furnace is presented. Precipitates have formed, but most of them were found to be empty with holes in the shell of the precipitates. Parts of the glass fall off during firing. The reason might be the redox reaction between Si and ZnO_{glass}. The boiling point of metallic Zn is at $T_b = 908.5°C$ [84] so that the vapour pressure at 800°C is supposed to be high. It is likely that Zn evaporates leaving behind the porous structure. In contrast in Figure 7.7(b) the cross section of the Bi_2O_3 based paste (AG2) after firing on a <111> oriented silicon substrate at identical conditions in the tube furnace is shown. The adhesion of the glass was strong. Precipitates were found in the bulk of the glass.
In a subsequent experiment the interaction of the Bi_2O_3 based glass with silicon was investigated in a fast firing sequence. The glass frit paste was prepared on a <100> oriented FZ silicon sample and fired in the RTP furnace with a ramp up rate of 120 K/s (dwell time: 0 s), a peak temperature of 850°C and a ramp down rate of 40 K/s. In Figure 7.7(c) a cross section picture of the Bi_2O_3 based glass on silicon after the peak firing is shown. EDX analysis revealed again that bismuth precipitates with different sizes have been formed, similar to the interaction of lead borosilicate glass with silicon. These precipitates do not wet the silicon. EDX analysis showed that these precipitates consists of pure bismuth, as no other glass constituent were found. It can be concluded that a redox reaction between silicon and $Bi_2O_{3,glass}$ has occurred with the reaction product bismuth and SiO_2 .

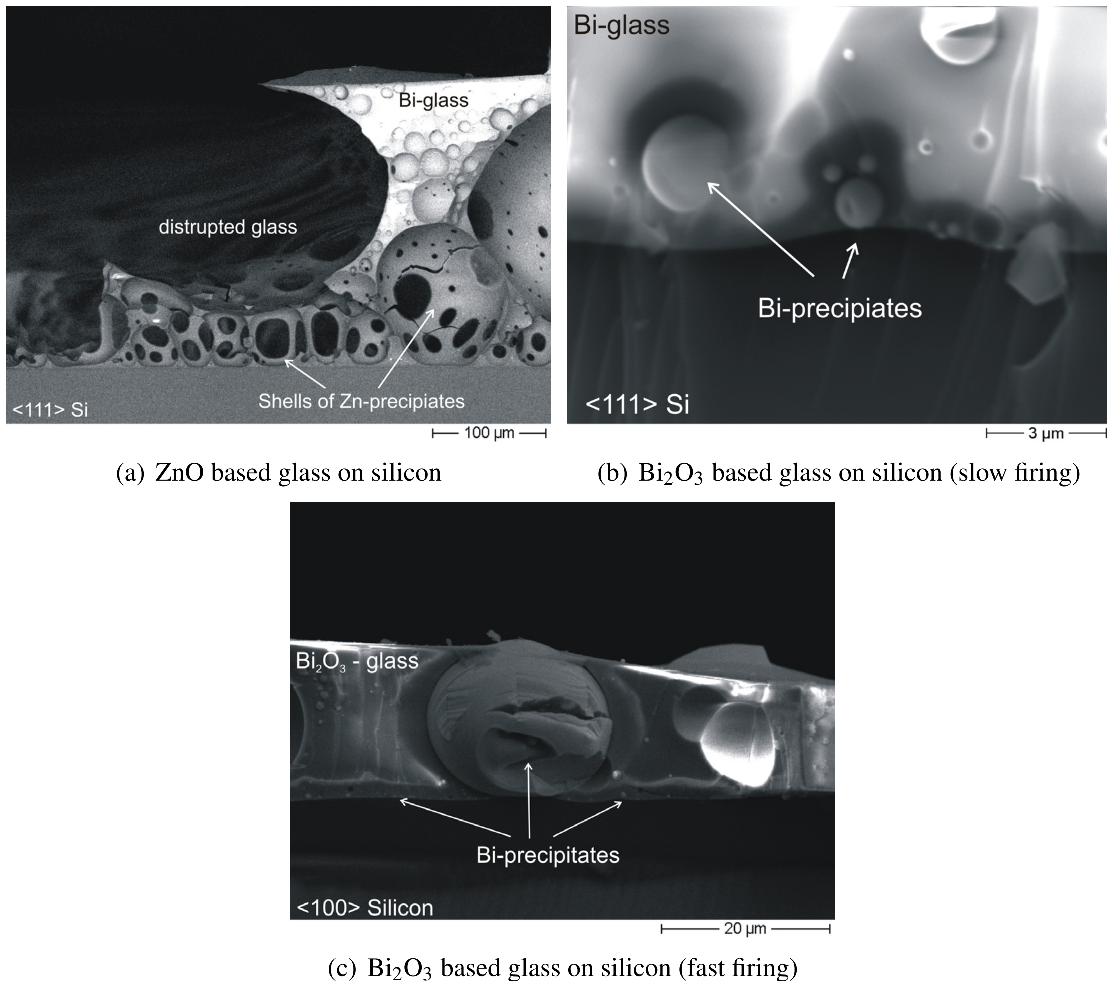

(a) ZnO based glass on silicon

(b) Bi_2O_3 based glass on silicon (slow firing)

(c) Bi_2O_3 based glass on silicon (fast firing)

Figure 7.7.: SEM cross section pictures of lead free glasses on silicon fired with different parameters. The adhesion of the ZnO based paste was very poor due to evaporation of zinc, the product of a (supposed) redox reaction between silicon and ZnO_{glass}.

7.3.3. Electrical properties

The electrical properties of silver pastes, containing lead free glasses, were tested. The four different glass frits (Table 7.4) were mixed with silver powder, binder and solvents using standard three roll mill techniques. The glass frit content was 5 wt.%. Paste preparation was done by Metalor.

In a first experiment the contact resistivity was measured. TLM test structures were printed on bare mc-Si without dielectric coating on a 35 Ω/sq emitter and dried on a hot plate. The samples were fired in the RTP furnace with varying peak temperatures (ramp up: 75 K/s, dwell time: 5 s, ramp down: as fast as possible). Initially, all pastes were fired at a peak temperature of 810°C. It turned out that the adhesion of the both ZnO based pastes, AG1 and AG3, was very poor. Most of the fingers fell off after firing. Therefore, further experiments were performed with the two Bi_2O_3 based frits. A peak temperature variation showed a tendency for higher peak temperatures (Figure 7.8).

These results show that it is possible to contact a typical emitter without using lead oxide in the glass frit. The achieved contact resistivities are, however, higher than standard values of Pb containing pastes (1-10 mOhmcm^2).

In a second experiment the contact resistivity to SiN_x coated mc silicon with a 35 Ω/sq emitter

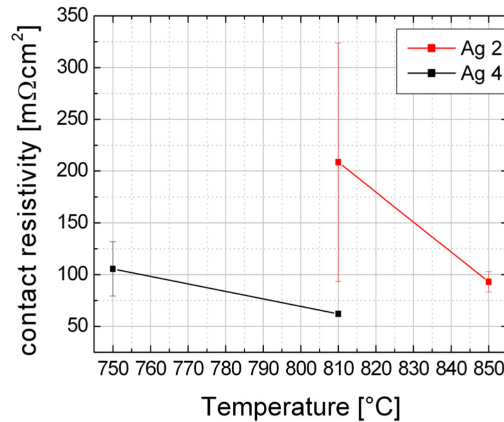

Figure 7.8.: Contact resistivity of paste Ag 2 and Ag 4 on a bare silicon emitter

was measured. After printing paste AG2 and AG4, the samples were fired with an improved firing sequences (ramp up: 70 K/s, $T_{peak} = 850°C$, dwell time: 2 s). After firing, ρ_C was determined using the TLM measurement setup. Subsequently, the samples were annealed in forming gas (Ar-H(10%)) at 400°C for 45 min and ρ_C was measured again. In Figure 7.9 the results are summarised.

After firing ρ_C of both pastes is high. The contact resistivity shows a great scattering. Some

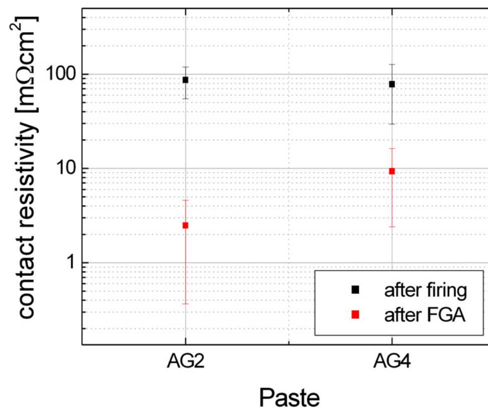

Figure 7.9.: Contact resistivities of lead free silver thick film pastes fired through a SiN_x layer before and after forming gas anneal (mean values of three measurements on 15 different fingers)

fingers seem to have established a better contact to the emitter than others. After the forming gas anneal the contact resistivity of all fingers is decreased drastically. Two important results can be extracted. The forming gas anneal has a beneficial effect on the contact resistivity of lead free pastes. Presumably, metal oxides in the glass, mainly Bi_2O_3 and dissolved silver, are reduced to precipitates that increase the tunnelling probability through the glass layer. The second result is that it is possible to achieve contact resistivities on an industrial silicon solar cell emitter using PbO free pastes that are comparable to those achieved with leaded pastes. In principle it is possible to substitute lead in the silver thick film paste. In the following the properties of Bi_2O_3 based glass frits are investigated in more detail.

7.3.4. Properties of Bi_2O_3 based glasses

As Bi_2O_3 based glasses turned out to be the most promising substitutes for PbO based glass in silver thick film pastes, a large range of Bi_2O_3 glasses were used for further testing, containing various amount of Bi_2O_3 and other active metal oxides. The exact composition was agreed to be non-disclosed by the project partners. The goal was to understand the role of glass frit components and to relate the frit properties to their performance on cell level. The following properties were investigated:

1. Transformation temperature
2. Silicon wetting
3. Silicon etching
4. Silver growth / Transfer process

Glass transformation temperature

The transformation temperature was determined using the DTA measurement setup (see chapter 7.1.3). In Figure 7.10 the dependency of T_g on the Bi_2O_3 content in the glass is shown for four different compositions. Using these glasses a decreasing Bi_2O_3 content leads to a decrease in T_g. Bi_2O_3 was substituted by another active metal oxide, while the concentrations of the other two components, SiO_2 and B_2O_3, was kept constant. The investigated glasses show consequently a glass transformation temperature similar to that of a typical lead borosilicate glass with a high PbO content used in silver thick film pastes (420°C). The relevance of the T_g for the contact formation is, however, not obvious so that further experiments were performed.

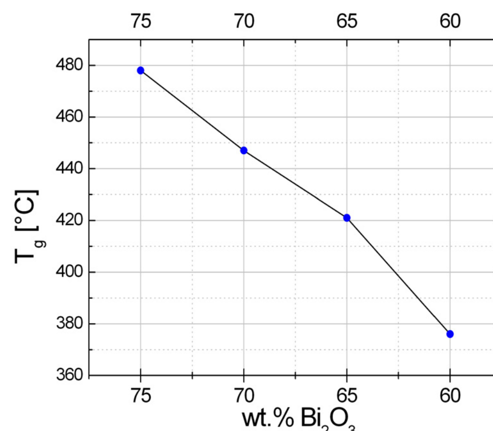

Figure 7.10.: The transformation temperature versus the Bi_2O_3 content

Silicon wetting

The wetting behaviour of Bi_2O_3 based frits differing in the Bi_2O_3 content was tested qualitatively. Three lead free glass frits (Bi1: 85 wt.% Bi_2O_3 , Bi6: 60 wt.% Bi_2O_3 and Bi8: 55 wt.Bi_2O_3) and one leaded glass with a PbO content of 81 wt.% (Pb25) were used to prepare test pastes containing 33 wt.% glass frit and 66 wt.% binder (ethyl cellulose) and solvent (terpineol). Two fingers of each paste were syringe-printed on one sample per temperature (<100> oriented p-type Cz silicon, chemically polished). The samples were fired in the RTP furnace using the following settings: Ramp up: 10 K/s, dwell time: 0 s, ramp down: 10 K/s, peak

temperatures: 800°C and 850°C. Although it was taken care to deposit comparable amount of glass frits on the sample, differences in the printed paste amount cannot be excluded. Surface profilometer measurements after firing showed a 40% reduced volume of the Bi1 fingers in comparison to Bi6 and Bi8 fingers which have a similar volume. The Pb25 fingers have a 10-20% reduced volume. The differences in finger volume are not necessarily due to a different amount of glass frit. Another possible explanation would be a higher density of glass Bi1 and Pb25. In Figure 7.11 SEM top view pictures on the glass fingers are shown. The SEM investigations of

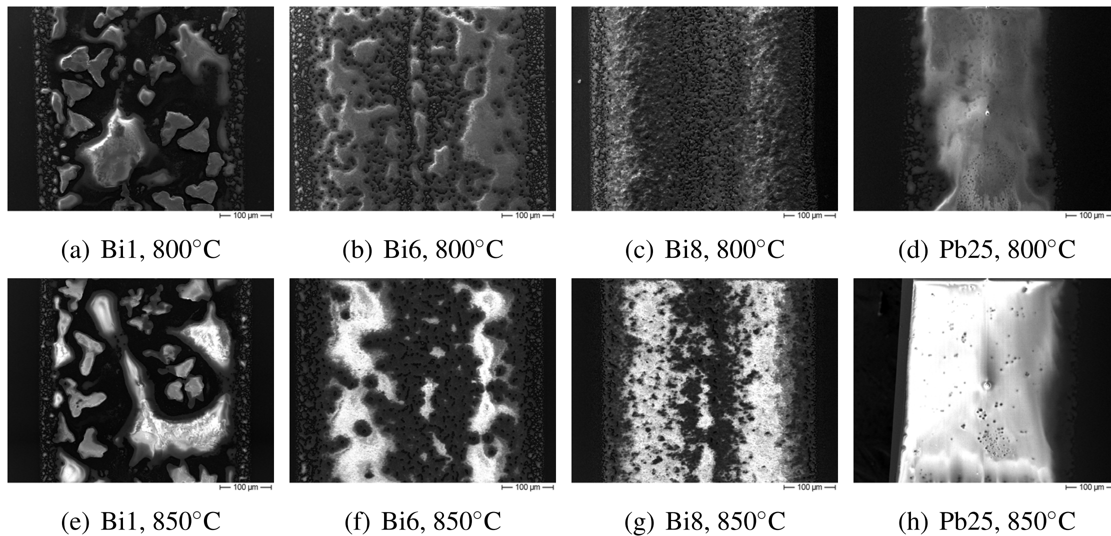

(a) Bi1, 800°C (b) Bi6, 800°C (c) Bi8, 800°C (d) Pb25, 800°C

(e) Bi1, 850°C (f) Bi6, 850°C (g) Bi8, 850°C (h) Pb25, 850°C

Figure 7.11.: Wetting behaviour of various glass frits on silicon. Details see text

paste Bi1 showed big islands of glass that are only partly connected. In contrast to Bi1 paste Bi6 wets silicon more homogeneously. The temperature dependence of wetting is not significant, however a slight tendency towards better wetting at higher temperatures can be deduced. The wetting behaviour of paste Bi8 is similar to Bi6 but with more grains. In contrast, Pb 25 wets the silicon completely even at 800°C. Wetting of silicon seems to be necessary to ensure a homogeneous contact. The frit composition seems to influence the wetting behaviour, however, it was not possible to determine the key component in the glass frit for optimised wetting.

Silicon etching

Initially, the etching behaviour of a Bi_2O_3 based glass Schott G018-198 (see Table 7.4) was studied similar to the study on high leaded glasses in chapter 5.3.3. The etching behaviour was studied in dependence of the peak firing temperature, ramp rate and dwell time. 0.4 g glass frit was mixed with a binder system and deposited on chemically polished <100> oriented, p-type silicon substrates. The samples were fired in the RTP furnace using the same parameters as for the leaded frit (ramp up: 20 K/s, 6 different peak temperatures, varied dwell times and ramp down rates). After firing the glass was completely removed in buffered HF. The average etching depth was measured using a DEKTAK surface profiler. In Figure 7.12 the temperature dependency of the average etching depth for both glasses, leaded reference and lead free, Bi_2O_3 based, is plotted. In fast firing processes (black points) the Bi-glass as well as the Pb-glass starts to etch significantly at $T > 650$°C. However, the etching rate is much higher in case of the specific Bi-glass. At $T_{peak} = 800$°C the Pb glass etches ≈400 nm deep whereas the Bi-glass etches ≈1100 nm deep. Long dwell times or slow cooling ramps lead to etching depths of 3300 nm

for the Bi-glass compared with at most 1100 nm for the Pb-glass.
The etching depth of the Bi_2O_3 glass G018-198 can therefore be estimated to be roughly three

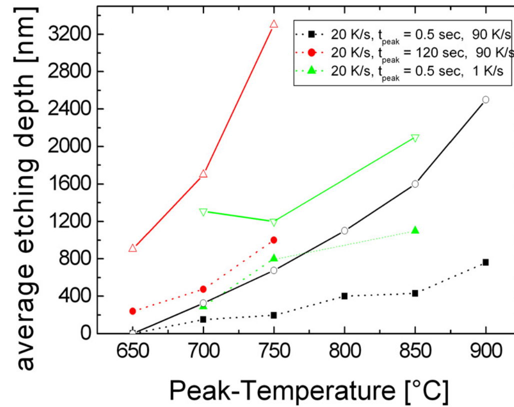

Figure 7.12.: Etching depth of Pb and Bi glass in <100> oriented silicon in dependence of the peak temperature. Bi-glass: full lines, non-filled symbols, Pb-glass: dotted lines, filled symbols.

times the etching depth of the Pb glass.

To study the etching rate dependency on the composition, measurements were performed on <100> oriented, chemically polished Cz p-type silicon without an emitter. Paste were mixed with Bi_2O_3 based glass frits differing in Bi_2O_3 content and in the content of other active metals (33 wt.% glass frit and 66 wt.% binder and solvent). The samples were fired in the RTP furnace with a ramp up and down rate of 2 K/s to 800°C and 850°C (dwell time: 0 s) to obtain etching depths measurable with the DEKTAK surface profiler. However, as the substrate roughness was relatively high, a reasonably etching depth determination was only possible for etching depths deeper than 100 nm (Figure 7.13). The results are therefore difficult to interpret. It was

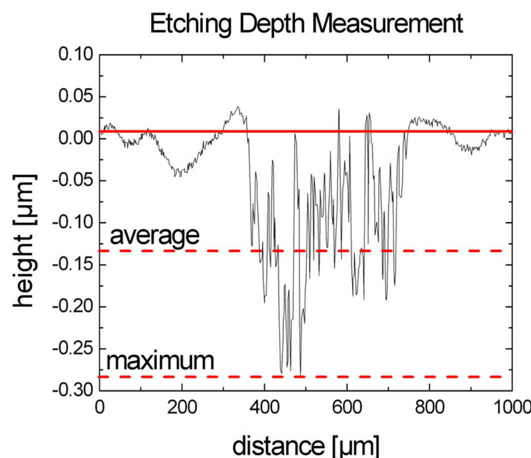

Figure 7.13.: Typical profile of the DEKTAK surface profiler. The surface roughness of the substrate was high.

found that the etch rate of pastes with a high Bi_2O_3 content was much lower (850°C: <100 nm ($\approx$ 25 nm)), than the etch rate of pastes with a lower Bi_2O_3 content (850°C: $\approx$ 250 nm).

The surface morphology of <100> oriented silicon below the glasses was investigated with SEM and EDX after etching off the glasses in buffered HF. In Figure 7.15 typical SEM pictures of the surface below the lead free and the leaded reference is shown. The sample was fired with a ramp up rate of 20 K/s to 800°C (dwell time: 0 s) and cooled down as fast as possible. It is obvious that <100>-oriented silicon is etched differently by the PbO- and the Bi_2O_3 -glass. Below the leaded glass the silicon surface under the glass is corrugated, whereas below the Bi-glass the silicon surface is more or less flat with hillocks. EDX analysis confirmed that these hillocks consist of silicon. The existence of hillocks might indicate an inhomogenous wetting of the Bi_2O_3 based glass.

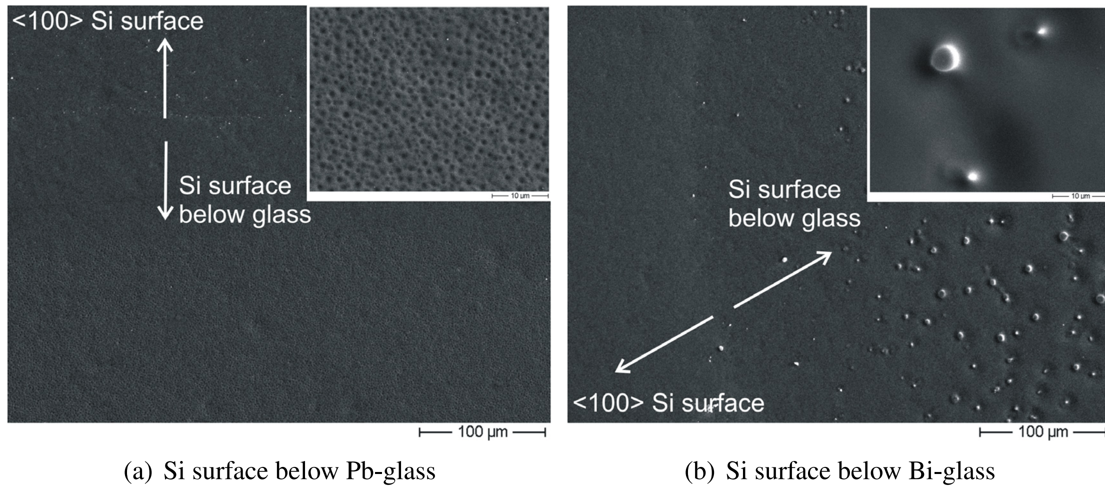

(a) Si surface below Pb-glass (b) Si surface below Bi-glass

Figure 7.14.: Silicon surface after etching off the glasses. The silicon is etched differently.

Silver growth

In a next study the silver crystal growth on silicon below lead free pastes was investigated. Six silver pastes with Bi_2O_3 containing glass frits were printed on etch polished p-type, <100> oriented FZ silicon with a 35 - 40 $\Omega/$sq emitter obtained by $POCl_3$ diffusion. The (lead containing) commercially available silver paste used throughout this work served as reference. Two fingers per paste were syringe-printed on each substrate to exclude any temperature deviation between two firing cycles. After drying, the samples were fired in the RTP furnace (ramp up/down: 20 K/s, $T_{peak} = 800$°C, dwell time: 0.5s). Subsequently, the fingers were removed in warm concentrated HCl (50°C) for 5 to 10 min followed by an HF(5%) dip for 7 to 10 min.

The silver growth using a Pb free paste is less effective than using the Pb containing reference paste. The density and size of the silver crystals increases with temperature. The SEM analysis of Ag-crystals below Pb free silver pastes with different compositions showed only very little differences. The crystal growth experiment showed clearly that Bi_2O_3 based frits need higher temperatures than the Pb reference frit to provide an efficient silver transfer process.

Summary

The main result of the experiments on Bi_2O_3 based frits is that the tested glasses need higher peak temperatures to perform similar to a lead containing reference. The main differences between lead free and leaded frits are the crystal growth and the wetting performance. The activation energies for these processes seem to be higher in the case of Bi_2O_3 based frits. These

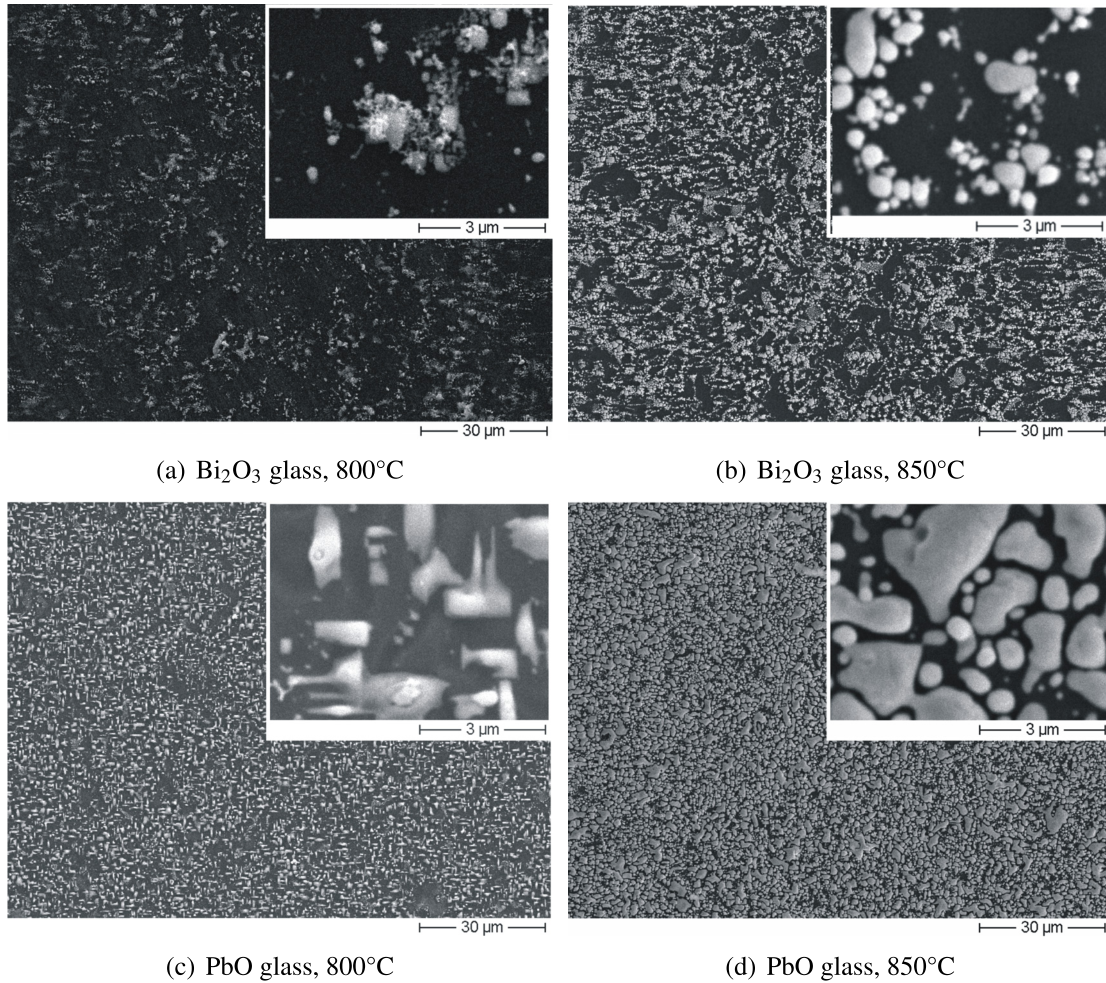

(a) Bi_2O_3 glass, 800°C

(b) Bi_2O_3 glass, 850°C

(c) PbO glass, 800°C

(d) PbO glass, 850°C

Figure 7.15.: Representative SEM pictures of the silicon surface after etching off the silver pastes. The silver crystal growth is more efficient below the leaded reference paste. However, the higher the peak temperature, the more efficient the crystal growth even below the Bi_2O_3 glass.

results lead to the assumption that the process window might be smaller in case of Bi_2O_3 fritted silver pastes: Higher temperatures are necessary for electrical contact formation but a higher temperature results in a higher etch rate.
The transformation temperature showed a clear correlation with the Bi_2O_3 glass composition. The silicon wetting also showed the same tendency. The composition of the glass frit seems to determine the etching rate into silicon to a great extend. The ability to provide an efficient silver crystal growth was very similar for all tested compositions. However, cell results obtained with the different pastes resulted in differences in efficiency and fill factor. The differences in fill factor were related to the contact resistance. As the crystal growth was found to be independent of the glass composition within the accuracy of measurement, the differences in the contact resistance are likely to be related to the homogeneity of the contact formation process determined by the wetting of silicon nitride and the wetting of silicon. Furthermore, the thickness of the glass layer separating silver crystals and silver finger is supposed to be responsible for the different contact resistances. As first tests revealed that a forming gas anneal can lower the contact resistance of Bi_2O_3 based pastes to a phosphorous doped emitter significantly, in the next section the influence of the forming gas anneal on solar cells with lead free front contacts is investigated.

7.4. Solar cells with lead free silver thick film metallisation

7.4.1. Influence of forming gas anneal

Comparing innovative just developed lead free front side silver pastes with an established leaded reference paste on cell level is difficult, because the performance of a paste depends not only on the glass frit but on many other parameters like printing properties, particle size, amount of glass frit, binder, etc. The firing conditions vary from paste to paste so that a time consuming optimisation would be necessary. An effective way to study the potential of a lead free silver paste is to apply a forming gas anneal after firing. The FGA was performed on cells processed at ECN and RWE SCHOTT Solar. Cz silicon solar cells (40Ω/sq emitter, pyramidal surface texture, SiN_x ARC) were screen-printed with a reference aluminium thick film paste and lead free silver test pastes provided by Metalor. At ECN and at RWE SCHOTT Solar different firing profiles were applied to reach high efficiencies. To demonstrate the potential of lead free silver thick film pastes, in the frame of this work a forming gas anneal was applied to several cells. In Figure 7.16 the potential of two lead free silver pastes is shown. After the forming gas anneal the fill factor of cells, printed with two different lead free thick film pastes, increased to values comparable to the fill factors reached on reference cells. The underlying mechanism is supposed to be similar to the mechanism described in chapter 6.5. The metal oxides (mainly Bi_2O_3) in the glass layer, separating silver crystals grown into silicon from the silver finger, are reduced to form homogeneously distributed precipitates. The tunnelling probability through the glass layer increases due to a multi-step tunnelling mechanism. It is likely that the bismuth precipitates are even more relevant for an increased tunnelling current than lead precipitates in a common lead borosilicate glass. The sheet conductivity of a lead borosilicate glass layer was found to be increased stronger after a forming gas anneal in case of containing Bi_2O_3 [112].

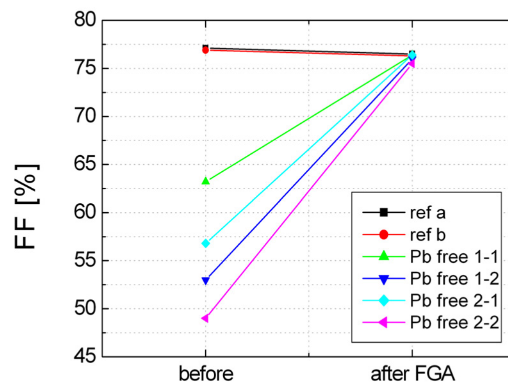

Figure 7.16.: Forming gas anneal applied to solar cells, printed with different lead free silver thick film pastes.

7.4.2. Results

The investigations on lead free glasses resulted in the development of an optimised lead free frit composition. These glasses were used to fabricate silver thick film pastes. Solar cell results obtained within the EC2Contact are very promising. Efficiencies, obtained on Cz p-type silicon with a pyramidal surface texture, SiN_x antireflection coating and a standard full area aluminium

back contact, were reached that are comparable with best performing lead containing silver pastes. It was not necessary to apply a forming gas anneal. In Table 7.5 results of the best cell are summarised [136,137]. To author's knowledge so far no higher efficiencies and fill factors

Paste	FF [%]	η [%]	J_{sc} [mA/cm^2]	Voc [mV]
Reference	77.7	17.0	35.7	614
Lead Free front	**77.2**	**17.0**	**35.9**	**615**

Table 7.5.: Best cell results with lead free silver front side paste

were reported for solar cells with a lead free silver thick film metallisation. The successful paste is currently commercialised by Metalor.

7.5. Summary

The development of lead free silver thick film pastes based on the contact formation model developed in chapter 5. A phase diagram survey showed that bismuth is the most promising candidate to substitute lead in the glass frit. This hypothesis was experimentally verified by studying the transport process of silver to grow onto silicon via liquid bismuth. In first tests based on the requirements of glass frits in silver pastes Pb free glass frit pastes with different active metal oxides were analysed. It was shown that bismuth based glasses are able to etch through a silicon nitride layer. Bismuth precipitates were found in the bulk of the glass after firing pure glass frit pastes on silicon, presumably due to a redox reaction between Si and $Bi_2O_{3,glass}$. ZnO based glass frit pastes showed a redox reaction, too, but the adhesion of the glass frit on silicon was reduced presumably due to the high vapour pressure of zinc at 800°C. A first test with silver pastes, based on these two pastes system, showed that the adhesion of the ZnO based silver pastes was poor. Therefore, further investigations were performed on Bi_2O_3 based glasses. It turned out that silver pastes containing these glasses need higher peak firing temperatures to provide an efficient growth of silver crystals. The etch rate and the wetting behaviour of the Bi_2O_3 based glasses on silicon depend on the glass frit composition, i.e. on the amount of Bi_2O_3 and other active metals. Silver pastes containing an optimised lead free glass frit prepared by Metalor led to the so far highest reported efficiencies for industrial Cz silicon solar cells with lead free thick film front contact metallisation obtained within the EC2Contact project. The efficiencies equal the efficiencies of an optimised leaded reference paste. The new developed pastes is currently commercialised by Metalor.

8. Development of lead and cadmium free aluminium paste

In most of the commercially available aluminium pastes a lead borosilicate glass is contained, similar to the glasses used for the silver pastes. As the aluminium paste is usually applied to the whole back surface of the wafer, the amount of consumed paste is much higher than on the front side. Consequently, the contribution of the aluminium paste to the total lead present in a finished solar cell is about 70% [131] underlining the necessity to apply lead free aluminium pastes. One task of the European research project EC2Contact [6] was therefore to develop beside a lead free silver paste a lead free aluminium paste.
In contrast to silver thick film contacts to silicon, thick film aluminium contacts to p-type silicon was subject to many publications addressing passivation quality, formation, bowing and other aspects (e.g. [138,5,139–141] and many more). Therefore, in this work the focus is on the transfer of the existing models to the development of lead free pastes. After a short review of contact formation and electrical properties the investigations on lead free fritted aluminium pastes are summarised. Within the framework of the EC2Contact project [6] a successful lead-free fritted aluminium paste was developed leading to similar electrical and superior bowing properties compared to a leaded reference. This paste is commercialised by Metalor.

8.1. Review of existing models

8.1.1. Contact formation

The basic principle of aluminium contacts to boron doped silicon is that aluminium acts as p-type dopant when incorporated into the silicon lattice. Independent of the deposition technology (evaporation or thick film techniques like screen-printing) an alloying step is incorporated that leads to the formation of an Al-doped back surface field in case of p-type silicon or to an emitter in case of n-type substrates (for latest results on this cell concept see e.g. [142]). Following the binary phase diagram of aluminium and silicon, both elements form an eutectic at $T = 577°\mathrm{C}$ [101]. Consequently, aluminium and silicon, supposed to be in intimate contact, form a liquid at temperatures exceeding the eutectic temperature. Further heating leads to dissolving of silicon in the liquid according to the phase diagram. On cooling down, silicon is transferred back to the silicon surface and recrystallises, incorporating aluminium in the concentration given by the solid solubility of Al in Si. At $T = 577°\mathrm{C}$ the melt solidifies in the eutectic composition (about 12% Si in Al). This process is well described by Loelgen [5].
The apparent difference between evaporated Al films and Al thick film pastes is that in the pastes aluminium particles are contained covered by an native oxide layer. This leads to a slightly modified contact formation process investigated amongst others by Sardi et. al [138] and more recently by Huster [140].
After combustion of the organics alloying starts at $T \geq 660°\mathrm{C}$, the melting point of aluminium, because only liquid Al is able to penetrate through the oxide shells [140]. Contact formation

starts therefore locally. During the firing process the Al_2O_3 layer grows, which has the beneficial effect that the structure is strengthened and held in place [138,140]. The transfer of silicon in liquid Al is nevertheless effective and complete. The volume in the Al_2O_3 shells is constant, however, aluminium and silicon exchange according to the phase diagram. On cooling down silicon is transferred back to the surface and recrystallises being doped with aluminium until the eutectic temperature is reached. The Al-Si melt in the particles solidify in the eutectic composition. This process is also fast and complete unless for very thick Al layers [140]. The cross section of an aluminium thick film contact on silicon after firing has the following structure according to Huster [140]. The regrown p^+-silicon, doped with aluminium, is covered by an Al-Si "lake". The amount of Al in this lake equals is the amount of Al in the thick film layer replaced by silicon. This "lake" determines the optical properties of the aluminium rear side.
Following basic argumentations, the peak temperature and the thickness of the printed Al layer defines the depth of the regrown Si layer and thus the depth of the BSF. However, it was found that for a defined thick film layer thickness a characteristic temperature exists at which the liquid Al-Si melt, present during firing, agglomerates locally [141]. At these points very deep back surface fields are measured, whereas in the surrounding of these islands only very thin BSFs are present.

8.1.2. Bowing

On cooling down the rear contact contracts more than the silicon wafer due to the large difference in the thermal coefficient of expansion (TCE) of aluminium and silicon ($TCE_{Al} = 23 \times 10^{-6}$ K^{-1}, $TCE_{Si} = 3.5 \times 10^{-6}$ K^{-1} [143]), leading to a convex bowing of the wafer. Following Huster [143] on cooling down, the contraction of the thick AL-Si layer leads to a strain of this layer and a resulting stress. The elastic limit is already reached at temperatures between 300°C and 400°C. Further cooling leads to a plastic flow of the Al-Si matrix. The stress is limited by the tensile stress. The total strain of 1.1% at room temperature divides in 0.4% elastic strain and 0.7% plastic flow.
This inherent phenomena gets more relevant with the use of thinner and larger wafer [144]. A too high bow can lead to severe problems in module fabrication. As the trend in photovoltaic industry is to minimise the consumed silicon per watt, the trend to large and thin wafers is given. Therefore, reducing the bowing is a very important issue for industrial solar cells. Several approaches are described in literature. The easiest is to reduce the amount of deposited Al. However, the BSF thickness and its homogeneity are related to the thickness of the deposited Al layer [140,145,141] leading to a loss in efficiency. Another approach is to weaken the interconnections between the particles in the rear contact, which determine the mechanical properties of the Al-Si layer after firing and therewith the maximal tensile stress. A weakening of the structure would therefore lead to a reduced bowing [143]. The interconnection between the particles can be influenced for instance by the amount of glass frit or by modifying the firing parameters [144]. A new approach was presented by Huster [143]. The bowing is completely eliminated by further plastic deformation of the Al-Si matrix. Further cooling to temperatures of about -50 K leads to a compensation of the elastic deformation by the plastic deformation. Re-heating to room temperature results in solar cells without a bow.

8.1.3. Role of the glass frit

In contrast to silver paste the glass frit in an aluminium thick film paste is not necessary for the contact formation. Al contacts and BSF formation can also be achieved by using fritless

aluminium pastes [34] or evaporated aluminium. For the development of lead free aluminium pastes it would be therefore straight forward to develop Al pastes without any glass.
However, a glass frit added to the aluminium paste has at least two important tasks. The glass, typically a lead borosilicate glass, is able to dissolve the Al_2O_3 skin covering the Al particles, at least partly. This leads to an increased sintering of the particles resulting in a significantly reduced sheet resistivity of the rear contact [138]. The strengthening of the structure as a consequence of sintering has the advantage that agglomeration of Al can be prevented thus a homogeneous BSF formation is expected. The disadvantage is, however, that this strengthening causes a higher bow (see above). Another task of the glass frit was recently investigated [146]. On cooling down boron contained in the glass can be incorporated into the silicon lattice acting as a p-type dopant as well. The doping concentration is therefore increased leading to a decreased sheet resistance of the BSF. The electrical quality is therefore frequently reported to be higher in case of fritted Al pastes [34]. It has to be taken into account that the optimal doping concentration of a BSF depends on its thickness and its gradient when considering free carrier absorption, Auger recombination, apparent electrical fields [34] and band gap narrowing effects [141].

8.2. Lead free, glass frit containing Al pastes

To make use of the beneficial effects of a glass frit, in the following an experiment is described that shows the potential of lead free glass frits in aluminium thick film pastes. This experiment, among others, served as the basis for the successful development of a lead free, glass frit containing Al paste within the EC2Contact project.

8.2.1. Experiment

Three lead free, fritted aluminium pastes, prepared by Metalor, were tested and characterised on cell level. The glass frit and its content was the same for all investigated pastes, however, the Al powder differed. Two commercially available, lead glass containing Al pastes served as reference. Two to five cells per paste were processed. Thin mc p-type silicon substrates (thickness: (169 ± 10) µm after saw damage etch (NaOH), size: (12.5x12.5) cm^2) were used because of two reasons: The sensitivity of the open circuit voltage and the effective diffusion length on the BSF properties are increased and differences in bowing can be studied easily. After an industrial cleaning procedure a 50 Ω/sq. emitter was diffused. A reference silver paste was used for screen-printing the front contacts. After drying, the Al pastes were screen-printed, dried and fired in an IR-belt furnace. The firing parameters were optimised for the reference paste system. As the front side has in general a smaller process window, the new developed rear side should match with the firing parameters of the front side. The cells were characterised measuring J-V characteristic, internal quantum efficiency and bowing. Additionally, the sheet resistance of the BSF was measured[1]. Optical microscope pictures of the silicon surface below the Al-Si structure were used to study the formation of bumps. For the latter two investigations the Al-Si contact was removed in HCL.

[1] Simplified, the sheet resistance of the BSF can be regarded as the parallel connection between the sheet resistance of the BSF and the sheet resistance of the base.

8.2.2. Results

In Figure 8.1 cell efficiencies are presented. In this experiment the two reference Al pastes performed slightly better due to a higher open circuit voltage (Figure 8.1(b)). The fill factor of all cells was high, exceeding 78% in all cases (8.1(c)), except for cells with paste EC2CAL17. Cells of the other groups showed even fill factors above 79%. This is a hint that the sheet resistance of the lead free Al contacts is not limiting, but in case of paste EC2CAL17 the powder system might have an influence on the series resistance.

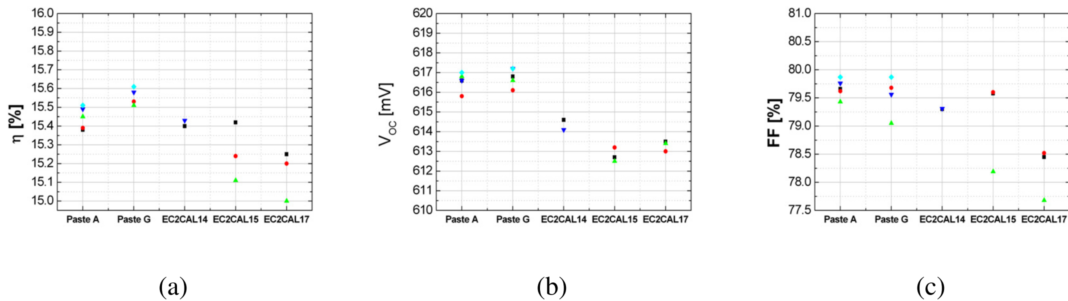

(a) (b) (c)

Figure 8.1.: Lead free Al pastes on thin mc silicon wafers

Measurement of the spectral response and the reflection led to internal quantum efficiencies showed in Figure 8.2. The quantum efficiency in the long wavelength range is lowered in case of the lead free Al pastes leading to lower effective diffusion length in correlation with the V_{oc} measurements. This indicates that the BSF performance in case of the lead free Al pastes is the limiting factor. Therefore, the electrical properties of the BSF was characterised in more detail.

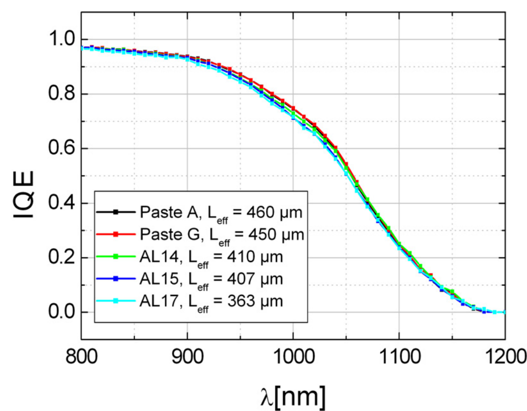

Figure 8.2.: Internal quantum efficiency of lead free Al pastes and leaded reference pastes

It was found that the sheet resistance of the BSF formed by the lead free pastes was higher than the sheet resistance of the leaded reference (see Table 8.1). A higher sheet resistance is a hint that the doping concentration in the BSF is lower and therefore the passivation quality of the BSF might be reduced. This would explain the reduced effective diffusion length and the lower open circuit voltage.
Careful weighting of the solar cells before and after printing, after drying and after firing led to the extraction of the amount of Al deposited on the wafer (Table 8.1). In case of the lead free

pastes less aluminium was deposited although using the same screen. This is likely to be one reason for the lower electrical performance. Another reason might be that the boron content in the lead free pastes was not high enough.
The investigation of the silicon surface below the Al thick film contact with an optical micro-

Paste	$R_{sheet,BSF}$ [Ω/sq]	dep. Al [g/cm^2]
A	17	11
G	23	12
EC2CAL14	43	6.9
EC2CAL15	43	7.6
EC2CAL17	38	7.5

Table 8.1.: Sheet resistance of the BSF.

scope revealed a tendency towards bump formation for all investigated lead free pastes (Figure 8.3). The firing conditions were, however, the same. As the amount of deposited Al was less in case of the lead free paste, the hypothesis of Meemongkolkiat et al. [141] that bump formation depends only on the thickness of the Al layer and the peak firing temperature and not on the paste composition could not be verified in this case[2]. The inhomogenous BSF is likely to be another reason for the reduced open circuit voltage.

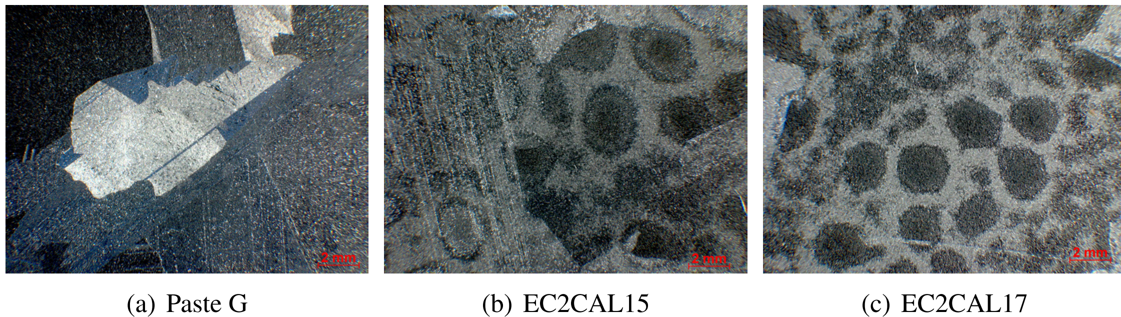

(a) Paste G (b) EC2CAL15 (c) EC2CAL17

Figure 8.3.: Optical microscope pictures of silicon surface below the formed Al thick film contact. Below the lead free pastes "potato" like structures are visible indicating agglomeration of the Al-Si lake during contact formation.

From Figure 8.4 it can be deduced that bowing is less in case of the lead free pastes. However, the different amount of deposited Al makes it difficult to interpret the origin for the measured bow.
Conclusively, it can be stated that the lead free, glass frit containing Al pastes have the potential to reach efficiencies comparable or higher than leaded reference pastes. The experiment described above served as one basis for further developments with modified pastes. The test pastes, fabricated by Metalor, were mainly tested by the project partner RWE SCHOTT Solar in an industrial solar cell production line. It could be shown that bowing is reduced by 20% in case of using lead free glass frits in Al pastes, even if comparable amounts of Al are deposited on a wafer [137].
It is likely that the reduced bowing originates from a weaker structure of the Al-Si particles after firing. It can be supposed that the lead free glass frit leads to less effective sintering. However,

[2]It is assumed that the cell temperature in the belt furnace differs only slightly with the different amount of deposited aluminium.

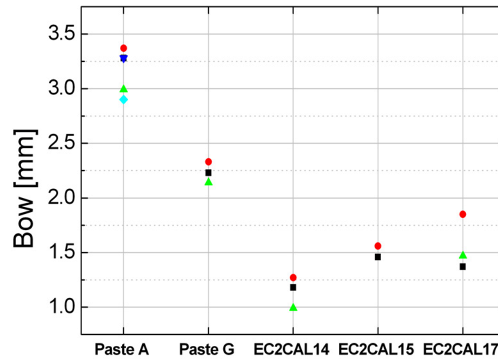

Figure 8.4.: Bowing of thin solar cells in dependence of the AL paste.

the sheet resistance of the lead free layer was not found to be reduced remarkably.

The optimised lead free, fritted Al paste led to comparable results as the reference paste on 100 cm^2 Cz solar cells with a 55-60 Ω/sq emitter [137] (Table 8.2). The bowing is reduced. This paste is currently commercialised by Metalor.

Paste	η [%]	FF [%]	J_{sc} [mA/cm^2]	V_{oc} [mV]	Bowing [µm]
Reference	17.1	76.8	36.2	614	598
Lead free rear	**17.1**	**76.5**	**36.4**	**614**	**500**

Table 8.2.: Best cell results for the developed lead free Al paste [137]

8.3. Summary

In this chapter the development of lead free, glass frit containing aluminium pastes is described. A review of contact formation models pointed out that the glass frit is not essential for the formation of a back surface field below an aluminium contact. However, the glass frit has two important beneficial effects. It reduces the sheet resistance of the Al-Si matrix after firing and boron is incorporated in the BSF leading to better passivation properties. Based on this model lead free, glass frit containing aluminium thick film pastes were prepared by Metalor and tested. First experiments on thin mc silicon solar cells showed that it was necessary to optimise the paste system slightly. The sheet resistance of the BSF was higher than the resistance obtained with leaded reference pastes and the BSF formation was partly inhomogenous. This analysis served as a basis for the development of further optimised lead free, glass frit containing aluminium pastes. Cells with the new developed Al paste processed in the production line of RWE SCHOTT Solar showed efficiencies equal to the efficiencies obtained with optimised reference pastes. Furthermore, the bowing was found to be reduced presumably due to less effective sintering of the Al-Si matrix.

9. Summary

This thesis dealt with the fundamental understanding of thick film contacts to crystalline silicon solar cells. The approach of this work was to separate competing processes and to develop models for contact formation and electrical conduction. These models were successfully applied to develop lead free silver and aluminium thick film pastes for the metallisation of crystalline silicon solar cells. Optimised pastes, developed within the EU research project EC2Contact and based on the fundamental studies, led to the fabrication of industrial solar cells with the highest efficiency for lead free metallisation pastes published so far (17% on Cz silicon), comparable to result obtained with optimised lead containing reference pastes. The pastes are currently commercialised by the project partner Metalor. In the following the results obtained in this work are described in more detail.

The analysis of the fabrication process of industrial crystalline silicon solar cells revealed that the co-firing process step used to form the front and rear side contact is the most complex one. Not only the metal - silicon contacts are formed, but the lateral resistance in the metal layers is lowered. Defects in the material are passivated by hydrogen diffusion from the silicon nitride layer, the antireflection coating, into the bulk of the silicon substrate. Additionally, the surface passivation quality of SiN_x improves and a back surface field is formed below the aluminium contact leading to an efficient rear side passivation.

Loss analyses of state-of-the-art industrial solar cells showed that silver thick film metallisation applied on phosphorous doped emitters is an essential limiting factor for reaching higher efficiencies. Only highly doped emitters with a low sheet resistance in the range of 40 Ω/sq to 70 Ω/sq are able to be contacted with specific contact resistivity below 10 mΩcm^2, low enough to allow for fill factor above 77%. The highly doped emitter with a deep junction depth leads to voltage and current losses due to excessive recombination. Therefore, the main focus of this work was on the fundamental understanding of silver thick film contacts and their formation.

The resistivity of silver thick film fingers is about two to three times higher than the bulk resistivity of pure silver. To study the potential of silver sintering in a fast firing sequence, a new measurement method was developed. With the in-situ line resistance measurement for the first time it was possible to gain insight in the kinetics of rapid sintering process. It was shown that rapid sintering of the silver particles starts at $T > 580°C$ for the investigated commercially available silver thick film paste. At this temperature typically used lead borosilicate glasses are fluid. Rapid sintering in fast firing sequences is therefore supposed to occur via a rearrangement process of the silver particles supported by the fluid glass. In fast firing sequences the differences in line resistance due to the various silver particle size and shape distributions is small. With the in-situ line resistance measurement it was shown that a dwell time $t > 50$ s at $T = 800°C$ leads to a saturation of the line resistance. The minimal resistivity achievable with silver thick film pastes is basically independent of the silver particle size and shape.

Microstructure analyses of formed silver thick film contacts to phosphorous doped emitters

showed that silver crystals have been grown into the silicon. These crystals are covered by a glass layer, separating them from the silver finger. The glass layer thickness increases with increasing firing temperature. No hints for direct interconnections between silver crystals and the silver of the bulk of the finger were found. However, the separating glass layer is very thin (below 1 nm) at some locations. The crystals grow preferentially on [111] planes of the silicon. The shape of the crystals depends on the silicon orientation and firing temperature. On <111> oriented silicon lens-shape crystals are obtained, on <100> oriented substrates the silver crystals grow in the shape of inverted pyramids. With increasing peak temperature the number and size of the crystals increase. The shape of most of the crystals is roundish and does not mirror the crystal orientation of the silicon any longer. Additionally, it was found that the bottom side of the silver finger is covered by lead containing precipitates.

The contact formation was studied in detail by following the approach of separating competing processes. The main focus was on the role of the glass frit. Typical lead borosilicate glasses were used to study the interaction of a glass with silver, silicon nitride and silicon. The glass wets all interaction partners equally well. Glass dissolves silver, but this process is slow at a peak temperature around 800°C.
Significant etching of a glass with a high lead oxide content in silicon starts at $T > 650$°C in fast firing processes. It was experimentally proven that silicon reduces lead oxide, contained in the glass. The lead precipitates do not wet silicon but conglomerate in the bulk of the glass.
A focus in this work was on the growth mechanism of the silver crystals. It was found that the silver growth is related to the interaction of lead oxide with silicon. Two mechanisms are supposed to occur simultaneously. One the hand silver is dissolved in the glass and the silver ions interact with the silicon in form of a redox reaction. However, the dissolution process is slow. On the other hand it was found that liquid lead, the reaction product of the glass - silicon interaction, interacts with silver and serves as a transport medium for silver to grow into the silicon. This process is fast and is therefore supposed to be dominating. In pastes with a high amount of silver lead is supposed to be dissolved in the silver finger so that no lead precipitates are found in the bulk of the glass layer. The existence of lead containing precipitates on the bottom of silver thick film fingers supports this hypothesis.
Silver crystal growth depends on the surface phosphorous concentration. On emitters with a chemical phosphorous concentration exceeding the solid solubility limit of phosphorous in silicon silver crystal growth starts to be significant at lower temperatures compared to silver growth on emitters with a surface phosphorous concentration below 1×10^{20} cm^{-3}. Higher peak temperatures or longer dwell times are necessary to enhance silver growth. One reason for unsuccessful contacting of moderately doped emitters so far was identified to be the insufficient silver crystal growth. Additionally, the silver crystal growth is supported by textured surfaces, exhibiting a large fraction of [111] oriented silicon planes.

Numerical simulations were performed to study the effect of the contact geometry and the doping profile on the contact resistivity in metal - semiconductor contacts. It was found that the geometry has only a minor effect on the contact resistivity. The surface near regions of the emitter determine the contact resistivity. The silver crystals grown into the silicon were found to be indispensable for the current transport. The contact resistivity of a single silver crystal to moderately doped emitters ($N_D = 6 \times 10^{19}\,\text{cm}^{-3}$) was measured to be in the range of $\rho_{C,\text{singlecrystal}} = 7$ to $60 \times 10^{-7}\ \Omega\text{cm}^2$), close to the simulated values. Even a crystal coverage of 0.1% would be sufficient to reach sufficient low macroscopic contact resistivities smaller than 10 mΩcm^2 assuming direct connections between silver fingers and crystals. Two limiting fac-

tors determine the macroscopic contact resistivity of silver thick film contacts. 1. The number of silver crystals grown into the silicon and 2. the current transport from the silver crystal to the silver finger. The current transport from the crystals into the silver finger is supposed to occur via tunnelling through the glass layer at locations where it is very thin. At higher temperatures the average glass layer thickness increases leading to a higher contact resistance.
The efficiency of overfired cells, limited by a thick glass layer between the silver crystals and the silver finger, can be improved by a forming gas anneal at $T > 375°C$ for at least 15 min in a tube furnace. The forming gas anneal has a significant influence on ρ_C and thus on the series resistance related losses, only. Other parameters are not remarkably influenced. No changes in the silver coverage or in the silver crystal size were detected. Hydrogen is necessary. Annealing in N_2 or O_2 led to a decrease of efficiency. It is likely that hydrogen reduces metal oxides in the glass. The metal precipitates are supposed to act as tunnelling centres. The current is then supposed to be transported via a multi-step tunnelling mechanism from precipitate to precipitate leading to an increased conductivity of the glass layer. The average resistance between crystals and finger was measured to drop to $\approx 1-2\%$ of the initial value. The reaction cannot be reversed by a subsequent anneal in oxygen. The beneficial effect proved to be long term stable for at least 17 months.

The combination of the contact formation and the current transport model led to the successful fabrication of a solar cell with a moderately doped emitter ($N_{D,surface} = 4 \times 10^{19}$ cm^{-3}). Standard commercially available silver thick film pastes were used in a co-firing process. The firing process was performed at a high peak temperature ($T = T_{opt} + 50$ K) so that enough crystals were grown. A subsequent forming gas anneal led to a series resistance of 0.7 Ωcm^2 being the lowest so far reported for silver thick film contacts on moderately doped emitters. FF and V_{oc} were limited by a high J_{02} current leading to an efficiency of 14.9% (untextured surface). It was shown that it is in principal possible to contact moderately doped emitters with silver thick film pastes even when using standard pastes. The process sequence has to be slightly modified due to the necessity of a forming gas anneal step. Regarding a transfer to the solar cell industry, it was shown that it is possible to anneal solar cells in a stack guaranteeing a high throughput rate.

The contact formation model was the basis to develop a lead free silver thick film paste. Bismuth was found to interact with silver, silicon nitride and silicon similarly to lead. In liquid phase bismuth can serve as a transport medium for silver to grow into silicon. Bi_2O_3 based glasses were characterised regarding wetting and etching of silicon and silicon nitride and the ability to serve as a transport medium for silver growth. Based on these studies an optimised glass frit was developed within the EC research project EC2Contact and successfully applied in silver thick film pastes. The best Cz industrial solar cell processed with the lead free silver paste within the EC2Contact consortium showed an efficiency of 17.0% and a fill factor of 77.2% on Cz silicon equal to an optimised leaded reference paste. To the author's knowledge this is the highest reported efficiency for lead free silver pastes so far.

To develop lead free aluminium pastes, it was made use of the beneficial effect of a glass frit to incorporate boron in the BSF and to reduce the sheet resistance of the Al-Si layer after firing due to effective sintering. Within the EC2Contact project a successful fritted but lead free aluminium thick film paste was developed. The best cell results are equal to the results obtained with the optimised reference paste. The lead free Al paste has the positive effect that the bow is reduced by 15-20%.

References

[1] W. P. Hirshman and M. Schmela, “Silicon shortage - so what! Market survey on cell and module production 2005,” *Photon International*, no. 3, pp. 100–125, 2006.

[2] “DIRECTIVE 2002/96/EC OF THE EUROPEAN PARLIAMENT AND OF THE COUNCIL of 27 January 2003 on the restriction of the use of certain hazardous substances in electrical and electronic equipment,” EC, 2003.

[3] M. de Wild-Scholten, K. Wambach, E. Alsema, and A. Jäger-Waldau, “Implications of European environmental legislation for photovoltaic systems,” in *Proc. 20th EC PVSEC*, Barcelona, 2005, pp. 3143–3147.

[4] A. D. Haigh, “Fired through printed contacts on antireflection coated silicon terrestrial solar cells,” in *Proc. 12th IEEE PVSC*, 1976, pp. 360–361.

[5] P. Lölgen, “Surface and volume recombination in silicon solar cells,” Ph.D. dissertation, University of Utrecht, 1995.

[6] EC2Contact, “FP5 program EC2Contact project (#enk6-ct-2001-00560),” EC, 2001.

[7] JSC Pillar, 2006. [Online]. Available: http://www.pillar.com.ua/

[8] C. Gerhards, “Mechanisch texturierte, großflächige mulikristalline Siliziumsolarzellen,” Ph.D. dissertation, University of Konstanz, 2002.

[9] A. Hauser, I. Melnyk, P. Fath, S. Narayanan, S. Roberts, and T. M. Bruton, “A simplified process for isotropic texturing of mc-Si,” in *Proc. 3rd WCPEC*, Osaka, 2003, pp. 1447–1450.

[10] A. Hauser, G. Hahn, M. Spiegel, H. Feist, O. Breitenstein, J. Rakotoniaina, P. Fath, and E. Bucher, “Comparison of different techniques for edge isolation,” in *Proc. 17th EC PVSEC*, Munich, Germany, 2001, pp. 1739–1746.

[11] W. Wolke, J. Catoir, R. Preu, G. Emanuel, J. Liu, and M. Ruske, “Surface passivation for solar cells by large scale inline sputtering of silicon nitride,” in *Proc. 20th EC PVSEC*, Barcelona, Spain, 2005, pp. 733–736.

[12] M. Ruske, J. Liu, S. Wieder, R. Preu, and W. Wolke, “A large area production technology for solar cells - sputter deposition of SiN:H,” in *Proc. 20th EC PVSEC*, Barcelona, Spain, 2005, pp. 1470–1473.

[13] C. Tool, G. Coletti, F. Granek, J. Hoornstra, M. Koppes, E. Kossen, H. Rieffe, I. Romijn, and A. Weeber, “17% mc-Si solar cell efficiency using full in-line processing with improved texturing and screen-printed contacts on high-ohmic emitters,” in *Proc. 20th EC PVSEC*, Barcelona, Spain, 2005, pp. 578–583.

[14] P. J. Holmes and R. G. Loasby, *Handbook of Thick Film Technology*. Glasgow: Electrochemical Publications Ltd, 1976.

[15] E. L. Ralph, “Recent advancements in low cost solar cell processing,” in *Proc. 11th IEEE PVSC*, Scottsdale, Arizona, 1975, pp. 315–316.

[16] Koenen GmbH, 2006. [Online]. Available: http://www.koenen.de

[17] K. Kautio, “Fine line screen printing in LTCC,” in *Research Activities in Optoelectronics and Electronics Manufacturing*. Finnland: VTT Electronics, 2002, pp. 32–34.

[18] M. Haskard and K. Pitt, *Thick Film Technology and Applications*. Glasgow: Electrochemical Publications Ltd, 1997.

[19] F. Huster, M. Spiegel, P. Fath, E. Bucher, T. Denner, and K. Schanz, “Progress of the roller-printing metallisation technique towards an industrially compatible alternative to screen printing,” in *Proc. 16th EC PVSEC*, Glasgow, Great Britain, 2000, pp. 1385–1388.

[20] F. Huster, P. Fath, and E. Bucher, “Roller printed mc-Si solar cells with optimized fill factors of 78%,” in *Proc. 17th EC PVSEC*, Munich, Germany, 2001, pp. 1743–1746.

[21] J. Hoornstra, S. Roberts, H. de Moor, and T. Bruton, “First experiences with double layer stencil printing for low cost production solar cells,” in *Proc. 2nd WPVSC*, Vienna, Austria, 1998, pp. 1527–1530.

[22] J. Hoornstra, 2006, private communication.

[23] G. Yao, J. Zhao, and J. E. Cotter, “Metal stencil-printed selective emitter silicon solar cell fabrication on CZ wafer,” in *Proc. 20th EC PVSEC*, Barcelona, Spain, 2005, pp. 749–752.

[24] P. Hahne, I. E. Reis, E. Hirth, D. Huljic, R. Preu, H. de Buhr, K. Schwichtenberg, and H. Ipsen, “Pad printing - a novel thick-film technique of fine line printing for solar cells,” in *Proc. 2nd WPVSC*, Vienna, Austria, 1998, pp. 1646–1649.

[25] P. Hahne, E. Hirth, I. E. Reis, K. Schwichtenberg, W. Richtering, F. M. Horn, and U. Eggenweiler, “Progress in thick-film pad printing technique for solar cells,” *Solar Energy Materials & Solar Cells*, vol. 65, pp. 399–407, 2001.

[26] D. M. Huljic, E. Hirth, R. Lüdemann, and G. Willeke, “Large area crystalline silicon solar cells with pad printed front side metallisation,” in *Proc. 17th EC PVSEC*, Munich, Germany, 2001, pp. 1582–1585.

[27] J. Hoornstra, A. W. Weeber, H. H. C. de Moor, and W. C. Sinke, “The importance of paste rheology in improving fine line, thick film screen printing of front side metallization,” in *Proc. 14th EC PVSEC*, Barcelona, Spain, 1997, pp. 823–826.

[28] Y. S. Chung and H. G. Kim, “Effect of oxide glass on the sintering behavior and electrical properties in Ag thick films,” *IEEE Transactions on components*, vol. 11, no. 2, pp. 195–199, 1988.

[29] H. Z. Wu and R. W. Vest, “Densification and adhesion of silver thick film conductors,” *International Journal of Hybrid Microelectronics*, vol. 10, no. 4, pp. 20–24, 1987.

[30] V. K. Nagesh and R. M. Fulrath, “Electrical conduction in glass-metal composite materials,” *Ceramic Bulletin*, vol. 58, no. 4, pp. 455–458, 1979.

[31] J. M. A. H. Lamneck, “A new electric field effect in silicon solar cells,” *Journal of Applied Physics*, vol. 44, no. 10, pp. 4785–4787, 1973.

[32] S. M. Sze, *Physics of Semiconductor Devices*. New York: John Wiley & Sons Inc., 1981.

[33] A. Goetzberger, B. Voß, and J. Knobloch, *Sonnenenergie: Photovoltaik*. Stuttgart: B.G. Teubner, 1997.

[34] B. Fischer, “Loss analysis of crystalline silicon solar cells using photoconductance and quantum efficiency measurements,” Ph.D. dissertation, University of Konstanz, 2003.

[35] B. Fischer, P. Fath, and E. Bucher, “Evaluation of solar cell J(V)-measurements with a distributed series resistance model,” in *Proc. 16th EC PVSEC*, Glasgow, Great Britain, 2000, pp. 1365–1368.

[36] A. S. H. van der Heide, A. Scönecker, J. H. Bultmann, and W. C. Sinke, “Explanation of high solar cell diode factors by non-uniform contact resistance,” *Progress in Photovoltaics*, vol. 13, no. 1, pp. 3–16, 2005.

[37] M. Stocks and D. Macdonald, “Non-ideal resistive effects in silicon solar cells,” in *Proc. 16th EC PVSEC*, Glasgow, Great Britain, 2000, pp. 1671–1674.

[38] M. A. Green, *Solar Cells, Operating Principles, Technology and System Applications*. Kensington: University of New South Wales, 1998.

[39] I. Melnyk, E. Wefringhaus, F. Delahaye, G. Vilsmeier, W. Mahler, and P. Fath, “High throughput in-line acidic texturisation and edge isolation: An industrial reality,” in *Proc. 20th EC PVSEC*, Barcelona, Spain, 2005, pp. 1403–1406.

[40] A. Hauser, I. Melnyk, E. Wefringhaus, F. Delahaye, G. Vilsmeier, and P. Fath, “Acidic texturisation of mc-Si using a high throughput in-line prototype system with no organic chemistry,” in *Proc. 19th EC PVSEC*, Paris, France, 2004.

[41] M. A. Green, *Silicon Solar Cells, Advanced Priciples & Practice*. Sydney: Centre for Photovolaic Devices and Systems, 1995.

[42] A. G. Aberle, *Crystalline Silicon Solar Cells - Advanced Surface Passivation and Analysis*. UNSW: Centre for Photovolaic Engineering, 1999.

[43] A. Bentzen, E. S. Marstein, R. Kopecek, and A. Holt, “Phosphorus diffusion and gettering in multi-crystalline silicon solar cell processing,” in *Proc. 19th EC PVSEC*, Paris, France, 2004, pp. 935–938.

[44] O. Schultz, S. W. Glunz, G. Willeke, A. Leimenstoll, H. Lautenschlager, and J. Goldschmidt, “Thermal oxidation processes for high-efficiency multicrystalline silicon solar cells,” in *Proc. 19th EC PVSEC*, Paris, France, 2004, pp. 604–607.

[45] A. Bentzen, G. Schubert, J. S. Christensen, B. Svensson, and A. Holt, “The influence of temperature during phosphorus emitter diffusion from a spray-on source in multicrystalline silicon solar cell processing,” *submitted to Progress in Photovoltaics*, 2006.

[46] G. Hahn, A. Schönecker, A. R. Burgers, R. Ginige, K. Cherkaoui, and D. Karg, “Hydrogen kinetics in crystalline silicon - PECVD SiN studies in mc and Cz silicon,” in *Proc. 20th EC PVSEC*, Barcelona, Spain, 2005, pp. 717–720.

[47] S. W. Glunz, E. Schäffer, S. Rein, K. Bothe, and J. Schmidt, “Analysis of the defect activation in Cz silicon by temperature-dependent bias-induced degradation of solar cells,” in *Proc. 3rd WCPEC*, Osaka, Japan, 2003, p. 919.

[48] K. Bothe and J. Schmidt, “Electronically activated boron-oxygen-related recombination centres in crystalline silicon,” *Journal of Applied Physics*, vol. 99, no. 1, p. 13701.

[49] A. Herguth, “Degradationsuntersuchungen an verschiedenen Silizium Solarzellen-Typen,” Master’s thesis, University of Konstanz, 2006.

[50] A. Herguth, G. Schubert, M. Kaes, and G. Hahn, “A new approach to prevent the negative impact of the metastable defect in boron doped cz silicon solar cells,” in *Proc. 4th WCPEC*, Hawaii, USA, 2006, in print.

[51] P. A. Basore, “Extended spectral analysis of internal quantum efficiency,” in *Proc. 23rd IEEE PVSC*, 1993, pp. 147–152.

[52] B. Fischer, M. Keil, P. Fath, and E. Bucher, “Scanning IQE-measurements for accurate current determination on very large area solar cells,” in *Proc. 19th IEEE PVSC*, 2002, pp. 454–457.

[53] A. Bentzen, A. Holt, J. S. Christensen, and B. G. Svensson, “High concentration in-diffusion of phosphorus in Si from a spray-on source,” *Journal of Applied Physics*, vol. 99, no. 6, p. 64502, 2006.

[54] S. M. Sze, *Semiconductor Devices Physics and Technology*. New York: John Wiley & Sons Inc., 1985.

[55] P. A. Basore and D. A. Clugston, “PC1D Version 5: 32-bit solar cell modeling on personal computers,” in *Proc. 26th IEEE PVSC*, Anaheim, 1997, p. 207.

[56] M. J. Kerr, J. Schmidt, A. Cuevas, and J. H. Bultmann, “Surface recombination velocity of phosphorus-diffused silicon solar cell emitters passivated with plasma enhanced chemical vapor deposited silicon nitride and thermal silicon oxide,” *Journal of Applied Physics*, vol. 89, no. 7, pp. 3821–3826, 2001.

[57] I. G. Romijn, H. Rieffe, A. Weeber, and W. Soppe, “Passivating mc-Si solar cells using SiNx:H: How to tune to maximum efficiencies,” in *Proc. 15th PVSEC*, Shanghai, China, 2005, in print.

[58] B. Fischer, "IV-CC - Program for evaluation of solar cell IV-Characteristics," University of Konstanz, 2000.

[59] D. K. Schroder, *Semiconductor Material and Device Characterization*. New York: John Wiley & Sons Inc., 1998.

[60] B. Fischer, "Metallisation of silicon solar cells," Master's thesis, ANU, Canberra, 1994.

[61] O. Breitenstein and O. Langenkamp, *Lock-in Thermography*. Berlin: Springer Verlag, 2003.

[62] M. Kaes, S. Seren, T. Pernau, and G. Hahn, "LIMOLIT - a novel thermographic characterisation method for p/n structures and solar cells," in *Proc. 19th EC PVSEC*, Paris, France, 2004, pp. 484–487.

[63] G. Schubert, "Untersuchung der Dickfilmmetallisierung für kristalline Silizium-Solarzellen," Master's thesis, University of Konstanz, 2002.

[64] F. Huster, S. Seren, G. Schubert, M. Kaes, G. Hahn, and O. Breitenstein, "Shunts in silicon solar cells below screen printed silver contacts," in *Proc. 19th EC PVSEC*, Paris, France, 2004, pp. 832–835.

[65] M. McCann, B. Raabe, W. Jooss, R. Kopecek, and P. Fath, "18.1% efficiency for a large area, multi-crystalline silicon solar cell," in *Proc. 4th WCPEC*, Hawaii, USA, 2006, in print.

[66] W. D. Kingery, "Densification during sintering in the presence of a liquid phase. i. theory," *Journal of applied physics*, vol. 30, no. 3, p. 301, 1959.

[67] R. M. German and B. H. Rabin, "Enhanced sintering through second phase additions," *Powder Metallurgy*, vol. 28, no. 1, pp. 7–12, 1985.

[68] R. M. German, S. Farooq, and C. M. Kipphut, "Kinetics of liquid phase sintering," *Material Science and Engineering*, vol. A105/106, pp. 215–224, 1988.

[69] P. E. Zovas, R. M. German, K. S. Hwang, and C. J. Li, "Activated and liquid-phase sintering - progress and problems," *Journal of Metals*, vol. 1, pp. 28–33, 1983.

[70] T. Sun, J. Miao, R. Lin, and Y. Fu, "The effect of baking conditions on the effective contact areas of screen-printed silver layer on silicon substrate," *Solar Energy Materials & Solar Cells*, vol. 85, pp. 73–83, 2005.

[71] O. V. Mazurin, M. V. Streltsina, and T. P. Shvaiko-Shvaikovskaya, *Physical Sciences data 15, Handbook of Glass Data, Part C Ternary Silicate Glasses*. Amsterdam: Elsevier Science Publishers B.V., 1987.

[72] M. Prudenziati, L. Moror, B. Morten, and F. Sirotti, "Ag-based thick film front metallization of silicon solar cells," *Active and Passive Electrical Compounds*, vol. 13, pp. 133–150, 1989.

[73] C. Ballif, D. M. Huljic, G. Willeke, and A. Hessler-Wyser, "Silver thick-film contacts on highly doped n-type silicon emitters: Structural and electronic properties," *Applied Physics Letters*, vol. 82, no. 12, pp. 1878–1880, 2003.

[74] M. Hilali, K. Nakayashiki, C. Khadilkar, R. Reedy, A. Rohatgi, A. Shaikh, S. Kim, and S. Sridharan, “Effect of Ag particle size in thick film Ag paste on the electrical and physical properties of screen printed contacts and silicon solar cells,” *Journal of the Electrochemical Society*, vol. 153, no. 1, pp. A5–A11, 2006.

[75] C. Khadilkar, S. Sridharan, T. Pham, A. Shaikh, and S. Kim, “Characterization of front contact in a silicon solar cell,” in *Proc. Technical Digest of the International PVSEC-14*, Bangkok, 2004.

[76] C. Khadilkar, S. Sridharan, D. Gnizak, T. Pham, S. Kim, and A. Shaikh, “Effect of glass chemistry and silicon orientation on the front contact microstructure formation in a silicon solar cell,” in *Proc. 20th EC PVSEC*, Barcelona, Spain, 2005, pp. 1291–1296.

[77] D. M. Huljic, C. Ballif, A. Hessler-Wyser, and G. Willeke, “Microstructural analysis of Ag thick-film contacts on n-type silicon emitters,” in *Proc. 3rd WCPEC*, Osaka, 2003.

[78] G. Grupp, D. M. Huljic, R. Preu, G. Willeke, and J. Luther, “Peak firing temperature dependence of the microstructure of Ag thick-film contacts on silicon solar cells - a detailed AFM study of the interface,” in *Proc. 20th EC PVSEC*, Barcelona, Spain, 2005, pp. 1379–1382.

[79] M. Hilali, M. Al-Jassim, B. To, H. Mountinho, A. Rohatgi, and S. Asher, “Understanding the formation and temperature dependence of thick-film Ag contacts on high-sheet-resistance Si emitters for solar cells,” *Journal of the Electrochemical Society*, vol. 152, no. 10, pp. G742–G749, 2005.

[80] R. Mertens, M. Eyckmans, G. Cheek, M. Honore, and R. V. Overstraeten, “Critical processing parameter optimization for screen printed semicrystalline silicon solar cells,” in *Proc. 17th IEEE PVSC*, 1984, pp. 1347–1351.

[81] G. C. Cheek, R. P. Mertens, R. V. Overstraeten, and L. Frisson, “Thick-film metallization for solar cell applications,” *Transactions on electron devices*, vol. ED-31, no. 5, pp. 602–609, 1984.

[82] C. Ballif, D. M. Huljic, A. Hessler-Wyser, and G. Willeke, “Nature of the Ag-Si interface in screen-printed contacts: a detailed transmission electron microscopy study of cross-sectional structures,” in *Proc. 29th IEEE PVSC*, 2002, pp. 360–363.

[83] M. V. Craen, L. Frisson, and F. Adams, “SIMS study of the penetration of metallic secondary impurities in screen-printed silicon solar cells,” *Surface and Interface Analysis*, vol. 6, no. 6, pp. 257–260, 1984.

[84] A. F. Holleman and E. Wiberg, *Lehrbuch der anorganischen Chemie*. Berlin: Walter de Gruyter, 1985.

[85] R. J. S. Young and A. F. Carroll, “Advances in front-side thick film metallisation for silicon solar cells,” in *Proc. 16th EC PVSEC*, Glasgow, Great Britain, 2000, p. VD3.63.

[86] W. Vogel, *Glaschemie*. Leipzig: VEB Deutscher Verlag für Grundstoffindustrie, 1979.

[87] G. Schubert, B. Fischer, and P. Fath, “Formation and nature of Ag thick film contacts on crystalline silicon solar cells,” in *Proc. PV in Europe Conference*, Rome, Italy, 2002, pp. 343–346.

[88] V. K. Nagesh, A. P. Tomsia, and J. A. Pask, “Wetting and reactions in the lead borosilicate glass-precious metal systems,” *Journal of Material Science*, vol. 18, pp. 2173–2180, 1983.

[89] B. Forti, A. F. Gualtieri, M. Leoni, M. Prudenziati, and C. C. Tang, “Kinetics of Ag distribution in high lead glass by real time synchrotron powder diffraction,” *Materials Science Forum*, vol. 321-324, pp. 1051–1055, 2000.

[90] L. Gmelin, *Gmelin Handbook of Inorganic and Organometallic Chemistry*. Berlin: Springer Verlag, 1995.

[91] D. M. Huljic, G. Grupp, J. Horzel, and R. Preu, “Comprehensive study of rapid thermal firing for industrial production of crystalline silicon thick-film solar cells,” in *Proc. 19th EC PVSEC*, Paris, 2004.

[92] R. Tölle, “Herstellung und Charakterisierung kristalliner low-cost Silizium Solarzellen,” Master’s thesis, University of Konstanz, 1997.

[93] P. Fath, “Processing, characterization and simulation of mechanically textured crystalline silicon solar cells,” Ph.D. dissertation, University of Konstanz, 1998.

[94] L. Weber, “Equilibrium solid solubility of silicon in silver,” *Metallurgical and Materials Transactions A*, vol. 33A, pp. 1145–1150, 2002.

[95] A. Hiraki, E. Lugujjo, M. A. Nicolet, and J. W. Mayer, “Low-temperature migration of silicon through metal films - importance of silicon - metal interface,” *Physica Status Solidi A*, vol. 79, pp. 401–406, 1971.

[96] A. Hiraki and E. Lugujjo, “Low-temperature migration of silicon in metal films on silicon substrates studied by backscattering techniques,” *Journal of Vacuum Science and Technology*, vol. 9, no. 1, pp. 155–158, 1972.

[97] L. Chen, Y. Zeng, P. Nyugen, and T. L. Alford, “Silver diffusion and defect formation in Si (111) substrate at elevated temperatures,” *Materials Chemistry and Physics*, vol. 76, pp. 224–227, 2002.

[98] T. Nakajima, A. Kawakami, and A. Tada, “Ohmic contact of conductive silver paste to silicon solar cells,” *International Journal of Hybrid Microelectronics*, vol. 6, no. 1, pp. 580–586, 1983.

[99] G. Schubert, F. Huster, and P. Fath, “Physical understanding of printed thick film front contacts of crystalline Si solar cells: Review of existing models and recent developments,” *Solar Energy and Materials*, vol. accepted for publication, 2006.

[100] W. Wendlandt, *Thermal Methods of Analysis*. New York: John Wiley & Sons Inc., 1974.

[101] T. B. Massalski, *Binary Alloy Phase Diagrams, 2nd Edition, Volume 1-3*. USA: ASM International, 1992.

[102] Y. Ugai, P. Fertsh, I. Mittova, V. Anokhin, and T. Gadesbskaya, “Certain general features of reactions of Si with metal oxides,” *Inorganic Materials*, vol. 13, no. 9, pp. 1304–1306, 1977.

[103] M. M. Hilali, A. Rohatgi, C. Khadilkar, S. Kim, T. Pham, J. Salami, A. Shaikh, and S. Sridharan, "Understanding and development of Ag pastes for silicon solar cells with high sheet-resistance emitters," in *Proc. 19th EC PVSEC*, Paris, 2004, pp. 1300–1303.

[104] A. S. H. van der Heide and M. J. A. A. Goris, "Contact optimisation on lowly doped emitters using the corescan on non-uniform emitter cells," in *Proc. 19th EC PVSEC*, Paris, France, 2004, pp. 701–704.

[105] H. Scholze, *Glas*. Braunschweig: Friedr. Vieweg & Sohn, 1965.

[106] R. H. Doremus, *Glass Science*. New York: John Wiley & Sons Inc., 1994.

[107] J. Zarzycki, in (R. W. Cahn, P. Haasen, and E. Kramer), *Glasses and Amporphous Materials*. Weinheim: VCH Publishers, 1991.

[108] K. Firor and S. Hogan, "Effects of processing parameters on thick film inks used for solar cell front metallization," *Solar Cells*, vol. 5, no. 1, pp. 87–100, 1981.

[109] K. Firor, S. J. Hogan, J. M. Barret, and R. T. Coyle, "Series resistance associated with thick- film contacts to solar cells," in *Proc. 16th IEEE PVSC*, 1982, pp. 824–827.

[110] O. Gzowski, L. Murawski, and K. Trzebiatowski, "The surface conductivity of bismuth contaminated lead-silicate glasses," *Journal of Non-Crystalline Solids*, vol. 41, pp. 267–271, 1980.

[111] M. Chybicki, J. Liwo, and K. Trzebiatowski, "Electrical surface conductivity modifications of lead-silicate glasses," *Physica Status Solidi A*, vol. 115, pp. K185–K189, 1989.

[112] O. Gzowski, L. Murawski, and K. Trzebiatowski, "The surface conductivity of lead glasses," *Journal of Applied Physics*, vol. 15, pp. 1097–1101, 1982.

[113] W. Schottky, "Zur Halbleitertheorie der Sperrschicht und Spitzengleichrichter," *Zeitschrift für Physik*, vol. 113, pp. 367–414, 1939.

[114] W. Schottky, "Vereinfachte und erweiterte Theorie der Randschichtgleichrichter," *Zeitschrift für Physik*, vol. 118, pp. 539–592, 1942.

[115] D. K. Schroder and D. L. Meier, "Solar cell contact resistance - a review," *IEEE Transactions on Electron Devices*, vol. 31, no. 5, pp. 637–647, 1984.

[116] E. H. Rhoderick and R. H. Williams, *Metal-Semiconductor Contacts*. Oxford: Clarendon Press, 1988.

[117] A. Y. C. Yu, "Electron tunneling and contact resistance of metal-silicon contact barriers," *Solid State Electronics*, vol. 13, pp. 239–247, 1970.

[118] J. Bardeen, "Surface states and rectification at metal semiconductor contact," *Physical Review*, vol. 71, pp. 717–727, 1947.

[119] J. M. Andrews and M. P. Lepselter, "Reverse current-voltage characteristics of metal-silicide schottky diodes," *Solid-State Electronics*, vol. 13, pp. 1011–1023, 1970.

[120] K. K. Ng and R. Liu, "On the calculation of specific contact resistivity on <100> Si," *IEEE Transaction on Electron Devices*, vol. 37, no. 6, pp. 1535–1537, 1990.

[121] J. M. Andrews, “The role of the metal-semiconductor interface in silicon integrated circuit technology,” *Journal of Vacuum Science and Technology*, vol. 11, no. 6, pp. 972–984, 1974.

[122] D. Z. Chi, W. D. Wang, S. J. Chua, and S. Ashok, “Reverse current transport mechanism in shallow junctions containing silicide spikes,” *Journal of Applied Physics*, vol. 92, no. 12, pp. 7532–7535, 2002.

[123] G. Grupp, D. Biro, G. Emanuel, R. Preu, F. Schitthelm, and G. Willeke, “Analysis of silver thick-film contact formation on industrial silicon solar cells,” in *Proc. 31st IEEE PVSC*, Orlando, Florida, 2005.

[124] A. Rohatgi, S. Narasimha, and A. Ebong, “Understanding and implementation of rapid thermal technologies for high-efficiency silicon solar cells,” *Transactions on electron devices*, vol. 46, no. 10, pp. 1970–1077, 1999.

[125] A. Ebong, M. Hilali, and A. Rohatgi, “Rapid photo-assisted forming gas anneal (FGA) for high quality screen-printed contacts for silicon solar cells,” in *Proc. 28th IEEE PVSC*, Anchorage, Alaska, 2000, pp. 264–267.

[126] U. Gerhardt, “A new conductive coating for channel electron multipliers,” *Review of Scientific Instruments*, vol. 44, no. 5, pp. 657–658, 1973.

[127] D. L. Meier, H. P. Davis, R. A. Garcia, J. A. Jesup, and A. F. Carroll, “Self-doping contacts to silicon using silver coated with a dopant source,” in *Proc. 28th IEEE PVSC*, 2000, pp. 69–74.

[128] D. L. Meier, H. P. Davis, P. Hacke, R. A. Garcia, S. Yamanaka, J. Salami, and J. A. Jesup, “Self-doping, screen-printed silver contacts applied to ibc and phostop dendritic web silicon solar cells,” in *Proc. 17th EC PVSEC*, Munich, Germany, 2001.

[129] A. Rohatgi, M. Hilali, D. L. Meier, A. Ebong, C. Honsbergh, A. F. Carrol, and P. Hacke, “Self-aligned self-doping selective emitter for screen-printed silicon solar cells,” in *Proc. 17th EC PVSEC*, Munich, Germany, 2001, pp. 1307–1310.

[130] M. Hilali, J.-W. Jeong, A. Rohatgi, D. L. Meier, and A. F. Carroll, “Optimization of self-doping Ag paste firing to achieve high fill factors on screen-printed silicon solar cells with a 100 /sq. emitter,” in *Proc. 29th IEEE PVSC*, 2002, pp. 356–359.

[131] S. Kim, T. Pham, S. Sridharan, C. Khadilkar, and A. Shaikh, “Towards development of lead-free thick film inks for crystalline silicon solar cells,” in *Proc. 20th EC PVSEC*, Barcelona, Spain, 2005, pp. 834–836.

[132] B. Ross, “Improved thick film semiconductor/solar cell contacts,” in *Proc. 2nd EC PVSEC*, 1979, pp. 222–231.

[133] B. Ross, “Screenable silver and base metal solar cell contacts,” in *Proc. 14th IEEE PVSC*, 1980, pp. 787–792.

[134] M. Eyckmans, “Fabrikatie van zonnecellen op semi-kristallijn silicium material met behulp van de zeefdruktechniek,” Ph.D. dissertation, Universiteit Leuven, 1987.

[135] W. H. Zachariasen, “The atomic arrangement in glass,” *Journal of the American Chemical Society*, vol. 54, pp. 3841–3851, 1932.

[136] J. Hoornstra, G. Schubert, K. Broek, F. Granek, and C. LePrince, “Lead free metallisation paste for crystalline silicon solar cells: From model to results,” in *Proc. 31st IEEE PVSC*, Orlando, Florida, 2005, pp. 1293–1296.

[137] J. Hoornstra, G. Schubert, C. LePrince, G. Wahl, K. Broek, F. J. Granek, B. Lenkeit, and J. Horzel, “Lead free metallisation for silicon solar cells: Results from the EC2Contact project,” in *Proc. 20th EC PVSEC*, Barcelona, 2005, pp. 651–654.

[138] L. Sardi, S. Bargioni, C. Canali, O. Davoli, M. Prudenziati, and V. Valbusa, “Some features of thick film technology for the back metallization of solar cells,” *Solar Cells*, vol. 11, pp. 51–67, 1984.

[139] A. Schneider, “Charakterisierungsverfahren und industriekompatible Herstellungsprozesse für dünne multikristalline Siliziumsolarzellen,” Ph.D. dissertation, University of Konstanz, 2004.

[140] F. Huster, “Investigation of the alloying process of screen printed aluminium pastes for the BSF formation on silicon solar cells,” in *Proc. 20th EC PVSEC*, Barcelona, Spain, 2005, pp. 1466–1469.

[141] V. Meemongkolkiat, K. Nakayashiki, D. Kim, R. Kopecek, and A. Rohatgi, “Factors limiting the formation of uniform and thick Al-back surface field and its potential,” *Journal of the Electrochemical Society*, vol. 153, no. 1, pp. G53–G58, 2006.

[142] T. Buck, R. Kopecek, J. Libal, I. Röver, K. Wambach, L. Geerligs, P. Sánchez-Friera, J. Alonso, and P. Fath, “14.4 % screen printed n-type mc-Si solar cells with Al back junction on thin large area wafers,” in *Proc. 15th PVSEC*, Shanghai, China, 2005, in print.

[143] F. Huster, “Aluminium-back surface field: Bow investigation and elimination,” in *Proc. 20th EC PVSEC*, Barcelona, Spain, 2005, pp. 635–638.

[144] A. Schneider, C. Gerhards, P. Fath, E. Bucher, R. Young, J. Raby, and A. Carroll, “Bow reducing factors for thin screenprinted mc-Si solar cells with al bsf,” in *Proc. 29th IEEE PVSC*, New Orleans, USA, 2002, pp. 336–339.

[145] V. Meemongkolkiat, M. Hilali, and A. Rohagti, “Investigation of RTP and belt fired screen printed Al-BSF on textured and planar back surfaces of silicon solar cells,” in *Proc. 3rd WCPEC*, Osaka, Japan, 2003, pp. 1467–1470.

[146] F. Huster and G. Schubert, “ECV doping profile measurements of aluminium alloyed back surface fields,” in *Proc. 20th EC PVSEC*, Barcelona, Spain, 2005, pp. 1462–1465.

List of Publications

G. Schubert, B. Fischer, and P. Fath, “Formation and nature of Ag thick film contacts on crystalline silicon solar cells,” in *Proc. PV in Europe Conference*, Rome, Italy, 2002, pp. 343–346.

G. Schubert, B. Fischer, F. Huster, and P. Fath, “The thick film front contact: Fundamentals and developments,” in *Proc. Freiberger Siliciumtage*, Freiberg, Germany, 2003, pp. 77–88.

G. Schubert, F. Huster, and P. Fath, “Physical understanding of printed thick film front contacts of crystalline Si solar cells: Review of existing models and recent developments,” *Technical Digest of the International PVSEC-14*, Bangkok, Thailand, 2004, pp. 441–442.

G. Hahn, P. Geiger, and G. Schubert, “Influence of bsf thickness and al-gettering steps on iqe and cell parameters in mc si solar cells,” in *Proc. 19th EC PVSEC*, Paris, France, 2004, pp. 1071–1074.

F. Huster, S. Seren, G. Schubert, M. Kaes, G. Hahn, and O. Breitenstein, “Shunts in silicon solar cells below screen printed silver contacts,” in *Proc. 19th EC PVSEC*, Paris, France, 2004, pp. 832–835.

G. Schubert, F. Huster, and P. Fath, “Current transport mechanism in printed Ag thick film contacts to an n-type emitter of a crystalline silicon solar cell,” in *Proc. 19th EC PVSEC*, Paris, France, 2004, pp. 813–816.

J. Hoornstra, G. Schubert, K. Broek, F. Granek, and C. LePrince, “Lead free metallisation paste for crystalline silicon solar cells: From model to results,” in *Proc. 31st IEEE PVSC*, Orlando, Florida, 2005, pp. 1293–1296.

F. Huster and G. Schubert, “ECV doping profile measurements of aluminium alloyed back surface fields,” in *Proc. 20th EC PVSEC*, Barcelona, Spain, 2005, pp. 1462–1465.

J. Hoornstra, G. Schubert, C. LePrince, G. Wahl, K. Broek, F. J. Granek, B. Lenkeit, and J. Horzel, “Lead free metallisation for silicon solar cells: Results from the EC2Contact project,” in *Proc. 20th EC PVSEC*, Barcelona, Spain, 2005, pp. 651–654.

G. Schubert, J. Horzel, R. Kopecek, F. Huster, and P. Fath, “Silver thick film contact formation on lowly doped phosphorous emitters,” in *Proc. 20th EC PVSEC*, Barcelona, Spain, 2005, pp. 934–937.

A. Herguth, G. Schubert, M. Kaes, and G. Hahn, “A new approach to prevent the negative impact of the metastable defect in boron doped cz silicon solar cells,” in *Proc. 4th WCPEC*, Hawaii, USA, 2006, in print.

A. Herguth, G. Schubert, M. Kaes, and G. Hahn, "Avoiding boron-oxygen related degradation in highly boron doped Cz silicon," *Proc. 21st EC PVSEC*, Dresden, Germany, 2006, pp. 530–537.

G. Schubert, and J. Horzel, "Investigations on the mechanism behind the beneficial effect of a forming gas anneal on solar cells with silver thick film contacts," *Proc. 21st EC PVSEC*, Dresden, Germany, 2006, pp. 1460–1466.

G. Schubert, F. Huster, and P. Fath, "Physical understanding of printed thick film front contacts of crystalline Si solar cells: Review of existing models and recent developments," *Solar Energy and Materials*, vol. 90, pp. 3399–3406, 2006.

A. Bentzen, G. Schubert, J. S. Christensen, B. Svensson, and A. Holt, "The influence of temperature during phosphorus emitter diffusion from a spray-on source in multicrystalline silicon solar cell processing," *accepted for publication in Progress in Photovoltaics*, DOI: 10.1002/pip.731, 2006.

Patent

A. Herguth, G. Schubert, M. Kaes, G. Hahn, and Ihor Melnyk, "Verfahren zum Herstellen eines Photovoltaikelements mit stabilisiertem Wirkungsgrad", German Patent Aktenzeichen 10 2006 012920.2, filed 21 March 2006

Zusammenfassung

In dieser Doktorarbeit wurde die Dickfilmmetallisierung von kristallinen Silizium-Solarzellen mit Hilfe eines neuen Ansatzes grundlegend untersucht. Konkurrierende Prozesse während der Kontaktbildung wurden getrennt voneinander analysiert. Aus den Erkenntnissen wurden Modelle für die Kontaktbildung und die elektrische Leitung in einem Dickfilmkontakt erstellt. Diese Modelle wurden erfolgreich angewendet, um blei- und cadmiumfreie Silber und Aluminium Dickfilmpasten zur Metallisierung von Solarzellen zu entwickeln. Mit optimierten Pasten, die innerhalb des Forschungsprojekts EC2Contact, gefördert von der europäischen Union, entwickelt wurden, konnten Industriesolarzellen hergestellt werden, die den Wirkungsgrad bleihaltiger Referenzpasten erreichten. Dies ist der bisher höchste publizierte Wirkungsgrad, der mit bleifreien Dickfilmpasten erzielt wurde. Die entwickelten Pasten werden derzeit vom Projektpartner Metalor in den Markt eingeführt. Im Folgenden werden die Ergebnisse der Doktorarbeit im Einzelnen vorgestellt.

Die Analyse des Herstellungsprozesses von industrierelevanten kristallinen Silizium-Solarzellen ergab, dass die Co-Feuerung, die simultane Kontaktbildung von Vorder- und Rückseitenkontakt in einem Hochtemperaturschritt, der komplexeste Prozessschritt ist. Es werden nicht nur die Vorder- und Rückseitenkontakte gebildet, sondern auch der laterale Widerstand in den Metallschichten gesenkt. Defekte im Siliziumsubstrat werden mit Hilfe von Wasserstoff passiviert, der aus der Siliziumnitridschicht während des Feuerns in das Silizium diffundiert. Ebenso nimmt die Oberflächenpassivierung des Siliziumnitrids zu und ein Back Surface Field wird unterhalb des Aluminiumrückkontaktes gebildet. Dieses dient als effiziente Rückseitenpassivierung.

Verlustanalysen von aktuellen Industrie-Solarzellen zeigten, dass die Silberdickfilmmetallisierung zur Kontaktierung von Phosphor-dotierten Emittern ein wesentlicher limitierender Faktor ist, um höhere Wirkungsgrade zu erzielen. Derzeit können nur hochdotierte Emitter (40 Ω/sq bis 70 Ω/sq) mit Silberdickfilmpasten kontaktiert werden, um Füllfaktorverluste zu vermeiden. Der hochdotierte Emitter ist aber die Ursache für Strom- und Spannungsverluste. Der Schwerpunkt dieser Arbeit lag deshalb auf dem grundlegenden Verständnis des Silberdickfilmkontakts und dessen Bildung.

Der spezifische Widerstand von Silberdickfilmfingern ist ca. 2 bis 3 mal höher als der spezifische Widerstand von reinem Silber. Mit Hilfe einer neu entwickelten Messmethode wurde das Potential des Silber-Sinterns während eines schnellen Feuerprozesses untersucht. Mit der In-Situ Linienwiderstandsmessung war es erstmalig möglich, einen Einblick in die Kinetik des Sinterprozesses in schnellen Feuerprozessen zu erhalten. Es konnte gezeigt werden, dass die Silberpartikel der untersuchten, kommerziell erhältlichen Silberpaste ab einer Temperatur größer 580°C anfangen, sehr schnell zusammenzusintern. Bei dieser Temperatur sind gebräuchliche Bleiborosilikat-Gläser flüssig. Das schnelle Zusammensintern der Silberpartikel lässt sich vermutlich auf einen Umordnungsprozess zurückführen, der durch das flüssige Glas unterstützt wird. Der Einfluss von Silberpartikelgröße und -form auf das Sintern in schnellen Feuer-

prozessen ist gering. Mit der neuen Messmethode wurde gezeigt, dass es nach einer Haltezeit von 50 s bei einer Temperatur von 800°C zu einer Sättigung des Linienwiderstandes kommt. Der auf diese Weise erreichbare, minimale Linienwiderstand ist im Wesentlichen unabhängig von der Form und Größe der Silberpartikel.

Die Analyse der Mikrostruktur des gefeuerten Silberdickfilmkontakts zu Phosphor-dotierten Emittern ergab, dass Silberkristalle in das Silizium gewachsen sind. Diese Kristalle sind von einer Glasschicht bedeckt, die die Silberkristalle von dem übrigen Silberfinger trennt. Die Dicke der Glasschicht nimmt mit steigender Feuertemperatur zu. Es wurden keine Hinweise auf direkte Verbindungen zwischen den Silberkristallen und dem Silber des Fingers gefunden. Allerdings kann die Glasschicht an einigen Stellen nur wenige Nanometer oder dünner sein. Die Silberkristalle wachsen vornehmlich auf den [111] Ebenen des Siliziumkristalls. Die Form der Kristalle hängt von der Feuertemperatur und der Siliziumorientierung ab. Auf <111> orientierten Substraten wachsen linsenartige Kristalle auf, auf <100> orientierten Substraten sind die aufgewachsenen Kristalle in Form von umgekehrten Pyramiden zu finden. Mit steigender Feuertemperatur wächst die Anzahl und Größe der Kristalle. Zudem verlieren die Kristalle ihre für die jeweilige Siliziumorientierung charakteristische Form. Zusätzlich wurde herausgefunden, dass die Unterseite des Silberfingers mit bleihaltigen Präzipitaten bedeckt ist.

Desweiteren wurde die Kontaktbildung detailliert untersucht. Dabei wurden konkurrierende Prozesse getrennt voneinander betrachtet. Der Schwerpunkt lag hierbei auf der Rolle des Glases. Typische Bleiborosilikat-Gläser wurden benutzt, um die Wechselwirkung des Glases mit Silber, Silizium Nitrid und Silizium zu untersuchen. Es wurde herausgefunden, dass ein solches Glas alle drei Partner ähnlich gut benetzt. Glas kann Silber lösen, allerdings ist dieser Prozess bei 800°C langsam im Vergleich zum schnellen Feuerprozess.
In typischen Feuerprozessen beginnt das Glas ab $T > 650$°C, signifikant in das Silizium hineinzuätzen. Es konnte experimentell gezeigt werden, dass Silizium das im Glas enthaltene Bleioxid reduziert. Das entstehende Blei benetzt Silizium nicht, sondern fällt als Präzipitat im Volumen des Glases aus.
Ein weiterer Untersuchungsschwerpunkt war der Wachstumsmechanismus der Silberkristalle. Es wurde herausgefunden, dass das Silberwachstum mit der Wechselwirkung des Bleioxids mit Silizium zusammenhängt. Vermutlich laufen hierbei zwei Prozesse simultan ab. Zum einen wird Silber im Glas gelöst. Die Silberionen können nun mit dem Silizium in Form einer Redox-Reaktion reagieren. Allerdings ist der Lösungsprozess des Silbers im Glas langsam. Zum anderen tritt das flüssige Blei, das Produkt der Glas - Silizium Reaktion, in Wechselwirkung mit Silber und dient als Transportmedium für den Aufwachsprozess des Silbers. Dieser Prozess ist schnell. Deshalb wird vermutet, dass dies der dominante Prozess ist. Bei optimalen Feuerbedingungen und bei Pasten mit einem hohen Silberanteil wurden keine Bleipräzipitate im Glas gefunden, was darauf hindeutet, dass Blei im Silber gelöst wurde. Die bleihaltigen Präzipitate auf der Unterseite des Fingers scheinen diese Hypothese zu unterstützen.
Das Silberwachstum hängt von der Oberflächenkonzentration des Phosphors im Emitter ab. Ist die Phosphorkonzentration an der Oberfläche größer als die Festkörperlöslichkeitsgrenze, wachsen im Vergleich zu niedrigeren Phosphorkonzentrationen mehr und größere Kristalle schon bei niedrigeren Temperaturen. Höhere Temperaturen ($T_{peak} > 810$°C) oder längere Feuerzeiten führen zu einem verstärkten Silberwachstum auch auf Emittern mit einer Dotierung unter 1×10^{20} cm^{-3}. Ein Grund für die erfolglose Kontaktierung von niedrig dotierten Emittern ist also der Einfluss des Phosphors auf das Silberkristallwachstum. Zusätzlich wurde herausgefunden, dass texturierte Oberflächen mit einer großen Anzahl an [111] orientierten Siliziumebenen das

Wachstum begünstigen.

Numerische Simulationen wurden durchgeführt, um den Effekt der Kontaktgeometrie und des Dotierprofils auf den spezifischen Kontaktwiderstand in Metall - Halbleiterkontakten abzuschätzen. Die Kontaktgeometrie hat nur einen geringen Einfluss. Unabhängig von der Geometrie bestimmen die hochdotierten oberflächennahen Bereiche den spezifischen Kontaktwiderstand. Die Silberkristalle, die in das Silizium gewachsen sind, sind unabkömmlich für den Stromtransport. Der gemessene spezifische Kontaktwiderstand eines einzelnen Kristalls zu moderat dotierten Emittern ($N_D = 6 \times 10^{19}\,\text{cm}^{-3}$) liegt im Bereich von $\rho_{C,\text{singlecrystal}} = 7$ bis 60×10^{-7} Ωcm^2. Nimmt man an, dass die Silberkristalle direkt mit dem Silberfinger verbunden sind, würde eine Bedeckung mit Silberkristallen eines solchen Emitters von 0.1% ausreichen, um ausreichend niedrige makroskopische Kontaktwiderstände von <10 mΩcm^2 zu erzielen. Zwei Faktoren limitieren den makroskopischen spezifischen Kontaktwiderstand von Silberdickfilmkontakten: 1. Die Anzahl der in das Silizium gewachsenen Kristalle und 2. der Stromtransport von den Kristallen in den Finger. Der Stromtransport von den Kristallen in den Silberfinger verläuft vermutlich über einen Tunnelprozess durch das trennende Glas, an Stellen, an denen die Glasschicht sehr dünn ist. Je höher die Feuertemperatur, desto dicker die Glasschicht. Deshalb steigt der Kontaktwiderstand beim Überfeuern.
Der Wirkungsgrad von überfeuerten Zellen, bei denen der Kontaktwiderstand durch eine dicke Glasschicht zwischen den Kristallen und dem Silberfinger limitiert ist, kann durch einen Formier-Gas Anneal (FGA) bei $T > 375°\text{C}$ für mindestens 15 min in einem Rohrofen gesteigert werden. Der FGA beeinflusst ρ_C und damit den Serienwiderstand einer Zelle. Andere Zellparameter werden nicht bemerkenswert beeinflusst. Änderungen in der Silberkristallbedeckung oder in der Kristallgröße nach einem FGA konnten nicht festgestellt werden. Es liegt nahe, dass Wasserstoff die in der Glasschicht enthaltenen Metalloxide reduziert. Diese agieren vermutlich als Tunnelzentren. Der Strom wird dann vermutlich über einen Tunnelmechanismus zwischen den fein verteilten Präzipitaten in der Glasschicht transportiert, was zur einer Erhöhung der Leitfähigkeit führt. Der gemittelte Widerstand zwischen Silberkristallen und Silberfinger sank nach dem FGA auf 1-2% des ursprünglichen Wertes. Die Reaktion während des FGAs kann nicht durch einen Anneal in Sauerstoff rückgängig gemacht werden. Es wurde gezeigt, dass der Wirkungsgrad einer Formier-Gas behandelten Zelle mindestens 17 Monate lang stabil bleibt.

Die Kombination des Kontaktbildungs- und Stromtransportmodells führte zu der erfolgreichen Herstellung einer Industrie-Solarzelle mit einem moderat dotierten Emitter ($N_{D,surface} = 4 \times 10^{19}$). Zur Metallisierung wurden kommerziell erhältliche Dickfilmpasten benutzt. Der Feuerprozess wurde bei erhöhten Temperaturen durchgeführt, um ein effizientes Kristallwachstum zu ermöglichen. Die Nachteile im Kontaktwiderstand durch das Überfeuern wurden durch einen Forming-Gas Anneal wieder rückgängig gemacht, was zu einem niedrigen Serienwiderstand von 0.7 Ωcm^2 führte. Die Zelle litt jedoch unter einem hohen J_{02} Strom, so dass ein Wirkungsgrad von 14.9% erreicht wurde. Es konnte somit gezeigt werden, dass es möglich ist, Solarzellen mit moderat dotierten Emittern mit Hilfe von Silberdickfilmpasten zu kontaktieren.

Das Modell der Kontaktbildung diente als Grundlage zur Entwicklung einer bleifreien Silberdickfilmpaste. Es wurde gezeigt, dass Bismuth hinsichtlich der Wechselwirkung mit Silber, Silizium und Siliziumnitrid ähnliche Eigenschaften wie Blei besitzt. Auf Grundlage der Untersuchungen an Bi_2O_3 Gläsern wurde im Rahmen des EC2Contact Projekts eine bleifreie Silberpaste entwickelt. Die beste Industriesolarzelle, die mit dieser Silberpaste innerhalb des Projekts hergestellt wurde, erzielte einen Wirkungsgrad von 17.0% und einen Füllfaktor von

77.2% auf Cz-Si Material. Nach Kenntnissen des Autors ist dies der bisher höchste Wirkungsgrad, der mit bleifreien Silberpasten erzielt wurde.

Basierend auf den positiven Eigenschaften von Gläsern für die Aluminiumkontaktbildung wurde innerhalb des EC2Contact Projekts eine glashaltige, bleifreie Aluminiumrückseitenpaste entwickelt. Die beste Zelle, die im Rahmen des Projektes mit einer bleifreien Paste hergestellt werden konnte, erzielt einen Wirkungsgrad der ebenso hoch ist wie der Wirkungsgrad von Zellen, die mit kommerziell erhältlichen Pasten hergestellt wurde. Als positiver Zusatzeffekt wurde festgestellt, dass die Verbiegung der Zellen mit bleifreien Pasten geringer ist.

Danksagung

An dieser Stelle möchte ich all denen danken, die zum Gelingen der Doktorarbeit beigetragen haben. Mein besonderer Dank gilt:

Prof Dr. Ernst Bucher für die Möglichkeit, diese Arbeit an seinem Lehrstuhl anfertigen zu können, und für die Betreuung der Arbeit.

Prof. Dr. Wim Sinke für die spontane Übernahme der Zweitkorrektur.

Dr. Peter Fath für die langjährige Leitung der Silizium-Solarzellengruppe, die Möglichkeit, auf dem EC2Contact EU-Projekt arbeiten zu können und für das Vetrauen, mir die Leitung der Industriesolarzellengruppe zu übertragen.

Pd. Dr. Giso Hahn und Dr. Kristian Peter für die Leitung der Photovoltaik-Abteilung, die nette Zusammenarbeit und die Unterstützung bei jeglichen Fragen.

Angela Schellinger für ihre Hilfsbereitschaft und die freundliche Atmosphäre an diesem Lehrstuhl.

Jaap Hoornstra, Dr. Jörg Horzel, Sibylle Ohl, Holger Knauss, Dr. Barabara Terheiden und Michelle McCann für das Korrekturlesen und die vielen guten Ratschläge.

Dr. Bernhard Fischer für die Mitgestaltung des EC2Contact Projekts, die Unterstützung, die vielen tollen Anregungen zu Beginn meiner Doktorarbeit und den Aufbau des Charakterisierungslabors.

Frank Huster für die spannenden Diskussionen, hilfreichen Ratschläge und für die Organisation des Kaffeeautomats.

Jaap Hoornstra für die freundschaftliche Zusammenarbeit und die interessanten Diskussionen.

Dr. Jörg Horzel für die fruchtbaren Gespräche und Diskussionen und die produktive Zusammenarbeit.

Dem gesamten EC2Contact Konsortium für die konstruktive Zusammenarbeit.

Erwin Biegger und Manfred Keil vom Lehrstuhl Rüdiger für die Hilfsbereitschaft, Unterstützung und Durchführung von DTA und XRD Messungen.

Sibylle Ohl für ihre Begeisterungsfähigkeit und ihr Engagement.

Dr. Eckard Wefringhaus für Diskussionen rund um die Chemie.

Meinem ehemaligen Diplomand Axel Herguth für die tollen Ergebnisse und seine uneingeschränkte Hilfsbereitschaft in auch für ihn anstrengenden Zeiten.

Meinen Bürokolleginnen Dr. Barbara Terheiden und Claudia Strümpel für die schöne Atmosphäre im Büro.

Said Riazi-Nejad für die Betreuung des Computernetzwerkes und die schnelle Hilfe bei jeglichen Problemen.

Holger Knauss für die nächtlichen Joggingrunden bei Minusgraden.

Allen anderen Kolleginnen und Kollegen an diesem Lehrstuhl für das gute Klima und die offenen Ohren bei Problemen.

Meiner Familie, die mich immer in jeglicher Weise unterstützt hat.

Und besonders meiner Frau Michaela für die uneingeschränkte Unterstützung, die Kraft, die sie mir gibt und für das Korrekturlesen.